# Numerical Modelling of Alkali Silica Reaction in Concrete Dams

By

**Mohammad Sadegh Pourbehi**


Dissertation presented for the degree of Doctor of Philosophy in Civil Engineering at
Stellenbosch University


Promoters:
Dr. J.A.v.B. Strasheim
Prof. Dr. Eng. Gideon P.A.G. van Zijl

December 2018

# Declaration

By submitting this dissertation electronically, I declare that the entirety of the work contained therein is my own, original work, that I am the sole author thereof (save to the extent explicitly otherwise stated), that reproduction and publication thereof by Stellenbosch University will not infringe any third party rights and that I have not previously in its entirety or in part submitted it for obtaining any qualification.

Signature: _____

Date: _____

UNIVERSITEIT·STELLENBOSCH·UNIVERSITY
jou kennisvennoot • your knowledge partner

## Plagiaatverklaring / Plagiarism *Declaration*

1 Plagiaat is die oorneem en gebruik van die idees, materiaal en ander intellektuele eiendom van ander persone asof dit jou eie werk is.
*Plagiarism is the use of ideas, material and other intellectual property of another's work and to present it as my own.*

2 Ek erken dat die pleeg van plagiaat 'n strafbare oortreding is aangesien dit 'n vorm van diefstal is.
*I agree that plagiarism is a punishable offence because it constitutes theft.*

3 Ek verstaan ook dat direkte vertalings plagiaat is.
*also understand that direct translations are plagiarism.*

4 Dienooreenkomstig is alle aanhalings en bydraes vanuit enige bron (ingesluit die internet) volledig verwys (erken). Ek erken dat die woordelikse aanhaal van teks sonder aanhalingstekens (selfs al word die bron volledig erken) plagiaat is.
*Accordingly, all quotations and contributions from any source whatsoever (including the internet) have been cited fully. I understand that the reproduction of text without quotation marks (even when the source is cited) is plagiarism.*

5 Ek verklaar dat die werk in hierdie skryfstuk vervat, behalwe waar anders aangedui, my eie oorspronklike werk is en dat ek dit nie vantevore in die geheel of gedeeltelik ingehandig het vir bepunting in hierdie module/werkstuk of 'n ander module/werkstuk nie.
*declare that the work contained in this assignment, except where otherwise stated, is my original work and that I have not previously (in its entirety or in part) submitted it for grading in this module/assignment or another module/assignment.*

| | |
|---|---|
| **Studentenommer / *Student number*** | **Handtekening / *Signature*** |
| **Voorletters en van / *Initials and surname*** | **Datum / *Date*** |

# Acknowledgements

Many people have contributed to this thesis in various ways. First of all, I would like to express the deepest appreciation to Professor Gideon P.A.G van Zijl of Stellenbosch University, for giving me the chance to work with him. His unwavering knowledge in the field of *Computational Solid Mechanics* opened a new horizon for me. Indeed, without his guidance and persistent help this dissertation would not have been possible. Also, I would like to express my sincere gratitude to my supervisor Dr. JAvB Strasheim lecturer at Stellenbosch University for his unconditional support and valuable advice especially during the write up of this dissertation.

I would like to acknowledge the support and advice provided by Professor Celeste Viljoen, professor at Stellenbosch University during my research in the Institute of Structural Engineering.

The permit issued from Department of Water and Sanitation in South Africa to conduct the technical investigation on Kleinplaas dam in Western Cape province is highly appreciated.

I would also like to appreciate the secretary and the staff of the Department of Civil Engineering for their support and help.

I am also grateful to my family, my colleagues of the Department of Civil Engineering and my friends for their continuous support and encouragement during my PhD studies.

Finally, I would like to express my deep gratitude and appreciation to my *FATHER* and *MOTHER* whose good wishes and prayers have always been with me.

# Dedication

I dedicate this dissertation to

my wife, *Andisheh*

and

my lovely son, *Pooria*

# Abstract

Dams are important infrastructure components and an asset for any country. Past earthquakes have highlighted their vulnerability to damage and even failure which can have major socio-economic consequences, losses and other cascading effects (e.g. water supply, power generation and irrigation). Hence, considerable research has been done to evaluating the safety of the aged dams and in some cases to pursue a suitable remedial action and rehabilitation strategy.

Alkali Silica Reaction (ASR), a deleterious chemical reaction between siliceous aggregate and cement paste in concrete, causes long term swelling and deterioration of concrete structures such as dams. Several important factors govern the ASR reaction kinetics, of which water and temperature are the most important. Numerical modelling should capture the impact of humidity, temperature, and confining stresses and material degradation during the ASR as the most prominent factors influencing ASR.

In general, numerical models for modelling ASR and its effects fall into three categories: (1) macrostructural models concerned with the analysis of structures affected by the reaction; (2) microstructural models which link the chemical reaction to its impact at the material level; (3) mesoscopic models that consider the multi-phases of the aggregate, cement paste, void and ASR gel, whereby anisotropy is explicitly represented.

In this study a chemo-damage-plastic model is developed, considering temperature, humidity, non-uniform time-dependent material degradation and 3D stress confinement effects on ASR evolution. The model is validated by modelling the structural behaviour and response of three concrete gravity dams namely Fontana dam, Kleinplaas dam and Koyna dam. Comparing the results with the actual data on macro crack appearance and crest displacement as well as with other numerical models available in literature. The model developed for Kleinplaas dam is calibrated with the measured data and the applicable ASR parameters are identified. An attempt is then made to simulate the past and current swelling behaviour of the dam and the associated damage. The results successfully predicted the displacements and ASR strain rates plus the development of irreversible plastic cracks.

While the structural behaviour of ASR affected structures under monotonic and quasi-static loading has been extensively investigated over the last decades, limited research has addressed dynamic loading. The combined effect of old and new cracks under dynamic excitation may

cause dam failure. Considering the predicted interaction between ASR and seismic loads, remedial measures can be adopted at the right point in time to safeguard the dam in the event of an earthquake. Fluid-Foundation-Structure Interaction (FFSI) also has received much attention in Finite Element Analysis (FEA) of dams. The SU-ASR (**S**tellenbosch **U**niversity ASR FE code) model developed, is used to analyse and predict dynamic behaviour of the Koyna dam, damaged by an earthquake. The combined ASR and seismic action are investigated and comparisons are made through a comprehensive study of the damage development and crest displacement. The seismic response of the deteriorated dam is subsequently analysed based on the state of the structure at the end of the long term ASR analysis. The results show that this combined action can significantly change the dynamic behaviour of typical concrete dams.

Finally, a rational prediction of the long term impacts of remedial actions such as the slot cutting technique and the justification of other remedial action based on analytical results, was done. This required the use of specialized software with an adequate constitutive law and time integration scheme. As an example, the slot cutting technique is implemented for a synthetic dam structure using the SU-ASR finite element based computer program code developed in this research. The results of this simulation are discussed and interpreted. The SU-ASR model predicted the behaviour of the dam before and after the slot cutting closure and the subsequent compressive stresses with good approximation.

# Opsomming

Damme verteenwoordig belangrike bates en ook komponente van die infrastruktuur van 'n land. Die voorkoms van aardbewings in die verlede het die vatbaarheid vir skade en selfs faling van hierdie strukture beklemtoon. Faling van damme kan drastiese sosio-ekonomiese gevolge, verliese en ander verdere gevolge hê (bv. watervoorsiening, krag opwekking en besproeiing). In die lig hiervan, word aansienlike pogings aangewend om die veiligheid van ouer damme te evalueer en ook om in sommige gevalle geskikte remediëringsaksies en rehabilitasie strategieë toe te pas.

Alkali Silika Reaksie (ASR), 'n skadelike chemiese reaksie tussen silikahoudende aggregate en sementpasta in beton, veroorsaak langtermyn uitsetting en agteruitgang van betonstrukture soos damme. Verskeie belangrike faktore bepaal die ASR reaksiekinetika, waarvan water en temperatuur die belangrikste is. Numeriese modellering behoort die effek van humiditeit, temperatuur, en inperkende spanning en materiaaldegradasie tydens die ASR as die mees prominente faktore wat ASR beïnvloed, te ondervang.

In die algemeen kan numeriese modelle vir die modellering van ASR en die effek daarvan in drie kategorieë geklassifiseer word:
(1) makro struktuurmodelle wat verband hou met die analise van strukture wat deur die reaksie geraak word;
(2) mikro struktuurmodelle wat die chemiese reaksie en die impak daarvan op die materiaalvlak met mekaar verbind;
(3) mesoskopiese modelle wat die meer-fases van die aggregaat, sementpasta, lugopeninge en ASR-gel beskou, waarmee anisotropie eksplisiet gemodelleer word.

In hierdie studie word 'n chemo-plastisiteit-skade-model ontwikkel, met inagneming van temperatuur, humiditeit, nie-uniforme tydafhanklike materiaaldegradasie en 3D-spanningsinperkings-effekte op ASR-ontwikkeling. Die model word gevalideer deur die strukturele gedrag en respons van drie beton swaartedamwalle naamlik Fontana-dam, Kleinplaasdam en Koynadam, te modelleer en die resultate te vergelyk met die beskikbare werklike makro-kraakvoorkoms en kruinverplasing data asook met ander numeriese modelle wat in die literatuur beskikbaar is. Die model wat ontwikkel is vir die Kleinplaasdam is gekalibreer met die gemete data en die toepaslike ASR-parameters is geïdentifiseer. Dan word daar gepoog om die voorafgaande en huidige uitsettingsgedrag van die dam en verwante skade

te simuleer. Die resultate kon die verplasings en ASR-vervormingstempos asook die ontwikkeling van onomkeerbare plastiese krake, suksesvol voorspel.

Alhoewel die strukturele gedrag en van ASR-strukture onder monotoniese en kwasi-statiese belasting die afgelope dekades omvattend ondersoek is, is beperkte navorsing oor dinamiese belastings gedoen. Die gesamentlike effek van ou en nuwe krake onder dinamiese aksie kan dam swigting veroorsaak. Met inagneming van die voorspelde interaksie tussen ASR en seismiese belastings, kan remediërende maatreëls op die regte tyd toegepas word om die dam te beveilig in die geval van 'n aardbewing. Daar is ook heelwat aandag aan Vloeistof-Fondament-Struktuur-interaksie (VFSI) in Eindige Element Analise (EEA) van damme gegee. Die SU-ASR model, wat ontwikkel is, is gebruik om die dinamiese gedrag van die Koynadam, wat deur 'n aardbewing beskadig is, te analiseer en te voorspel. Die gekombineerde ASR en seismiese aksie word ondersoek en vergelykings word gemaak deur 'n omvattende studie van die struktuurskade en kruinverplasing te doen. Die seismiese gedrag van die verswakte dam is vervolgens ontleed aan die hand van die toestand van die struktuur aan die einde van die langtermyn-ASR-analise. Die resultate toon dat hierdie gekombineerde aksie die dinamiese gedrag van betondamme aansienlik kan beïnvloed.

Ten slotte is daar 'n rasionele voorspelling van die lang termyn impak van remediërende werk soos die groef-sny tegniek en die regverdiging van ander remediërende werk gebaseer op analitiese resultate, gedoen. Hiervoor is daar gebruik gemaak van gespesialiseerde sagteware met 'n voldoende materiaalwet modellerings- en die tyd integrasie skema vermoë. As 'n voorbeeld word die groef-sny tegniek geïmplementeer vir 'n sintetiese dam struktuur met behulp van die SU-ASR eindige element baseerde rekenaar program kode ontwikkel in hierdie navorsing. Die resultate van hierdie simulasie word dan bespreek en geïnterpreteer. Die SU-ASR-model voorspel die gedrag van die dam voor en na die slot-sluiting en die daaropvolgende drukspanning met 'n aanvaarbare vlak van akkuraatheid.

# List of Publications

***International conference papers***

1- **M. S. Pourbehi**, G. P. A. G. Van Zijl, and J. A. v. B. Strasheim, (2018), "*Modelling of Alkali Silica Reaction in Concrete Structures for Rehabilitation Intervention*", in Proceedings of ICCRRR2018, Cape town.

2- **M. S. Pourbehi**, G. P. A. G. Van Zijl, and J. A. B. Strasheim, (2018),"*Seismic Analysis of Concrete Dams Affected by Alkali Silica Reaction Considering Fluid-Structure-Interaction*," in Proceedings of *ConMod Conference*, Delft, The Netherlands, (*This Paper was awarded PhD grant from RILEM as one of the best PhD student paper submitted to the conference from Africa continent*).

3- **M.S. Pourbehi**, G.P.A.G. van Zijl and J. A. v. B. Strasheim, (2018) "*Numerical modelling of the Alkali Silica Reaction affected Kleinplaas dam considering anisotropic swelling and concrete material deterioration*. In Proceeding of SANCOLD 2018, 7-9 November, Somerset, Cape Town, South Arica.

# Table of Contents

# List of Figures

# List of Tables

# Symbols and Abbreviation

## Symbols

| | |
|---|---|
| $A_0$: | Kinetics constant to be experimentally determined |
| $A_m$: | Reaction affinity |
| $B$: | Calibration parameter in ASR induced damage function |
| $C$: | Volumetric heat capacity |
| $C_0$: | Acoustic wave speed in Helmholtz equation |
| $c_1$: | Material constant of tensile stress-COD equation |
| $c_2$: | Material constant of tensile stress-COD equation |
| $COD$: | Crack opening displacement |
| $d_{asr}$: | ASR damage variable |
| $d_{t,c}$: | Tensile and compressive damage variable in concrete damage plastic model |
| $d_m$: | Mechanical damage variable |
| $\boldsymbol{D}_0^{el}$: | Initial elastic stiffness tensor of the concrete |
| $\boldsymbol{D}^{el}$: | Deteriorated elastic stiffness tensor |
| $D_\theta$: | Thermal diffusivity |
| $e_{sc:}$ | Thickness of the slot cutting |
| $E_0$: | Initial values of Young's modulus |
| $E_s$: | Spring modulus of chemo-elastic device |
| $F$: | Yield function |
| $f_{c0}$: | Initial compressive strength |
| $f_{cm}$: | Mean cylindrical concrete compressive stress |
| $f_t$: | Concrete tensile strength |
| $G_F$: | Tensile fracture energy |
| $G_c$: | Compressive fracture energy |
| $g(h)$: | Humidity function |
| $g_k$: | Dissipation energy of concrete material |
| $h_w$: | Water head in reservoir |
| $I_1$: | First stress invariant |
| $J_2$: | Second deviatoric stress |
| $K_c$: | Concrete damage plasticity parameter |

$K_d$: Coefficient that relates chemical extent to affinity

$l_{max}$: Maximum characteristic length of FE mesh

$P_g$: Swelling pressure

$Q$: Flow potential function

$S_t$: Tensile parameter in concrete damage plastic model

$S_c$: Compression parameter in concrete damage plastic model

$t$: Time

$t_c(\theta_0, \xi)$: Characteristic time in kinetics equation

$T$: Absolute temperature

$\bar{T}$: Reference temperature

$U_c$: Activation energy constant of characteristic time

$U_L$: Activation energy constant of latency time

$w_c$: Maximum Crack mouth opening

$W_i$: Weight function to distribute ASR volumetric strain

**Greek symbols**

α: Coefficient of thermal expansion

$\beta^m$: Calibration factor

$\Gamma_t$: Function accounts for ASR reduction due to tensile cracking

$\Gamma_c$: Function accounts for the reduction in ASR volumetric expansion under compressive stresses

$\gamma$: Parameter of the yield function in damage plastic model

$\delta$: Kronecker's delta

$\varepsilon$: Total strain measurable by experiment

$\boldsymbol{\varepsilon}$: Principal strains

$\varepsilon^{asr}$: ASR strain

$\varepsilon^{el}$: Elastic strain

$\varepsilon^{pl}$: Plastic strain

$\varepsilon^{th}$: Thermal strain

$\epsilon(\infty)$: Asymptotic volumetric expansion strain in the stress-free experiment

$\epsilon(t)$: ASR expansion strain

$\epsilon$: Eccentricity parameter in concrete damage plastic model

$\varepsilon_c$: Concrete compression strain

$\varepsilon_{ec}$: Equivalent strain corresponding to the maximum compression stress

$\varepsilon_{uc}$: Fracture strain

$\tilde{\varepsilon}_t^{pl}$: Equivalent plastic strain for tension

$\tilde{\varepsilon}_c^{pl}$: Equivalent plastic strain for compression

$\theta$: Temperature

$\theta_0$: Reference temperature

$\upsilon$: Poisson's ratio

$\kappa$: Conductivity in heat transfer equation

$\xi$: Extent of the chemical reaction

$\bar{\xi}$: Material constant

σ : Macroscopic stress due to external forces

$\boldsymbol{\sigma}$: Principal stresses

$\bar{\boldsymbol{\sigma}}$: Effective stress in concrete damage plasticity model

$\sigma_\mu$: Stress in elastic spring

$\bar{\sigma}$ : Hydrostatic pressure

$\sigma_v$: Sum of the compressive stresses in principal direction

$\bar{\sigma}_v$: Stress limit below which ASR strain could be suppressed.

$\tau_c$: Characteristic time

$\tau_L$: Latency time

$\Psi$: Free energy

$\psi$: Dilation angle in concrete damage plastic model

**Abbreviations**

AAR: Alkali aggregate reaction

ASR: Alkali silica reaction

ASTM: American society for testing and materials

COD: Crack mouth opening displacement

CDP: Concrete damage plasticity

FE: Finite element

FEM: Finite element method

FFSI: Foundation fluid structure interaction

FPZ Fracture process zone

| | |
|---|---|
| FV: | Field variable |
| ITZ: | Interfacial transition zone |
| pH: | potential of Hydrogen |
| RH: | Relative humidity |
| RVE: | Representative volume element |
| SDV: | Solution dependent state variable |
| SEM: | Scanning electron microscopy |
| SU-ASR: | Stellenbosch University ASR finite element model |
| UCP: | Uniaxial confinement parameter |
| UPVC: | Unplasticized polyvinyl chloride |
| XFEM: | Extended finite element method |
| XRF: | X-Ray Fluorescence |

# CHAPTER 1

# Introduction

**Highlights:**

Background

Research questions

Thesis contribution

Thesis outline

## 1.1 Background

The impact of water supply shortages due to the climate change in many regions of the world imply that a high level of operational reliability needs to be maintained for dams and the associated water distribution systems. Meeting these requirements has become a growing concern of dam owners.

A number of hydraulic structures such as dams and hydro-power plants in Southern Africa designed during the last decades, e.g. since 1960, have been deteriorating due to deleterious Alkali Silica Reaction (ASR) phenomenon. ASR within the group of Alkali Aggregates Reaction (AAR), is a harmful chemical reaction between alkalis in Portland cement paste and certain types of silica found in a various natural aggregates which usually results in structural distress due to expansion of the structure, material degradation, cracking, presence of gel, discoloration and pop outs of the reacting components near the surface of the concrete. Also, suitable environmental conditions such as temperature and relative humidity play a vital role in the initiation and advancement of ASR.

Many concrete structures, such as dams and bridges and more recently nuclear power plants, have been deteriorated by ASR. This problem was first reported in 1940 by Stanton (1940) in the USA and in South Africa the problem was first identified in structures in the Cape Peninsula in the 1970s (Owens, 2009). Extensive research on the material and structural scale has been done focusing on the physics and chemistry of the ASR. Laboratory techniques such as accelerated test methods to study the expansion mechanism and also techniques for the analysis of concrete structures affected by ASR have been developed. These include the development of strategies to reduce the effects of ASR induced damage (Blight & Alexander, 2011).

Because ASR in actual structures usually needs prolonged periods of more than 10 years to develop, it is challenging to research this phenomenon in the laboratory environment. Laboratory experimental approaches such as Accelerated Mortar Bar Test (ASTM C1260, 2007) and Concrete Prism Test (ASTM C1293, 2008) have been developed to accelerate the process of ASR and to overcome the difficulties regarding the determination of material and environmental parameters influencing ASR. Experimental tests as part of research carried out within days or months depend extensively on the control of environmental conditions of the specimens. Using these accelerated tests on specimens affected by ASR, variables such as kinetics of the reaction and material properties can be determined in a few days or months.

## 1.2 The main problem statement

It is mentioned in the previous section that ASR is a harmful chemical reaction between siliceous aggregate and cement paste in concrete that causes long term swelling and deterioration of concrete structures such as dams. The hydrophilic ASR gel expands in the presence of water, and initially fills the pores and micro cracks in the interfacial transition zone (ITZ). Further expansion induces a build-up of internal pressure, which is assumed to be the main mechanism of initiation and propagation of cracks and degradation of elastic properties. Several important factors govern the ASR reaction kinetics, of which water and temperature are the most important (Alaud, 2016; Larive, 1998; Multon & Toutlemonde, 2006). ASR is thermo-activated; that is, the higher the temperature, the faster it occurs (Ulm *et al*., 2000).

ASR can be confined through different constraints. The effects from 3D confinement stresses due to internal and external loads could reduce the volumetric ASR strain and create anisotropy of the swelling. It is now widely accepted that a sufficiently high confinement stress would

stop the ASR expansion completely (Liaudat *et al.*, 2018). The effects from this 3D confinement stress should be incorporated in the numerical modelling of dam structures suffering from ASR.

ASR expansion may be strongly coupled with internal damage (Giorla *et al.*, 2015). The majority of research has ignored the long term effects of material degradation that may lead to change in the engineering properties of the concrete material during the service life of the dam. Material degradation may cause to change to the dynamic behaviour of the dam, and it is necessary to estimate the seismic safety of dams suffering from the ASR taking the time-dependent material deterioration into account. Research has been performed on aged concrete dams assuming a uniform material time dependent degradation index along the dam body, due to physical and chemical attacks such as freeze-thaw cycles, fatigue and expansive chemical reactions (Valliappan & Chee, 2009). However, a uniform material deterioration index for the dam may overestimate the structural dynamic response and behaviour of the damaged structure.

Whether degraded structures can still resist natural events such as seismic excitation is a concern. While the mechanical performance of ASR affected structures under monotonic and quasi-static loading has been extensively investigated over the last decades, limited research has addressed dynamic loading (Pan *et al.*, 2014). The combined action of old and new cracks under dynamic excitation may cause dam failure. Considering predicted interaction between ASR and seismic loads, remedial measures can be adopted at the right time to safeguard the dam in the event of an earthquake. Fluid-Foundation-Structure Interaction (FFSI) also has received much attention in Finite Element Analysis (FEA) of dams. They include the effects of hydrodynamic pressure on the dam-water interface, and assumed boundary conditions on the fluid domain, such as far-field non-reflective and the admittance boundary condition for modelling the sediments in the reservoir bed (Calayir & Karaton, 2005; Tan & Chopra, 1995).

So far there is no way to stop or decrease the ASR in the current concrete dam structures. Hence, remedial and rehabilitation techniques to relieve the pressure and associated damage in the dam structures are inevitable. Among the several intervention strategies, slot cutting is one of the main techniques that has been applied successfully to some dams in the real world (Charlwood, 2009; Sellier *et al.*, 2017). A specialized numerical software tool should be used

to analyse and predict the impact of slot cutting on deteriorated structures such as dams suffering from ASR.

However, a unified chemo-thermo-mechanical finite element numerical model that can integrate the key phenomena involved in the ASR such as kinetics of the reaction, temperature, humidity and confining stresses to predict the expansion and subsequent non-uniform time dependent material deterioration considering the non-linear behaviour of concrete and cracking still to be developed. The goal of this research is to develop such a model to predict the behaviour of the dam affected by ASR and then simulate the slot cutting technique as a rehabilitation strategy to relieve the harmful compressive stresses inside the dam.

## 1.3 ASR in South Africa and need for research

The most cases of diagnosed ASR deterioration in South Africa occur in the Cape Peninsula and environs and the aggregates involved are from the Malmesbury Group (Alaud & van Zijl, 2017). As a result, many hydraulic structures such as several storage dams and related structures for power generation, a large number of bridges, concrete highways, sport stadiums, a large concrete dome structure, the hard-standing slab of a container terminal and electric mast foundations, have been affected (Blight & Alexander, 2011). In the Eastern Cape, also some exposed concrete structures have been suffering from ASR and the aggregates involved are Table Mountain Group quartzite, Enon Formation quartzite pebbles and Quaternary gravels. The structures involved are several irrigation and water storage dams, bridges, an airport apron and airport building pile caps, retaining walls and electric mast foundations (Owens, 2009). In the Pretoria-Johannesburg-Heidelberg-Welkom area, structures such as reservoirs, bridges, reinforced concrete portal frames of highway bridges and an airport runway have shown some symptoms of ASR. In all cases, the aggregate used contained quartzite and shale of the Witwatersrand Super-Group (Alaud, 2016).

While the scope of this research is mostly numerical modelling of ASR in concrete dams, it is considered necessary to provide some data of ASR affected dams in South Africa. Table 1-1 contains a summary of data on dams and related facilities which have been suffering from ASR in recent years. Symptoms of the ASR in Table 1-1, range from displacement of the crest, cracks and damage in the body of dams, to misalignment of mechanical facilities such as spillway gates and stop beams.

**Table 1-1**. Hydraulic structures in South Africa suffering from ASR effects (Blight & Alexander, 2011; Sims & Poole, 2017)

| No | Name of Dam | Typology | Year of construction | Height (m) | Symptoms | Treatment | Type of treatment |
|---|---|---|---|---|---|---|---|
| 1 | Churchill (Eastern Cape) | Multiple arch buttresses | 1943 | 39 | Horizontal cracking on the downstream face, vertical movement | Strengthening Buttresses of reinforced concrete | R |
| 2 | Keerom | Gravity arch | 1954 | 38 | Diagonal cracking, open joints and loss of concrete strength | injection and fissures together | I |
| 3 | Kleinplaas | spillway concrete | 1982 | 20 | Cracking in galleries | Injection and sealing together | I |
| 4 | Kouga (Eastern Cape) | Gravity arch | 1978 | 78 | Horizontal and vertical movement and cracking above water facing | Installation of monitoring devices | M |
| 5 | Paul Sauer | Gravity arch | 1969 | 82 | Cracking in joints construction and block movements | No treatment | N |
| 6 | Poortjieskloof | Gravity arch | 1955 | 38 | Horizontal cracking, Permanent upstream movement up to 20 mm over a period of 15 years | Surface repair | S |

| | | | | | | | |
|---|---|---|---|---|---|---|---|
| | | | | | and upward movement of about 2 mm over a period of 2 years | | |
| 7 | Pietersfontein | Gravity arch | 1968 | 29 | Low concrete flexure resistant | No treatment | N |
| 8 | Roode Elsburg | Gravity arch | 1968 | 72 | Cracking and vibration in the turbine | Repair of the turbine | S |
| 9 | Steenbras (Western Cape) | Central hydropower | 1964 | | remaining movements | no intervention till the date | N |
| 10 | Stompdrift | Multiple arch and gravity | 1965 | 49 | Extended cracking and seals opening | Injection to construction joints | I |
| 11 | Clan-William dam (Western Cape) | Concrete gravity | 1935 | Current height: 43 | Vertical and horizontal offsets at joints | Installation of monitoring devices | M |

Note: I: Injection, S: Strengthening, R: Reinforcement, M: Monitoring and N: No action.

The Kariba and Kleinplaas dams, two well-known cases of affected dam on the African continent are shown in Figures 1-1 and 1-2. It is observed that these dams are seriously affected by ASR. The Kleinplaas concrete gravity dam is simulated and analysed using the developed chemo-thermo-mechanical model in this research to predict the structural behaviour of the dam due to service loads and ASR phenomenon.

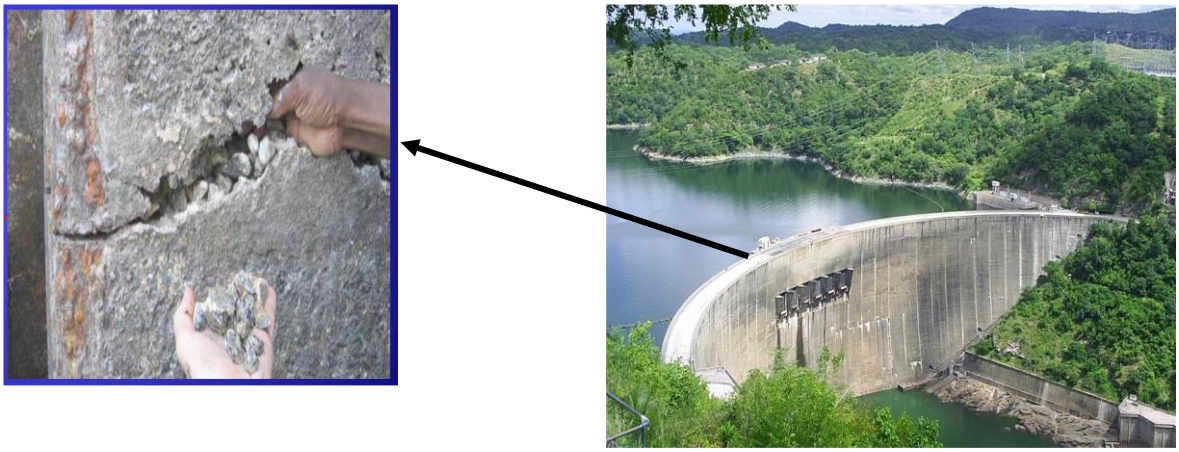

(a) (b)

**Figure 1-1**. Kariba double arch dam in the border of Zambia and Zimbabwe affected by ASR, a) damage and concrete spalling in upstream wall of the dam, b) perspective view of the dam (Mhalanga, 2014).

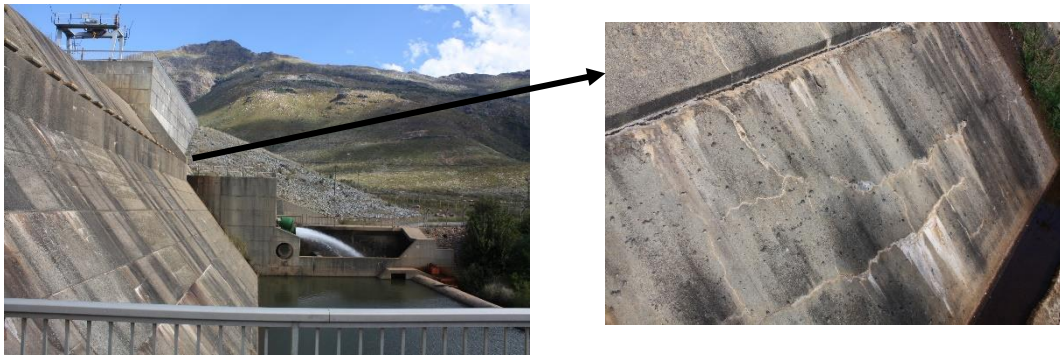

(a) (b)

**Figure 1-2**. Kleinplaas dam, a concrete gravity dam in the Jonkershoek River in Stellenbosch, a) a view from downstream of the dam, b) damage and cracking in the downstream wall.

## 1.4 Research Scope

In this research, four important aspects of the chemo-thermo-mechanical numerical modelling of ASR induced expansion in concrete are addressed:

1. Favourable environmental conditions such as temperature and relative humidity and their influences on the ASR kinetics.
2. Effects of confining stress on ASR evolution.
3. Deterioration of concrete material due to ASR swelling.
4. Nonlinear behaviour and fracture mechanics of concrete material due to ASR induced expansion and related material degradation.

Since chemically induced volumetric expansion is likely to cause substantial nonlinear deformation, a nonlinear material model for the concrete is required, hence this study is composed of two parts focusing on different scales. The first part which is the subject of Chapters 3 and 4 deals with material modelling, and the second part focuses on structural modelling which is presented in Chapters 6,7 and 8. For the material modelling the study is divided to two sections:

1. Parameter identification and calibration of the model for the constitutive law with provided laboratory test results and

2. Prediction of the material response.

Mathematical principles and numerical solution through finite element analysis are applied to develop and validate a numerical model to analyse and predict the behaviour of ASR affected concrete structures taking primarily thermal environmental conditions into account. Then the behaviour of constructed dams affected by ASR is analysed and the results interpreted in detail. Finally, an attempt is made to predict the long term material and structural behaviour of structures subject to ASR and to provide proposals for management programmes and for remedial action. A review of the repair and rehabilitation strategies of the dam affected by ASR accompanied by application of the proposed model in this research to analyse a slot cutting remedial technique for a synthetic dam subjected to ASR swelling is illustrated.

## 1.5 Research questions

Although ASR and its effects on concrete structures have been studied for a number of years, there are still quite a number of aspects of this phenomenon which needs to be assessed and studied. This research is a part of broader research in this field in department of Civil Engineering at Stellenbosch University aimed at the understanding of the key phenomena involved in ASR and prediction of the behaviour of structures suffering from ASR. Alaud and van Zijl (2017) studied the role of reactive aggregates, which are available in Western Cape area, on ASR development of the cylindrical and cubic concrete samples by conducting an extensive laboratory experiments. Also, they performed combined analysis on mechanical loads and ASR affected specimens which resulted in a new insight into the understanding of the problem. Considering the research which has been done experimentally, a lack of numerical modelling techniques that could analyse and predict the behaviour of structures affected by ASR is evident. Hence, in this research the main questions are:

1. What are the important parameters and phenomena that govern the ASR expansion constitutive model in concrete material?
2. How do these parameters need to be incorporated into a numerical model to capture the nonlinear behaviour of concrete?
3. How do concrete structures suffering from ASR behave?
4. What impact does ASR degradation have on the seismic behaviour of a dam?
5. Could the proposed model predict the effects of remedial measures such as slot cutting in a dam?

## 1.6 Thesis contribution

In this research a chemo-thermo-mechanical model is developed to predict the kinetics of the reaction, structural expansion, damage in material and stiffness degradation and cracks in concrete dams affected by ASR. Parameters such as temperature, relative humidity, non-uniform material degradation, effect of micro cracking in ASR development and effects of 3D confinement stresses are included in the model. In summary, the main contributions from this thesis are:

1. A novel formulation for prediction the ASR strain, expansion and damage in concrete structures considering the 3D state of stress in the context of continuum damage mechanics,

2. Analyses of actual concrete dams suffering from ASR,
3. Study of the combined action of seismic loads and ASR,
4. And analyses of a synthetic dam suffering from ASR subjected to the remedial slot cutting technique.

The model developed in this research can predict the long term effects of the ASR on concrete dams i.e. ASR strain rate, displacement and damage development. The model is implemented in nonlinear finite element code software, and is used to analyse actual concrete dams suffering from ASR. By interpreting the results of and information gained from the analysis, the management and evaluation of the remedial measures regarding the repair and maintenance programmes for dam suffering from ASR can be supported.

## 1.7 Thesis outline

This thesis is composed of 9 chapters. After the introduction and main problem statement in Chapter 1, the features of concrete under ASR are thoroughly discussed in Chapter 2. Important parameters involved in ASR process such as kinetics of the reaction, temperature effects, confining stress and material degradation are assessed. In addition, numerical and experimental researches which have been developed considering the scale of the study (micro-meso-macro) are address. This chapter serves as a foundation for developing the ASR constitutive law in the next chapter by determination of key phenomena identified in this chapter.

Chapter 3 is devoted to development of ASR chemo-thermo-mechanical model. The mathematical formulation for the ASR induced strain rate including key variables and functions are developed. The role of material damage due to ASR induced expansion in concrete structures is illustrated. A weighting function in terms of the 3D state of stress that can reproduce the anisotropy of the ASR expansion in principal directions is introduced.

Chapter 4 explores the nonlinear behaviour of concrete and presents concrete damage plasticity model to capture the inelastic behaviour of concrete under ASR. Typical mechanical properties of concrete under uniaxial, biaxial and multiaxial states of stress in tension and compression are presented.

Then in Chapter 5, the validation of the proposed model on material scale through different laboratory examples is illustrated.

The application of the proposed model to the real dams affected by ASR is presented in Chapter 6. Two dam case studies are analysed and results to validate the model on structural scale are presented.

As structures dams are vulnerable to seismic loading, hence, in Chapter 7 the analysis of combined ASR and seismic loads is done. Different strategies are used to model the hydrodynamic effects of reservoir and fluid-structure interaction due to seismic excitation. The results and information of the analysis are compared with the ASR affected dam coupled with seismic excitation.

One of the main goals of developing a finite element model to analyse a dam affected by ASR is to predict the long term behaviour and to support the possible interventions and remedial actions which can be considered. In Chapter 8 strategies for rehabilitation and repair of dams suffering from ASR are presented and reviewed. The model developed is then used to predict the behaviour of a dam suffering from ASR where remedial slot cutting incorporated. The effect of the slot cutting on stress field in the dam wall before and after sawing in the structure is studied.

Finally, in Chapter 9 the concluding remarks and recommended future research is discussed. Figure 1-3 shows a brief review of research methodology and required steps from initiation of the research to the final stage.

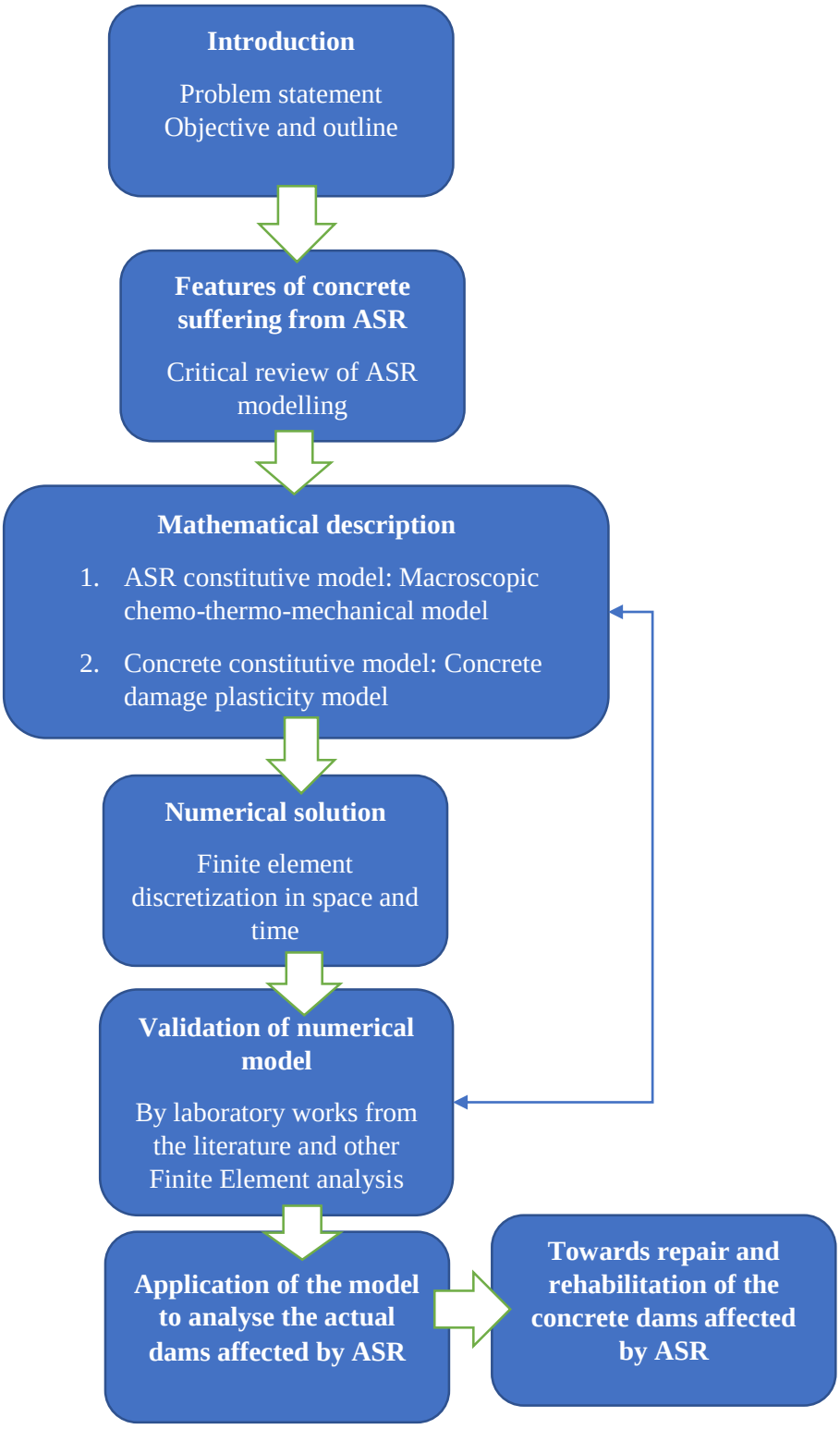


**Figure 1-3**. Flowchart of the proposed research methodology.

# CHAPTER 2

# Effects of ASR on Concrete (Literature review)

**Highlights:**

Key phenomena involved in ASR evolution

Material deterioration due to ASR

Experimental research review

Numerical modelling research review

## 2.1 Features of concrete under ASR

ASR is a deleterious chemical reaction between certain siliceous aggregates and with the alkalis which are available in the cement that typically leads to the formation a gel product. This reaction causes an increase in the molar volume of the gel product and depending on the micro porous structure of the concrete material, introduces a build-up of pressure in the material. At first this pressure, is relieved by the gel filling the voids, micro cracks and pores of the concrete matrix and once there is no more space to relieve the pressure, expansion due to induced cracking occurs.

Several factors can influence the ASR induced expansion of a structure. These include the amount of alkali in the cement, the type and size of the aggregate, confining 3D stresses and the environmental temperature and relative humidity. In Figure 2-1, the cracking and swelling of the concrete material with the effects from confining stresses are shown. The horizontal tensile stresses in the surface of the concrete develop mainly due to the action of the parallel in-plane confining compressive stresses (Saouma, 2014).

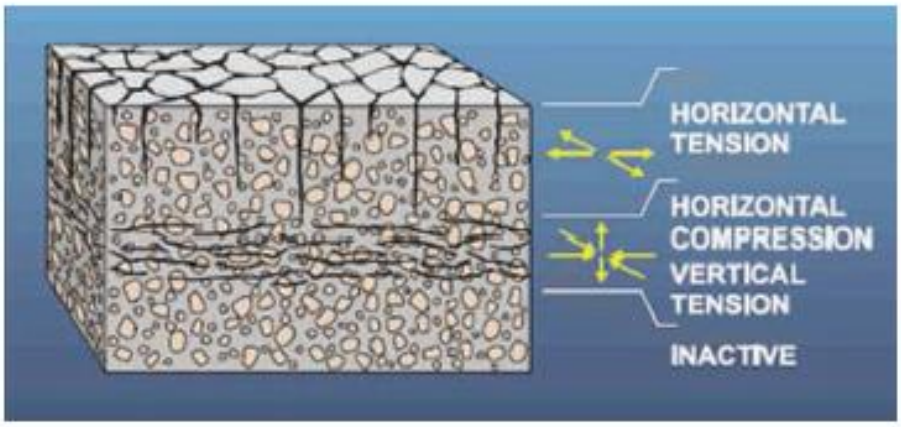


**Figure 2-1**. Internal damage and surface map pattern cracking in the concrete material due to the ASR expansion (Saouma, 2014).

## 2.2 Alkali-silica gel formation

The chemistry of ASR is multi-staged and complex. In Portland cement Alkalis are available in the form of the Alkali-silicate or Alkali-aluminate. (Saouma *et al.*, 2015). When the process of precipitation of ettringite is completed, the counter ions of the alkalis become hydroxides. Evidence exists that an increase in the pH of the pore solution is caused by both alkali ions ($Na^+$ $K^+$) and hydroxide ions ($OH^-$) concentrating at a sufficiently high level. Due to this process the ions are ready to penetrate the silica which exists in the aggregate to form alkali-silica gel. See Figure 2-2. At the interface between Alkali solution a topochemical reaction takes place and the aggregate hydroxyl ions are available to attack and penetrate the silanol groups, $Si-OH$, and the siloxane bonds, $Si-O-Si$. These processes can be described stoichiometrically as follows (Glasser & Kataoka, 1981):

$$\underbrace{-\overset{|}{\underset{|}{Si}}-O-\overset{|}{\underset{|}{Si}}-}_{Siloxane}+\underbrace{R^+ + OH^-}_{Hydroxyl\ ions}\rightarrow\underbrace{-\overset{|}{\underset{|}{Si}}-O-R}_{Alkali-silica\ (gel)}+\underbrace{H-O-\overset{|}{\underset{|}{Si}}-}_{Silicic\ acid} \qquad (2\text{-}1)$$

$$\underbrace{H-O-\overset{|}{\underset{|}{Si}}-}_{Silicic\ acid}+\underbrace{R^+ + OH^-}_{Hyroxyl\ ions}\rightarrow\underbrace{-\overset{|}{\underset{|}{Si}}-O-R}_{Alkali-silica\,(gel)}+\underbrace{H_2O}_{Water} \qquad (2\text{-}2)$$

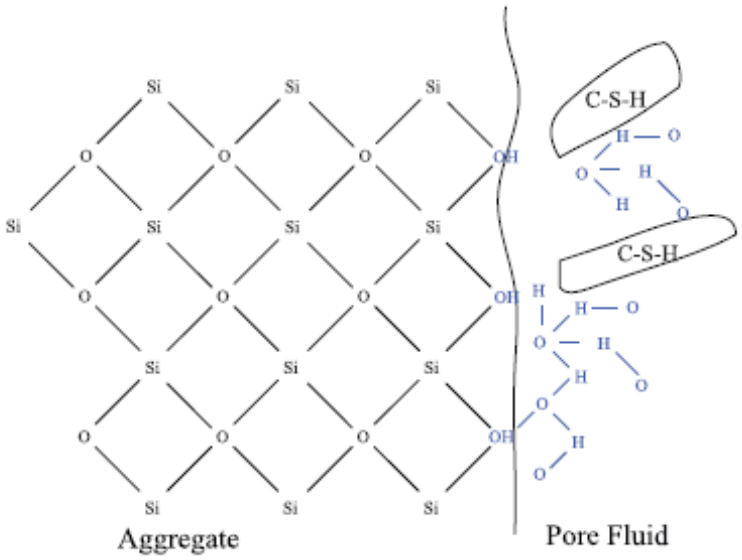


**Figure 2-2**. Aggregate-cement paste interface. Aggregate is attacked by Alkali hydroxyls ions (reproduced from (Glasser & Kataoka, 1981)).

$$\underbrace{-\overset{|}{\underset{|}{Si}}-O-R}_{Alkali-silica\ (gel)} + \underbrace{nH_2O}_{Water} \rightarrow \underbrace{-\overset{|}{\underset{|}{Si}}-O + H_2O + R^+}_{Expansive\ alkali-silica\ (gel)} \qquad (2\text{-}3)$$

The reaction product (ASR gel) which depends on the location and the hygral properties of concrete i.e. amount of water available, could generate an increasing internal pressure in the cementitious matrix on the concrete material. It is widely accepted that this pressure build-up is the main mechanism of the expansion of concrete under ASR and the consequential material degradation (Ulm *et al.*, 2000). ASR in concrete often leads to damage and deterioration of structures, mainly depend on several coexisting conducive factors. Three vital factors are: (i) the presence of potentially reactive silica in the required critical proportion. (ii) sufficiently high alkali hydroxide concentration to trigger and sustain the ASR reaction (iii) available water to initiate the reaction and then drive the swelling of the gel (Newman & Choo, 2003).

## 2.3 Factors influencing Alkali-silica gel formation

Factors that can influence the likelihood, rate and severity of the ASR expansion and/or resulting deterioration and damage include:

1. Alkali availability,
2. Aggregate constitutive properties,

3. Environmental conditions
   3.1. moisture (Relative Humidity)
   3.2. temperature
4. Confining stresses and mechanical loads.

The role of these factors in ASR affected concrete material and the expansion thereof can be set out as follows.

### 2.3.1 The role of Alkali content in ASR

An increase in the alkali concentration in the pore solution and especially the ratio of reactive silica to alkali play a significant role in swelling of concrete material due to ASR. Results of experiments indicate an increase in pH due to increase in the alkali concentration in the pore solution of concrete material (Dyer, 2014). Figure 2-3 illustrates the effect of reactive silica to alkali ratio on ASR expansion. In this figure a 'pessimum' amount of this ratio is evident in which the expansion is a maximum. One needs to take note of the difference between the silica/alkali ratio and alkali content variable in Figures 2-3 and 2-4.

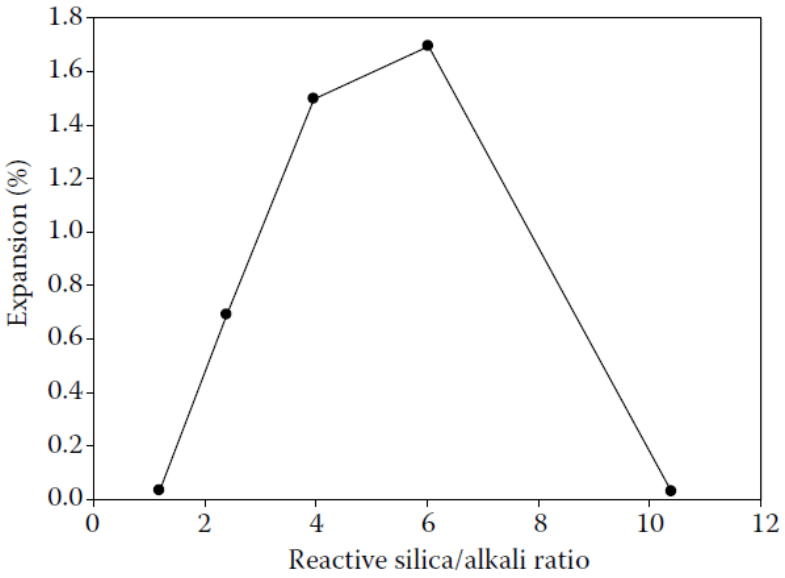


**Figure 2-3**. Relation between expansion of concrete and alkali/silica ratio for 112 days, adopted from (Dyer, 2014).

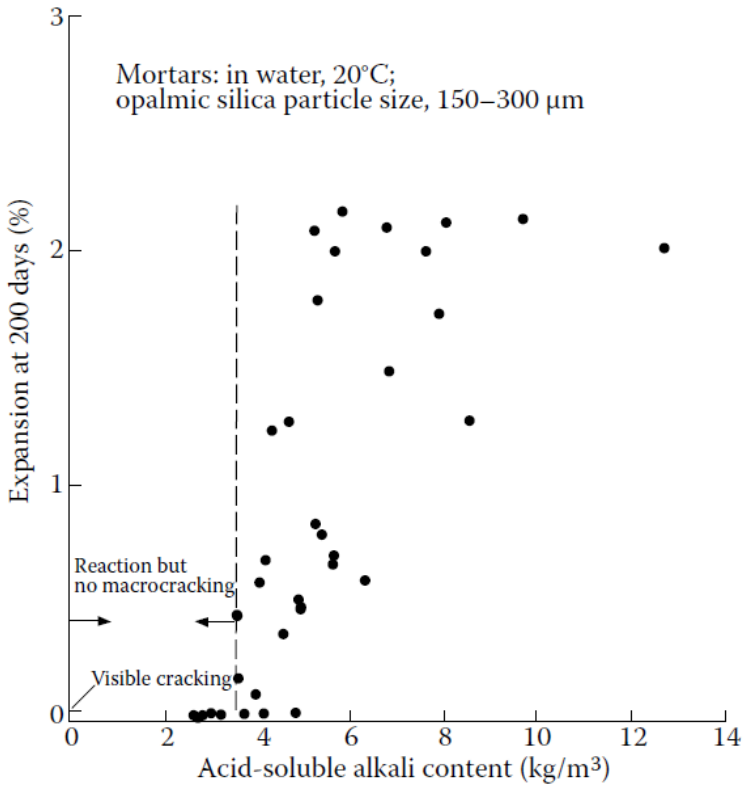


**Figure 2-4**. Relation between swelling of mortars containing opaline silica aggregate and alkali content at 20 ℃ (Dyer, 2014).

### 2.3.2 The role of aggregates in ASR

Two main categories of aggregates are found, namely early reactive and late reactive, manufactured from rocks which contain specific types of minerals. Aggregates belonging to the first category are composed of amorphous components. Volcanic glass and opal are two typical examples of this category that react quickly with harmful effects, typically about a year after the structure was built.

The second group of aggregates are manufactured from crystalline rocks. A number of tectonic activities during the evolution of the earth crust cause to significant deformation and thermal variations in these rocks. Quartz is one of these constituent minerals that can be found in rocks in the strained and/or deformed state (Ponce & Batic, 2006).

Alaud and van Zijl (2017) studied the ASR effects on two types of aggregates which are widely used in South African construction namely Granite and Greywacke. They pointed out that concrete samples made using the Greywacke aggregates show late expansive behaviour, but

the ultimate expansion was significantly more than the samples which were made by using Granite aggregates. Also, the reduction in elasticity modulus (E-Modulus) for the samples with Greywacke aggregates was more than that the Granite aggregates. Figure 2-5 and Figure 2-6 show the results of Alaud's experiments for the expansion and E-Modulus for the two different samples.

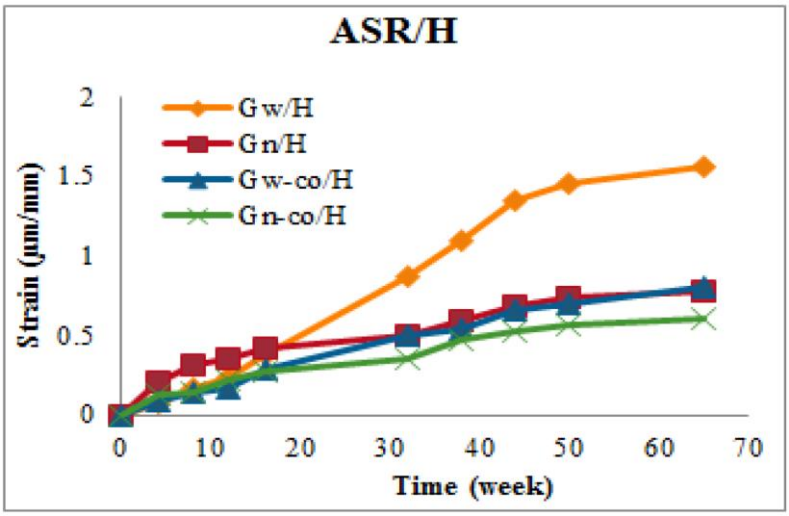


**Figure 2-5**. Comparison of ASR strains of samples made by different aggregates. In this figure Gw/H refers to Greywacke samples cured in high humidity condition and Gn/H shows the samples made by Granite in high humidity condition. The Gw/H mixes show more strain but later than the Gn/H. (Gw-co/H: Greywacke samples including Corex slag in high humidity, Gn-co/H: Granite samples including Corex slag in high humidity).

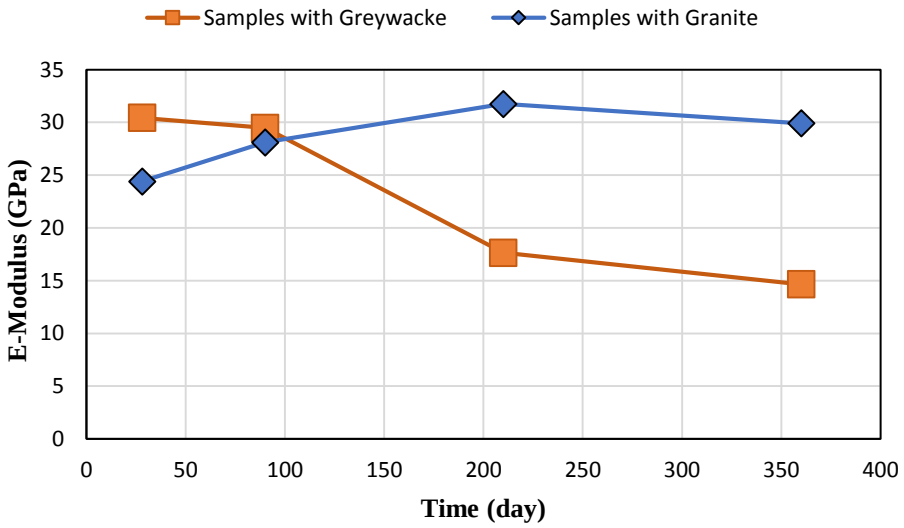


**Figure 2-6**. Comparison of reduction in E-Modulus in concrete samples made with two types of reactive aggregate.

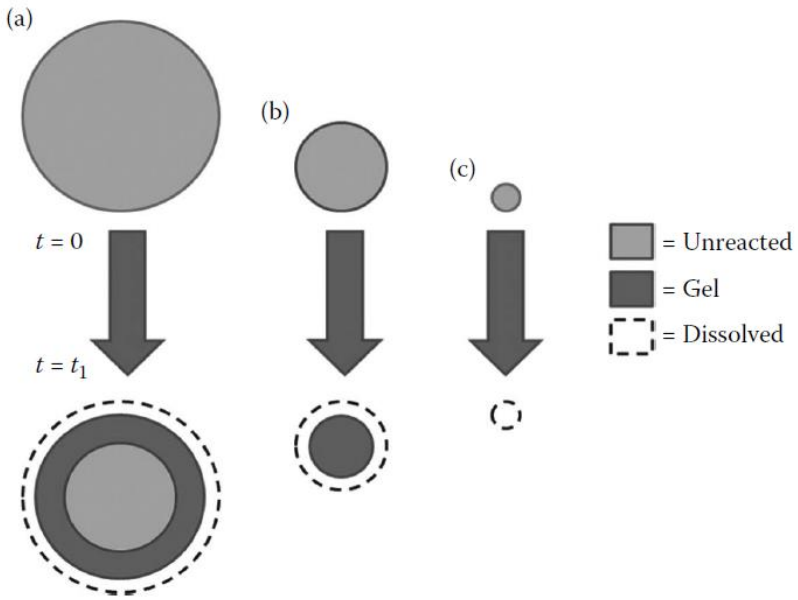


**Figure 2-7**. Effect of aggregate size on ASR gel formation and gel dissolution over a period $t_1$, a) large volume of gel is produced for relatively large particles, b) smaller particle is converted entirely to gel, which then gradually dissolves, (c) very small particle is totally dissolved in a relatively short time (reproduced from (Dyer, 2014)).

Similar to the effect of the pessimum silica/alkali ratio which discussed in section 2.3.1, a pessimum size for aggregate is also recognized. Figure 2-7 illustrates the role of aggregate size on ASR evolution.

Generally, the accessibility of the alkaline pore solution to reactive silica can be considered as a criterion of aggregate reactivity. If the aggregate is composed of reactive silica (such as volcanic and synthetic glasses) the aggregate surface may react in early stages with the alkaline pore solution to form ASR gel on the surface of the aggregate. However, if the reactive silica is not available at the surface and is contained some fine reactive components distributed within a non-reactive matrix of the particle (such as siliceous limestones and Greywackes aggregates), it takes time for the pore solution to diffuse into the aggregate and reach the reactive silica components. Therefore, the reaction proceeds more slowly and the gel forms within the aggregate. Also, pre-existence of micro cracks has an effective role in the alkali silica reaction as shown in Figure 2-8. Finally, according to the mineralogy of aggregates, expansive gel may occur at the interior of the aggregate, or within the reaction rim, or at the cement paste-aggregate interface. As a result, ASR can be divided into two distinct categories: early-expansive ASR (E-ASR) and late- expansive ASR (L-ASR).

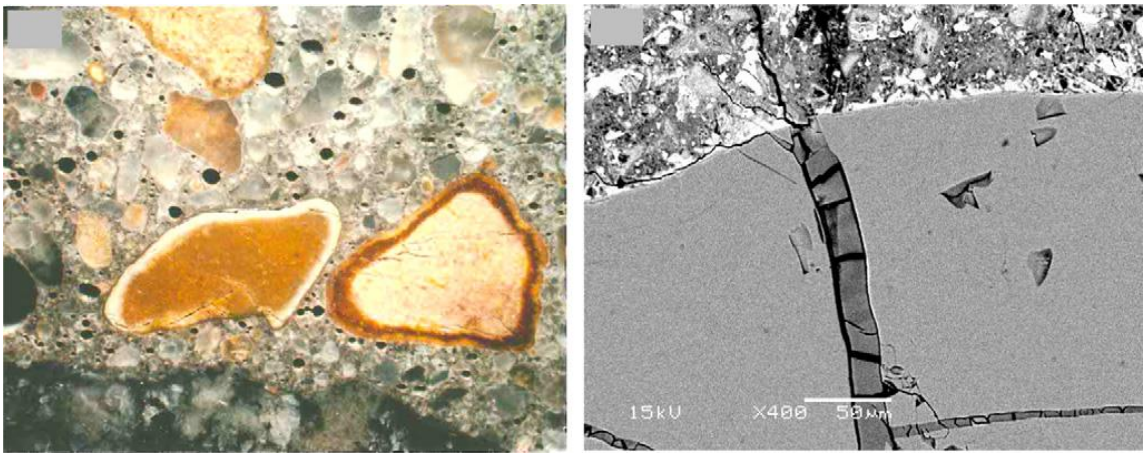


(a) (b)

**Figure 2-8**. Scanning electron microscopy (SEM) analysis of the samples affected by ASR, a) effect of ASR on granite aggregate surface. The reaction rim is evident on the surface of this particle (right aggregate in left picture) and chert particle (left aggregate), b) ASR occurs inside the particle through available micro cracks, (reproduced from (Rajabipour *et al.*, 2015)).

### 2.3.3 The role of relative humidity in ASR

Figure 2-9 presents the role of relative humidity on ASR swelling. The ASR gel is highly hydrophilic and when water as solvent agent enters the medium this results in gel expansion. Thus, the extent to which expansion occurs is dependent on the amount of water available within the concrete. in addition, the humidity of the air surrounding the concrete could affect the expansion. Experiment on the role of relative humidity in ASR expansion shows that a relative humidity below approximately 75% ASR cannot produce significant expansion.

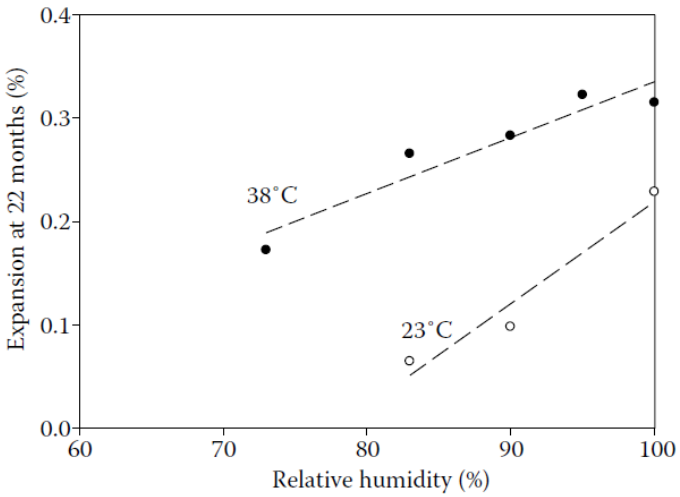


**Figure 2-9**. Relation between RH and ASR-induced expansion of mortar bar at the two temperatures, adopted from (Dyer, 2014).

### 2.3.4 The role of temperature in ASR

Figure 2-10 illustrates the role of temperature in ASR expansion. When the temperature is below a threshold level of approximately 40 °C the swelling increases with the increase of temperature while for a temperature value higher than this level expansion declines. The ASR is a thermo-activated process and thermal conditions of the concrete structure should be considered in a numerical model of the process (Ulm *et al.*, 2000).

The lower viscosity of the ASR gel at higher temperatures could be the reason for decreasing the expansion at the elevated thermal conditions (Newman & Choo, 2003).

### 2.3.5 Effects of stress confinement on ASR development

ASR can be described as two simultaneous but uncoupled processes: The production of expansive silica gel, and its mechanical consequences. In addition, mechanical stress could affect both processes (Morenon *et al.*, 2017; Multon & Toutlemonde, 2006). Indeed, some chemical reactions and dissolution processes are known to be hindered or promoted by external pressure. However, the results from Larive (1998) indicate that such phenomena do not occur in ASR, at least in the range of stresses encountered in the field. To the contrary, in a recent experimental research by Liaudat *et al.* (2018) it has been shown that a 3D state of permanent compressive stress of about 9.7 MPa can hinder the development of ASR volumetric strains. See Figure 2-11.

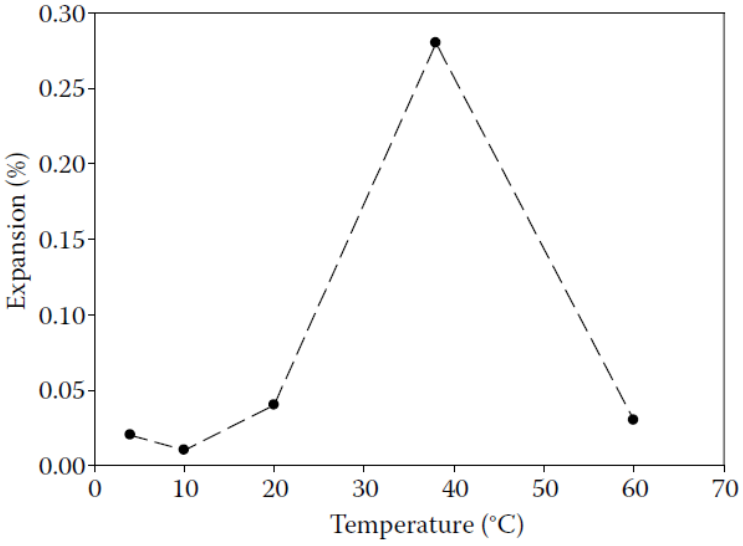


**Figure 2-10**. The relation between temperature changes and expansion of mortar bar test specimens for a period of 6 months (adopted from (Dyer, 2014)).

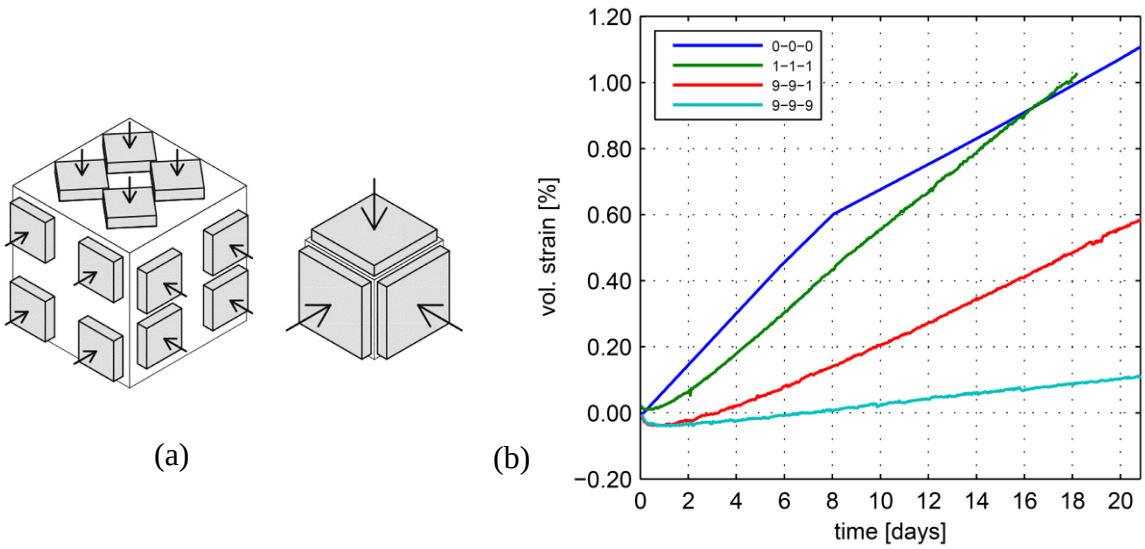


**Figure 2-11**. Triaxial confinement test on cubic samples, a) a view of the cubic samples, b) comparison of average ASR volumetric strain at different triaxial confinement stress, adopted from (Liaudat *et al.*, 2018).

Mechanical loads also affect the fracture processes in the material, and therefore the expansion as it is, in ASR, may be strongly coupled with internal damage (Giorla *et al.*, 2015).

In summary, Figure 2-12 illustrates the key factors that affect ASR kinetics and evolution of the expansion of concrete material under ASR.

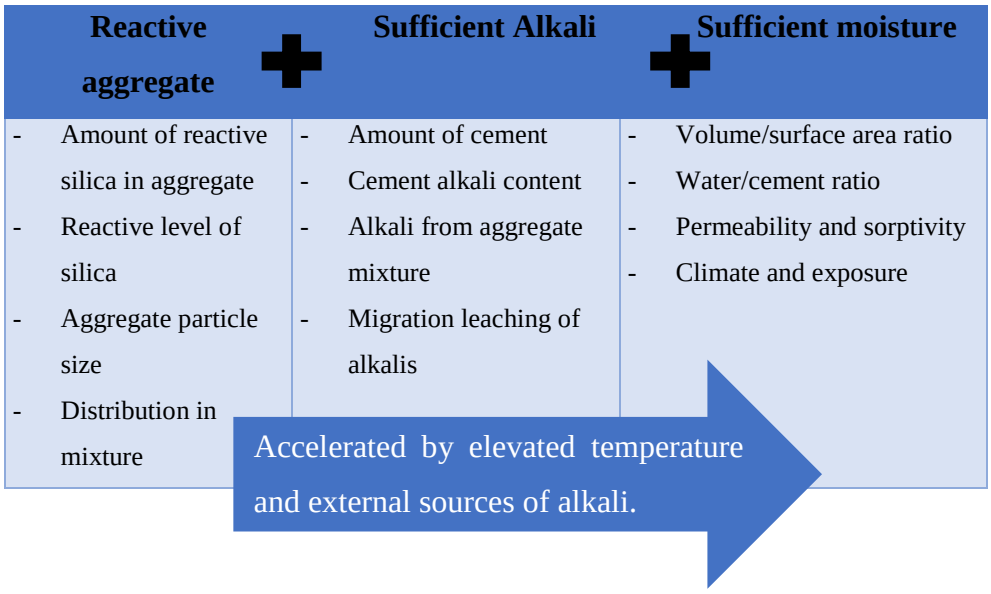


**Figure 2-12**. Factors that affect ASR kinetics and progress.

## 2.4 Expansive and cracking mechanism of concrete due to ASR

It is now widely accepted that the water absorption by the gel and resulting swelling, are the main reasons for concrete expansion and deterioration of ASR affected structures (Ulm *et al.*, 2000; Larive,1998). The expansion of the ASR hydrophilic gel produces a pressure build-up, and when the tensile strength of the concrete is reached results in the development of cracks. Because the mechanism of swelling and cracking of concrete due to ASR is still not clearly understood, extensive research has been done to investigate this mechanism recently. Alternative theories for the swelling of the gel and the cracking mechanism which have been developed are:

1. Theory of osmotic pressure (Glasser, 1979; Sims & Poole, 2017)
2. Interfacial Transition Zone (ITZ) theory (Bazant & Steffens, 2000)
3. Diffusion of dissolved silica into the interconnected pores from reacted aggregates (Camacho & Ortiz, 1996)
4. Theory of dependency of ASR on the mineralogical nature of aggregate (Ben Haha *et al.*, 2007; Dunant & Scrivener, 2010; Garcia-Diaz *et al.*, 2006; Ichikawa & Miura, 2007; and Ponce & Batic, 2006).

As discussed in section 2.3.2, some aggregates such as opaline, shale, andesite, glassy rhyolite which are early-expansive the reaction rim is evident, but in some late-reactive aggregate such as schist, gneiss, quartzite, limestone the rim is less noticeable (Saouma *et al.*, 2015). From an evolutionary point of view, the following stages for the reaction can be identified: 1) micro nucleation, 2) progress of the reaction, 3) increase in the rate of the reaction and degradation process, and finally 4) significant degradation of material. See Figure 2-13 a. A petrographic interpretation of the aggregate affected by ASR is shown in Figure 2-13 b. The SEM analysis shows that the following stages could possibly explain the ASR progress: 1) formation and development of reaction rim in the surface of the aggregate; 2) rimming of the ASR gel on the reacted aggregate; 3) cracking of aggregate filled with gel; 4) cement paste cracking due to the gel propagation from the aggregate and finally 5) precipitation of the ASR gel into air voids some distance from the aggregate. From this figure it can be concluded that each stage of the ASR progress can be related to one of the stages identified above. For instance, initiation of micro nucleation can be related to the formation of reaction rim in ITZ and deterioration

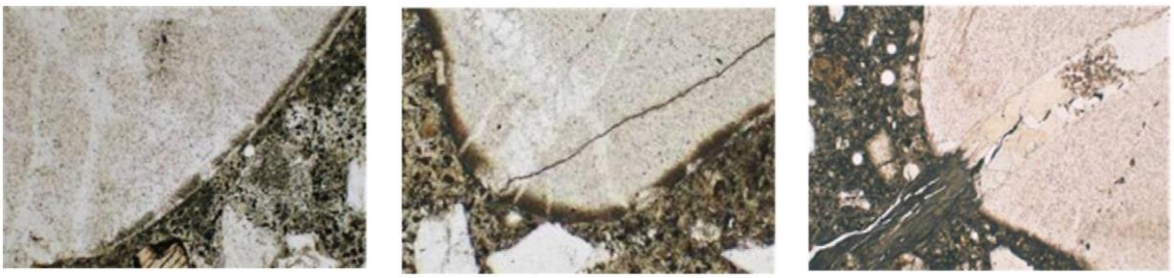

Formation of reaction rim | Crack in aggregate | Propagation of crack into cement paste

(a)

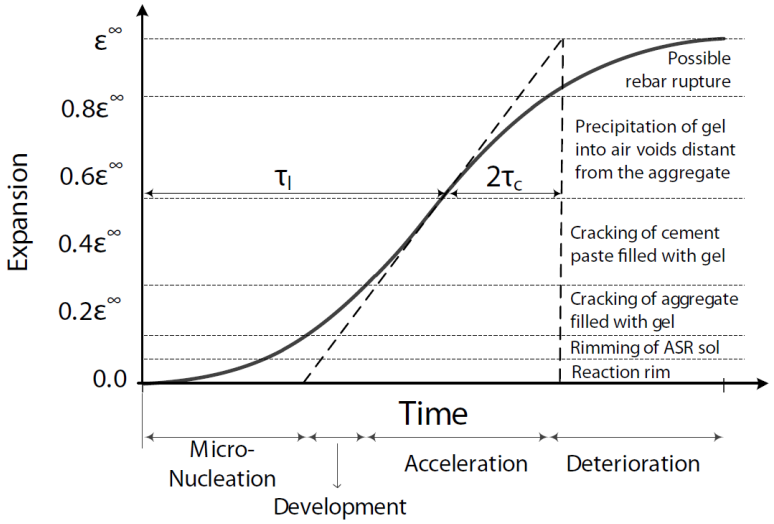


(b)

**Figure 2-13**. Interpretation of the reaction using petrographic tests. The symbols $\tau_l$ and $\tau_c$ are the latency and characteristic times respectively (reproduced from (Saouma *et al.*, 2015)).

mechanisms of concrete material affected by ASR could be related to the precipitation of ASR gel into voids and pores adjacent to the reacted aggregate.

## 2.5 Damage and deterioration of concrete material due to ASR

The majority of research conducted to date has not studied the long term effects of material degradation due to ASR that may change the engineering properties of the concrete material during the service life of typical structures e.g. dams. More recently, Sposito and Hendriks (2016) has performed extensive research which included experimental and numerical modelling work on the deteriorating impact of ASR on concrete material. They used micro-poro-fracture mechanics theory to develop a pressure based multi scale material model to evaluate the effect of ASR on the degradation properties such as the compressive and the tensile strength and elastic modulus. They concluded that the elastic modulus could be a better indication to measure the deteriorating impact of ASR on concrete. This assumption is used in

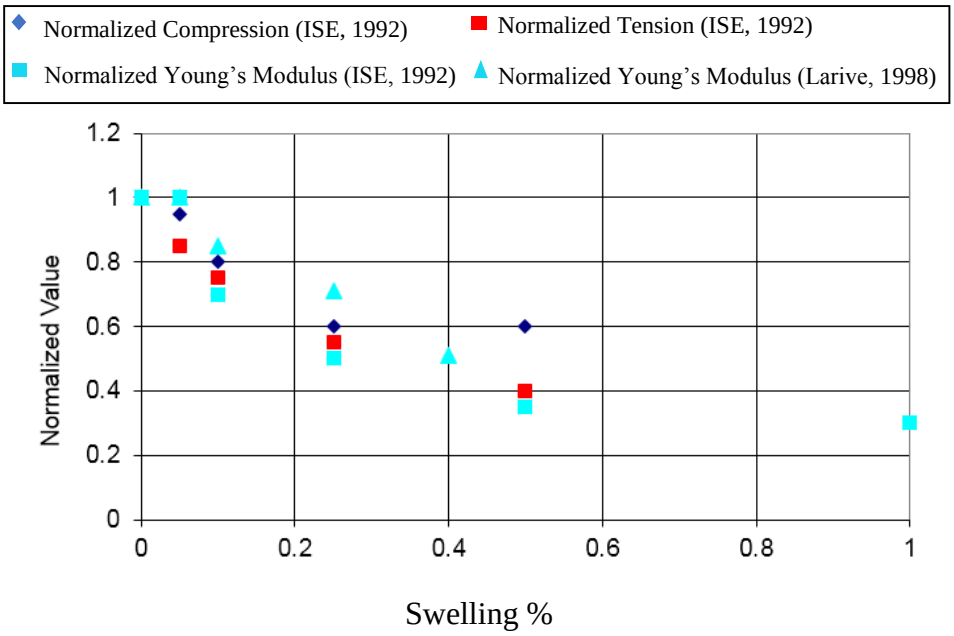


**Figure 2-14**. Evolution of mechanical characteristic vs. ASR expansion of concrete, (reproduced from (ISE, 1992)).

the next chapter to model the deterioration of concrete material in time and space with ASR expansion evolution. Figure 2-14 shows the degradation of concrete properties with evolution of ASR expansion.

Furthermore, material degradation may significantly change the seismic behaviour of the concrete structures such as dams, and it is also necessary to predict the seismic safety of e.g. dams suffering from ASR considering the time dependent material deterioration. Research has been performed on aged concrete dams assuming a uniform material time dependent degradation index along the dam body, due to physical and chemical attacks such as freeze-thaw cycles and fatigue and expansive chemical reactions (Nayak & Maity, 2013; Valliappan & Chee, 2009). However, using a uniform material deterioration index for the dam structures as a whole may lead to an overestimation of the structural dynamic response and the dynamic behaviour of the damaged structure.

## 2.6 Strategies for the modelling of ASR: From material to structural level

ASR evolves during the time and results in expansion which often leads to permanent deformations and cracking in concrete structures in locations that are more than concrete tensile strength. Because this harmful process, which includes internal swelling due to ASR, could

compromise the durability and integrity of the structures, numerical modelling and continuous monitoring are required to analyse the behaviour of the affected structures and to evaluate the long term safety level and structural performance.

As is shown in section 2.3 several parameters may profoundly control the ASR formation, and evolution. Thus, numerical modelling should be able to capture the impact of these parameters. Among these, humidity, temperature, amount of alkali, aggregate size and confining stresses are the most prominent factors. Due to the complexity of developing a general model, based on the current understanding of the ASR phenomenon, that can accurately capture the behaviour of a typical structure, mathematical, analytical, numerical and semi-empirical models have mainly been developed (Pan *et al.*, 2012).

In general, numerical models for modelling ASR and its effects fall into three main categories: (1) macrostructural models concerned with the analysis of structures affected by the reaction (Capra & Sellier, 2003; Charlwood, 2009; Li & Coussy, 2004; Saouma & Perotti, 2006; Steffens *et al.*, 2003; Ulm *et al.*, 2000); (2) microstructural models which link the chemical reaction to its impact at the material level (Bazant & Steffens, 2000; Lemarchand *et al.*, 2002) and (3) mesoscopic models used for analysis of the ASR mechanism (Comby-Peyrot *et al.*, 2009; Dunant & Scrivener, 2010). Anisotropy can be explicitly represented in these mesoscopic concrete models which consider the multi-phase behaviour of aggregate, cement paste, voids and ASR gel products. In the following section, several ASR models which have been developed by the researchers and scientist in recent years and in different scale are reviewed and discussed.

### 2.6.1 Microscopic models

On the microscopic modelling scale, a representative volume element (RVE) comprising a single aggregate particle within the surrounding cement paste is generally considered. The mass transport equation is used to model the gel, which the formation of in the first instance leads to the saturation of the capillary pores with gel, (Bazant & Steffens, 2000); (Lemarchand *et al.*, 2002); (Suwito *et al.*, 2002); (Multon *et al.*, 2009); (Puatatsananon & Saouma, 2013) and (Dormieux *et al.*, 2006). These theoretical approaches are used to determine the "*pessimum"* size of aggregate which induces the maximum expansion in the concrete material. While it is essential for proper understanding of the underlying phenomenon causing ASR, this level of

modelling is of limited value for the structural analysis of ASR-affected structures. An example of this category, the micro model presented by Puatatsananon and Saouma (2013) is explored here. They assumed that the reaction may occur at the surface of the aggregate and Fick's law is used to model the diffusion of alkali ions into the aggregate. Also Darcy' law is used to model the permeation of the ASR gel to the cement paste. See Figure 2-15.

a)

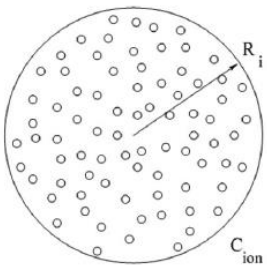


Aggregate before reaction

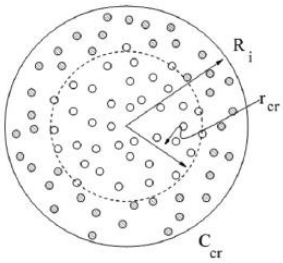


Diffusion of alkali ions to the surface of aggregate within a critical radius

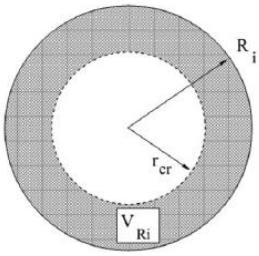


Volume of the reacted aggregate

b)

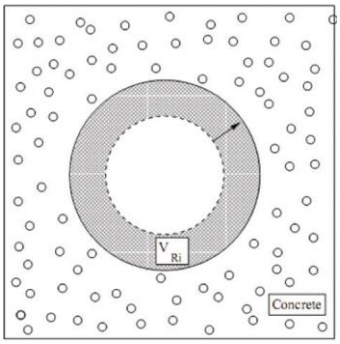


Aggregate saturate by ASR gel

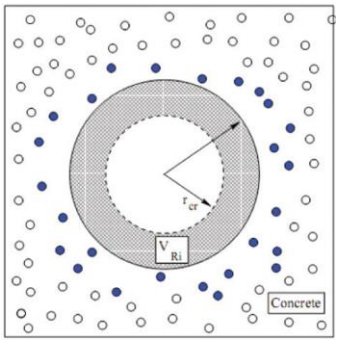


Diffusion of the ASR gel to the concrete pores

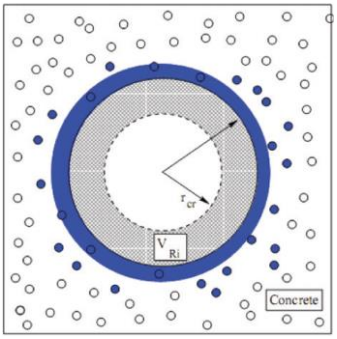


Pressure build up by the ASR gel saturation in concrete

**Figure 2-15**. Process and evolution of ASR in ITZ of concrete, a) shows the initial stage where alkali ions diffuse to the aggregate, b) presents the second stage defining diffusion of ASR gel into the concrete that results in pressure build up and expansion (reproduced from Puatsananon & Saouma (2002)).

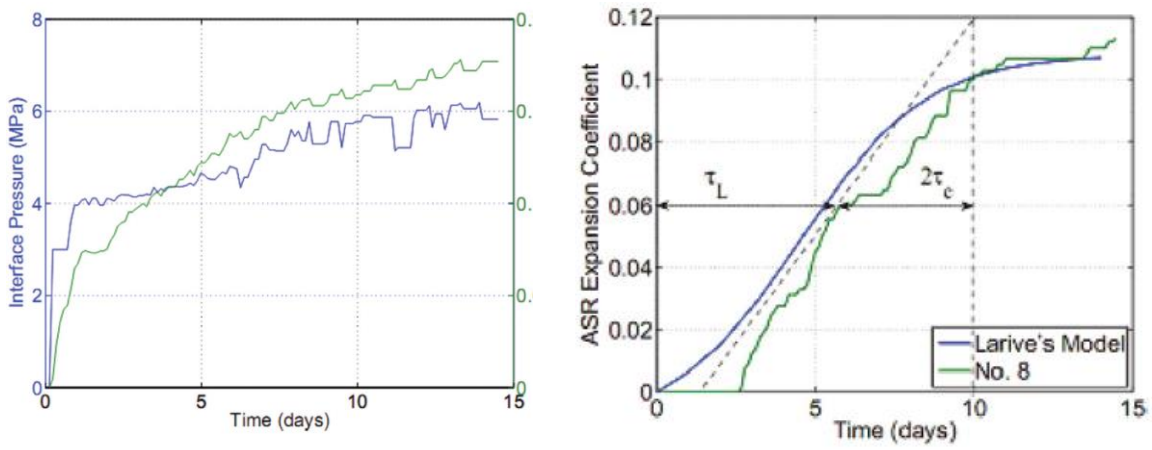


**Figure 2-16**. Gel pressure and swelling versus time (reproduced from (Puatatsananon & Saouma, 2013)).

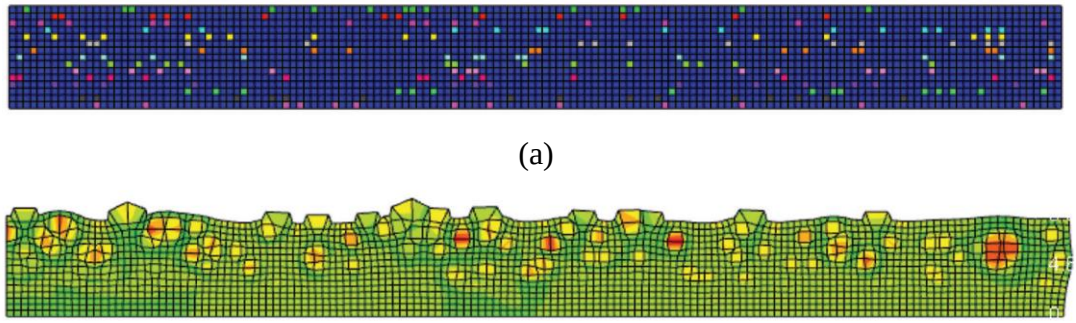

(a)

(b)

**Figure 2-17**. Finite element analysis of mortar bar a) Random locations of expansive aggregate b) inhomogeneous deformation of the mortar bar due to ASR (reproduced from (Puatatsananon & Saouma, 2013)).

In this model the behaviour of a mortar bar is examined to study aggregate reactivity. However, this test cannot show the real expansion of concrete structures in the field, but is intended to study localised effects of aggregate reactivity. See Figure 2-17.

### 2.6.2 Mesoscopic models

This is an extension of the previous approach, in which both particle size distribution and interaction among individual particles are considered. The mesoscopic models basically consider the anisotropy in the concrete material by assuming the multiphase of aggregate, cement paste, pores and voids and ASR gel. In a mesoscopic model developed by Dunant and Scrivener (2010), ASR expansion is modelled by the equivalent swelling of aggregate components or the expansion of the ASR gels distributed in the aggregate. Refer to

Comby-Peyrot *et al*. (2009) as well. To understand the mechanism of the ASR reaction and to construct a constitutive model for gel migration and the pressure exerted on the cement paste on the meso level by the gel, a petrographic investigation using SEM is required. Without such an experiment, the knowledge about the location in which gel concentrates is incomplete. According to Ben Haha *et. al*. (2007) the damage, for three different circular aggregates from the Swiss Alps which were studied experimentally, mainly occurs on the inside of aggregate and not in the cement paste around it.

Figure 2-18 illustrates different microscopic foundations for the prediction of ASR kinetics. In this figure a micro structure model to predict the kinetics of the ASR can be described by using:

1. a homogenised or an explicit technique to define the micro structure of the concrete material,
2. formation of the gel pocket inside the aggregate or on the aggregate surface
3. a separation of the different phenomena involved in the ASR
4. or assuming an integrate diffusion technique. (Rajabipour *et al.*, 2015).

### 2.6.3 Macroscopic ASR models

Several macroscopic models have been recently developed to analyse the global behaviour of ASR at structural level. These models, mainly focus on the strain field, stress field and damage

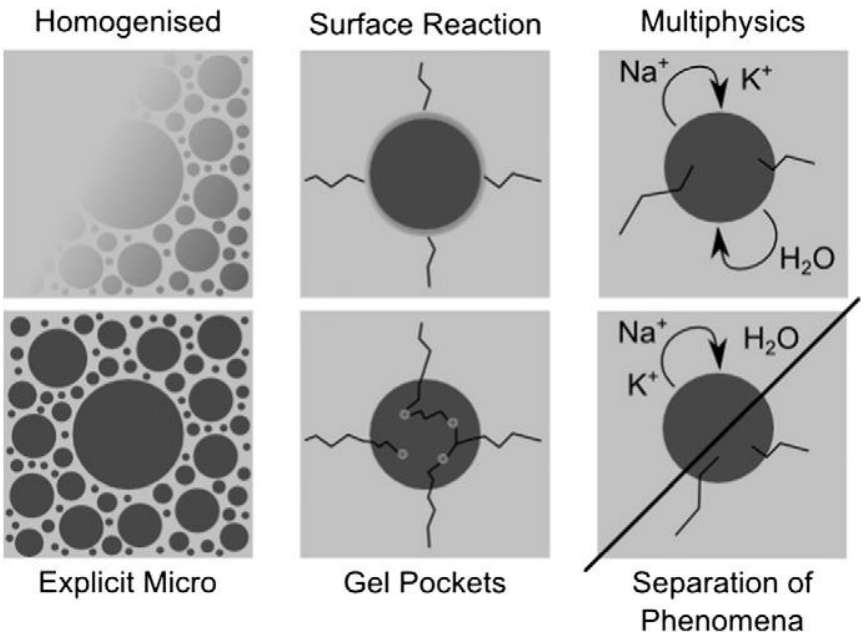


**Figure 2-18**. Different microscopic foundations for ASR models which treat the microstructure explicitly or through homogenization techniques, consider the formation of the gel inside the aggregate or through a surface reaction or include diffusion of the ions to the particle, (reproduced from (Rajabipour *et al.*, 2015)).

mechanism of cracking in the concrete at structural levels. These models simulate the observed behaviour of real structures and investigate the deterioration mechanism in concrete. In these models ASR kinetics is considered according to the laboratory accelerated tests to determine the ASR characteristic parameters. Linear or nonlinear constitutive laws can be used to model the structural behaviour. Where it is necessary to model the creep, shrinkage and crack behaviour in the concrete structure, nonlinear fracture mechanics models can preferably be used.

### *2.6.3.1 Phenomenological models*

One of the earliest models that were developed in the 1990s was a phenomenological model, developed by Charlwood *et al.* (2012) and Thompson *et al.* (1994). In these models, the anisotropic swelling is based on the confining stress state and is determined as a function of the stress tensor. The kinetics of the chemical reaction is not considered. The anisotropic expansion rate in the principal stress directions, is given by:

$$\epsilon_{ASR}(\sigma) = \begin{cases} \epsilon^0_{ASR} & if\ \sigma < \sigma_L \\ \epsilon^0_{ASR} - K \log_{10}(\sigma/\sigma_L) & if\ \sigma_L < \sigma < \sigma_{max} \\ 0 & if\ \sigma > \sigma_{max} \end{cases} \quad (2\text{-}1)$$

where $\epsilon^0_{ASR}$ denotes the free expansion strain due to ASR, a value of 0.3 MPa is used for $\sigma_L$ which represents a limit that ASR expansion starts to decrease, $\sigma_{max}$ is the compressive stress (5 to 10 MPa) above which there is no ASR expansion. *K* is the slope of the line defining the rate of ASR expansion versus log-stress directions. This curve is shown in Figure 2-19.

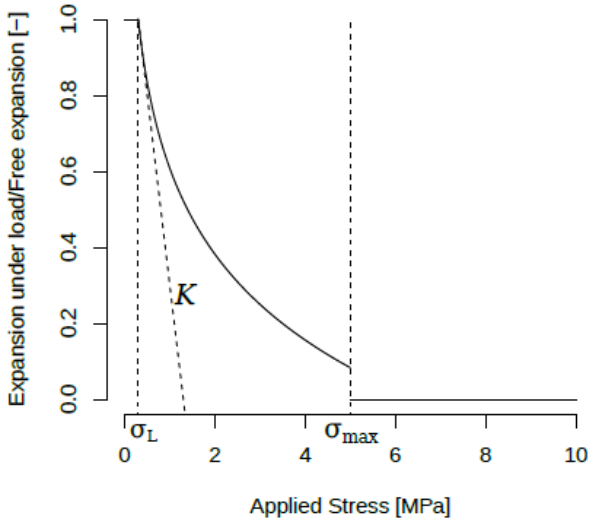


**Figure 2-19**. Effect of uniaxial confining stress on ASR expansion.

Subsequently, more refined models have been proposed by Léger et al. (1996), Bournazel and Moranville (1997), Capra and Bournazel (1998). Among these methods, Léger *et al.* (1996) used a Finite Element (FEM) formulation which included the compressive stress state, temperature, moisture and reactivity of the concrete constituents as parameters. The procedure was then used to analyse the displacement of concrete dams affected by ASR. Herrardo *et al.* (2009) combined creep effects in this model to investigate the core-drilled specimens extracted from the Blesar Dam in Spain which suffered from ASR. This kind of parametric models which often use the thermal expansion equivalent strain as a representation of ASR strain, might be successful engineering models, but do not reflect the physical mechanism of the ASR phenomenon. The main shortcoming of these models is lack of a link between kinetics of the reaction and subsequent expansive strains.

#### *2.6.3.2 Chemo-mechanical models*

A more refined model that can be categorized as a chemo-mechanical model, is one that was proposed by Pietruszczak (1996). In this model the evolution of the ASR in concrete is coupled with the damage in mechanical properties, which is characterized using the elastic-plasticity constitutive law for the concrete material. The effects of humidity and temperature on ASR expansion are neglected. The model was later refined by them to include the effects of these factors (Huang & Pietruszczak, 1999). The swelling rate was calculated by the alkali content in the cement, the magnitude of the confining stress as well as the temperature history in space and time. The deterioration of mechanical properties such as E-modulus and tensile strength due to ASR was also included in the model.

The kinetics of the ASR has been explored by researchers according to the scale of the model adopted. At macro-level for instance when a finite element analysis is performed to obtain full structural behaviour, empirical kinetics models based on 1D bar expansion experiments have been developed. One of the earliest models was proposed by Capra and Bournazel (1998) who expressed the expansion strains as follows:

$$\epsilon(t,\theta) = \frac{1}{A_0}\left(1 - A_0 - e^{K_0 e^{-E_a/R\theta} t}\right)\epsilon^{\infty} \qquad (2\text{-}2)$$

where $\epsilon^{\infty}$ is the asymptotic expansion, and $A_0$ is a constant to be experimentally determined, $E_a$ is the activation energy and $R$ is the gas constant. In 1998, extensive laboratory research in LCPC-France by Larive (1998) lead to the development of the most promising model formulation for the reaction kinetics:

$$\xi(t) = \frac{1-\exp(-t/\tau_c(\theta))}{1+\exp(-t/\tau_c(\theta)+\tau_L(\theta)/\tau_c(\theta))} \quad (2\text{-}3)$$

where $\theta$ is the absolute temperature, and $\tau_l$and $\tau_c$ are as defined in section 2-4. See Figure 2-20. It is worth noting that in these cases, kinetics equations are empirical and applicable to macro-structural modelling by FEM. Based on the Larive experiment 2 years later, Ulm *et al*. (2000) developed a chemo-mechanical model that more precisely considered ASR kinetics and the swelling effects. In this model, the gel is produced in pores and fills micro cracks of the cementitious matrix and exerts a pressure on the surrounding concrete skeleton. This model is shown in Figure 2-21. The parameters of this model under stress free conditions are mainly the internal swelling pressure $P_g$ of the expansive gel, $\sigma_\mu$ the tension stress in the concrete skeleton, $\sigma$ is the stress due to external loads, and $\varepsilon$ is the total strain. The stress state in a 1D chemo-elastic device is given by:

$$\sigma = \sigma_\mu - P_g = E_s\varepsilon + E_g(\varepsilon - \kappa\xi) \quad (2\text{-}4)$$

where $E_s$ and $E_g$ are the spring moduli of the chemo-elastic device and $\xi(t)$ is the extent of the ASR computed by using equation (2-3). The model is also generalized to the 3D using an energy approach according to thermodynamic principals. The free energy in the 1D chemo-elastic device is obtained as:

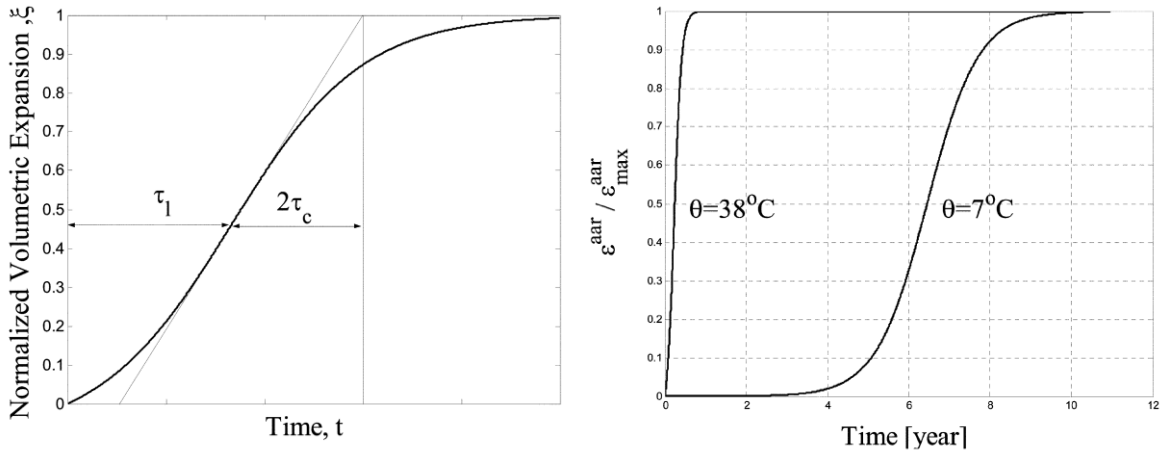


(a) (b)

**Figure 2-20**. Swelling evolution of ASR-affected concrete, a) curve showing normalized volumetric expansion vs. time, b) comparison of normalized volumetric strain at two temperatures.

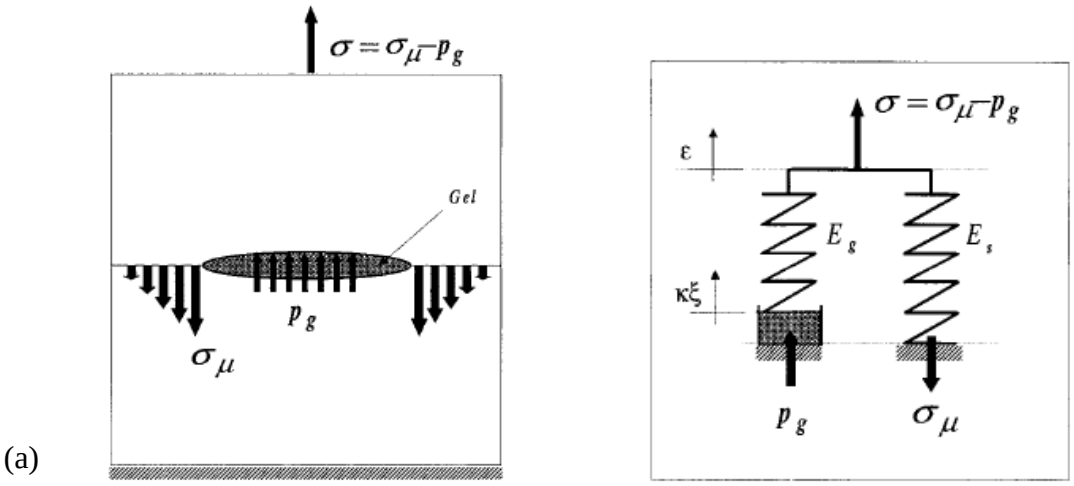


**Figure 2-21**. Chemo elastic device of ASR modelling, a) Mechanism of ASR swelling, b) Chemo-elastic pressure-spring device of ASR expansion, after (Ulm *et al.*, 2000).

$$\Psi = \frac{1}{2}\left[E_s\varepsilon^2 + E_g(\varepsilon - \kappa\xi)^2\right] + g(\xi) \tag{2-5}$$

The function $g(\xi)$ corresponds to the free energy in the chemical pressure cell shown in Figure 2-21 b and represents the driver agent of the reaction. According to the expression of dissipation in thermodynamics $\varphi dt = \sigma d\epsilon - d\psi \geq 0$ yields:

$$\varphi dt = \left[\sigma - \left(E_s\varepsilon + E_g(\varepsilon - \kappa\xi)\right)\right]d\varepsilon + \left[\kappa E_g(\varepsilon - \kappa\xi) - \frac{\partial g}{\partial \xi}\right]d\xi \geq 0 \tag{2-6}$$

The generalisation to the 3D case is obtained by replacing the scalar stress and strain variables with the applicable tensor values for the isotropic case:

$$\sigma_{ij} = \frac{\partial \Psi}{\partial \varepsilon_{ij}} = \left(K - \frac{2}{3}G\right)\epsilon\delta_{ij} + 2G\varepsilon_{ij} - 3\beta K\xi\delta_{ij} \tag{2-7}$$

where $\epsilon = \boldsymbol{\varepsilon}_{ii}$, $K = E/2(1-2\upsilon)$ and $G = E/2(1+\upsilon)$ are the overall bulk modulus and shear modulus, respectively. $E = E_s + E_g$ is the overall Young's modulus; $\upsilon$ is the Poisson's ratio and $\beta = \kappa\, E_g/E$ is the chemical dilatation coefficient.

The reaction extent $\xi$ is the only unknown parameter in this model. The rate of reaction extent is defined by a first order chemical reaction law, a rate equation relating the reaction affinity $A_m = A_m(\xi)$ to the reaction rate $\dot{\xi} = d\xi/dt$. For the stress free condition:

$$A_m(\xi) = K_d \frac{d\xi}{dt} \tag{2-8}$$

where the affinity $A_m(\xi)$ indicates the local reaction imbalance driving the ASR gel formation according to the reaction order used in typical physical chemistry formulation:

$$1 - \xi = t_c(\theta_0, \xi) \frac{d\xi}{dt} \quad \text{or} \quad \epsilon(\infty) - \epsilon(t) = t_c(\theta_0, \xi) \frac{d\xi}{dt} \tag{2-9}$$

where the $t_c$ defines the characteristic time of the reaction, and laboratory stress-free expansion test can be used to determine this parameter. According to Larive (1998), this time $t_c$ depends on reaction extent and temperature. Finally, the ASR strain in free-stress state is expressed as:

$$\epsilon(t) = \xi(t)\epsilon(\infty); \tag{2-10}$$

where $\xi(t)$ is defined in equation (2-3) and $\epsilon(\infty)$ is the volumetric asymptotic strain in free-stress state determined by experimental methods at the reference temperature.

Currently, models assume an Arrhenius law as a first-degree engineering approach to estimate the ASR parameters in the field according to laboratory experiments. However, although this might be suitable for the computing of expansion and strain from ASR, it is likely to provide erroneous results for the evolution of mechanical properties, particularly strength and stiffness (Coussy, 2004).

The chemo-mechanical model proposed by Ulm *et al.* (2000) was improved by many researchers. A more refined version of this model presented by Li and Coussy (2004) in which chemo-elastic model by Ulm was extended by using a chemo-plastic constitutive law including thermal-hydrometric conditions. They applied the model to analyse a reinforced concrete pier of a bridge affected by ASR. The numerical results were promising when compared to the experiment. In addition, Farage *et al*. (2004) proposed a smeared crack finite element approach to analyse the concrete structures suffering from ASR effects according to the kinetics od ASR proposed by Ulm *et al*. (2000). Also, Fairbairn *et al*. (2006) presented an ASR chemo-mechanical model, in which the stress anisotropy was considered by the smeared crack approach. They applied this model to predict the swelling of a concrete dam, and the results showed good agreement with the field measurements.

In 2006, a loosely coupled chemo-mechanical model was presented by Saouma and Perotti (2006) in which the free volumetric strain due to ASR is given as follows:

$$\epsilon_V^{AAR}(t) = \Gamma_t\, \Gamma_c\, g(h)\, \xi(t,\theta)\epsilon^{\infty} \tag{2-11}$$

here the expression $0 \leq \Gamma_t \leq 1$ is a function that reduces the expansion in the presence of large tensile stresses under the hypothesis that macro cracks play a role in absorbing the gel, Similarly, $0 \leq \Gamma_c \leq 1$ is a function that accounts for the reduction in ASR volumetric expansion under relatively high compressive stresses. This mechanism is possibly due to reduction in micro cracks under high 3D compressive stresses and reduction in the gel expansion due to axial state of compressive stresses. $\epsilon^{\infty}$ is the asymptotic volumetric expansion as determined from experimental tests at temperature $\theta_0$, $0 \leq g(h) \leq 1$ is a function that accounts for the humidity effects and is less than 1 if the humidity is lower than 80%. Typically, the humidity inside a massive concrete structure such as a dam is 90 to 100%. Finally, $\xi(t,\theta)$, represents the reaction extent according to equation (2-3).

Volumetric ASR strain is then decomposed into tensor components based on a weight function of principal stresses which can determine the strain rate in each principal direction as shown in equation (2-12), and as a result, the expansion is now anisotropic. Finally, concrete material degradation properties during the evolution of ASR are given by Huang and Pietruszczak (1999) model. This model was applied to analyse a 2D gravity dam structure affected by ASR.

$$\varepsilon_i = W_i\, \epsilon_V^{ASR} \tag{2-12}$$

Another chemo-mechanic model using a different kinetic reaction law is proposed by Poyet *et al.* (2006) in which the effects of temperature and water are considered. In equation (2-13) below $A$ is a dimensionless ASR advancement variable which represents the progress of the ASR development given by:

$$\dot{A}(S,T,t) = \alpha_0 \left[\frac{U_a}{R}\left(\frac{1}{\bar{\theta}} - \frac{1}{\theta}\right)\right] \frac{(S_r - S_r^0)^+}{(1 - S_r^0)} [S_r - A(S_r,\theta,t)]^+ \tag{2-13}$$

where $\alpha_0$ is a material constant that determines the ASR kinetics, $(.)^+$ is the positive part of the equation, $\theta$ is the current temperature, $\bar{\theta}$ is the reference temperature and $S_r^0$ is the minimum saturation ratio required to allow the initiation of the ASR.

The volumetric ASR strain $\epsilon_{ASR}$ is related to the rate of advancement $A$ by equation (2-14):

$$\begin{cases} \dot{\epsilon}_{ASR} = 0 & A < A_0 \\ \dot{\epsilon}_{ASR} = K\dot{A} & A \geq A_0 \end{cases} \quad (2\text{-}14)$$

where $A_0$ denotes the minimum ASR advancement necessary to initiate swelling. It is worth noting that in this model, kinetics of the reaction which is basically pressure based, the variations of the volume of gel and saturation degree of the structure are included in the model. However, in the kinetics proposed by Larive (1998) the saturation degree of the structure is implicitly considered by measuring the different characteristic time and latency time for the concrete specimens under several hygral ambient conditions developed in the laboratory. In the current research, it is assumed that concrete dam walls represent saturated medium and therefore the reaction kinetics expression used in equation (2-3) is considered to be sufficient for the modelling of concrete dams.

## 2.7 Conclusion

In this chapter a comprehensive review of the literature on the study and modelling of concrete affected by ASR is done. A number of modelling techniques for ASR affected concrete at different scales (micro-meso and macro scale) are presented and discussed. Parameters that are important for ASR initiation and progress are critically reviewed and discussed. The variables such as temperature, relative humidity, kinetics of the reaction, 3D confining stresses and material degradation due to swelling of concrete are identified as the key parameters to model the ASR. In the next chapters, a chemo-thermo-mechanical model based on concrete damage plasticity constitutive law is developed considering the parameters and phenomena that are found to be important in the modelling of concrete dams suffering from ASR.

While the most current numerical models that have been developed to analyse the effect of ASR on structures are phenomenological models, future research will likely be on ASR modelling in combination with micro, meso and macro scales, where the macroscopic models are derived from the microscopic analysis. Modelling of the anisotropy of the expansion partially caused by the internal swelling of concrete under various loading conditions is an open question remaining in the study of ASR. A model on micro-mechanical scale which combines thermodynamics, chemistry and fracture mechanics of materials is still forthcoming.

Finally, the interaction of long term strains such as creep, relaxation and shrinkage with strains from ASR in structures is critical in planning for remedial measures (van Zijl, 1999).

# CHAPTER 3

# Solid mechanics based modelling of ASR in concrete

**Highlights:**

Constitutive modelling of ASR

Kinetics of the chemical reaction

Confining effects from stress state

Concrete deterioration due to ASR

Anisotropic nature of the expansion of concrete due to ASR

## 3.1 Introduction

In this chapter the solid mechanics based mathematical formulation of ASR is presented. To correlate the material degradation with the material expansion due to ASR, various parameters are incorporated in the model. These include temperature effects, kinetics of the reaction, characteristic time scales, 3D state of the stress and confining effects and non-uniform time dependent material degradation. Also, anisotropy of the ASR swelling in principal directions is considered using a weighting function in terms of the 3D state of stress. Subsequently, a mathematical description of all the phenomena involved in model is presented.

## 3.2 Chemo-mechanical modelling of ASR

Currently, no practical methods to curb or arrest the swelling chemical reaction in concrete dams due to ASR have been developed. A numerical model that can predict the long term behaviour of and the potential damage to a structure subject to ASR can provide engineers with a tool to properly plan the rehabilitation and remedial action. In this research a chemo-thermo-mechanical model is developed to predict the structural expansion, degradation of mechanical

properties, cracks and damage in concrete structures affected by ASR. The finite element based model can simulate the temperature field in the structure and the kinetics of the chemical reaction to predict the long term effects of the ASR on a typical concrete structure including displacement, cracking and damage development.

## 3.3 ASR constitutive modelling

In this research, it is assumed that the strain due to ASR is volumetric in nature in configurations without confining stresses. This assumption is considered by many researchers and experimental works demonstrated a reasonable agreement with numerical models considering volumetric strain (Multon & Toutlemonde, 2006; Saouma & Perotti, 2006). In recent experiments by Liaduat *et al*. (2018), an ad-hoc device is introduced which is able to apply triaxial loads on ASR specimens for a long period of time. The results indicate that the ASR expansion is volumetric in free stress state tests and transfers to the less compressed direction for configurations where confining stresses are present. Also, they observed that a triaxial compressive stress state equal to 9.7 MPa could hinder the volumetric strain rate. Therefore, a refined model from Saouma and Perotti (2006) to estimate the expansion from ASR strains in each principal direction can be defined by a rate form which is suitable for integration:

$$\dot{\varepsilon}_i^{asr} = \Gamma_c(\sigma_v)\dot{\xi}[\tau_L(\theta,\sigma_v, f_c^{'}),\tau_c(\theta)]\beta W_i(\sigma_v) \tag{3-1}$$

where in this equation $\xi \in [0,1]$ represents an extent of the chemical reaction. In 1998, extensive laboratory research in LCPC-France by Larive (1998) led to the development of the most promising chemical kinetics formulation. The reaction extent in the rate form is given by:

$$\dot{\xi} = \frac{e^{t/\tau_c}\left(e^{\tau_l/\tau_c}+1\right)}{\tau_c\left(e^{t/\tau_c}+e^{\tau_c/\tau_l}\right)^2} \tag{3-2}$$

The characteristic time $\tau_c$ and latency time $\tau_l$ can be estimated using an Arrhenius relation:

$$\tau_c(\theta) = \tau_c(\theta_0)\exp[U_c(1/\theta - 1/\bar{\theta}_0)],$$
$$\tau_L(\theta,\sigma_v, f_c^{'}) = f(\sigma_v, f_c^{'})\,\tau_L(\theta_0)\exp\left[U_L(1/\theta - 1/\bar{\theta}_0)\right] \tag{3-3}$$

The latency time and characteristic time are functions of the current temperature $\theta$ and the temperature $\bar{\theta}_0$. Iso-thermal laboratory tests have been conducted for their identification (Larive, 1998). In addition, in equation (3-3) $U_c$ and $U_L$ are activation energy constants of the characteristic time and latency time, respectively in Kelvin (K) and are defined as:

$$U_c = 5400 \pm 500 \ K$$
$$U_L = 9400 \pm 500 \ K. \quad (3\text{-}4)$$

Furthermore, $\beta$ is the asymptotic volumetric expansion strain in the stress-free experiment and can be estimated according to the moisture content of and type of aggregates and the other mix proportion parameters (Ulm *et al.*, 2000).

### 3.3.1 The effects of micro cracking on volumetric expansion

Equation (3-5) presents a retardation function that considers the increase in latency time due to the fact that micro cracks relevant to volumetric compressive stresses could likely absorb some gel which is produced during the chemical reaction. This mechanism could delay the ASR swelling initiation (Saouma & Perotti, 2006):

$$f(\sigma_v, f_c^{'}) = \begin{cases} 1 & \sigma_v > 0 \\ 1 + \alpha_0 \dfrac{\sigma_v}{3 f_{cm}} & \sigma_v \le 0 \end{cases} \quad (3\text{-}5)$$

in equation (3-5) $\alpha_0$ is 4/3 according to the Multon's tests (Multon & Toutlemonde, 2006), $\sigma_v$ is the sum of compressive stresses in principal directions.

### 3.3.2 The effect of confinement stresses on volumetric expansion

ASR can be confined through different constraints. The forces from these constraints can be applied by loads such as gravity forces or imposed loads such as hydrostatic loads on a dam structure. Also, the forces may arise due to ASR swelling itself. The effect of confinement stress on ASR expansion is considered through a reduction function which is shown in equation (3-6):

$$\Gamma_c = \begin{cases} 1 & \sigma_v \geq 0 \\ 1-\left(\sigma_v/\bar{\sigma}_v\right)^2 & 0 \geq \sigma_v \geq \bar{\sigma}_v \\ 0 & \sigma_v \leq \bar{\sigma}_v \end{cases} \tag{3-6}$$

where $\bar{\sigma}_v$ is a limit below which ASR could be prevented. In this research, it is assumed that $\bar{\sigma}_v$ is equal to -9.7 MPa.

### 3.3.3 Effect of stress state on anisotropy of the swelling of concrete

The effects from confinement stresses could reduce the volumetric ASR strain and create anisotropy of the swelling. It is now widely accepted that a sufficiently high confinement stress would stop the ASR expansion completely (Liaudat *et al.*, 2018). In this research, a weight function is used to model the anisotropy of the ASR expansion due to external and internal stresses. The maximum and minimum stress limits are parameters that should be provided by the user. The lower limit stress is a value that reduction in ASR expansion occurs.

The calculation of the anisotropic distribution function starts by defining the volumetric confinement parameter. This parameter determines the level of stress at which ASR expansion would start to reduce and at what level it would stop completely. As shown in the previous section a 3D confinement stress equal to -9.7 MPa could totally suppress the ASR (Liaudat *et al.*, 2018).

For the purpose of the distribution of ASR volumetric strain as a function of stress, $W_i(\sigma_v)$ is introduced as a weighting function in equation (3-1). The introduction of this parameter proposed by Gocevski and Yildiz (2017) and improved in this research, represents an effective technique for the pro-rata distribution of the ASR strain in the principal stress directions. Practically, this method can determine the weight of the ASR strain rate in each principal direction by introducing a function which links the weight in each direction to $\sigma_v$ the volumetric stress equal to sum of the stresses in all principal direction. To enhance the understanding of all the aspects of these weighting techniques an application example is presented below.

Assume a stress state in a material point according to the Figure 3-1 is given. The uniaxial confinement parameter (UCP) is introduced in Figure 3-2. Gocevski and Yildiz (2017)

considered a linear function of the stress for estimating of this parameter while in this research equation (3-6) is used to develop this function which is linked to the stress state at each material point. This function is a parabolic function of the volumetric stress providing the directional stress at each material point. It is assumed that a value of compressive stress equal to -9.7 MPa could possibly stop the ASR in the same direction. It is also assumed that at a lower limit of stress (-1.5 MPa) the ASR starts to reduce.

The percentage of expansion in each principal direction is estimated using the calculated value of UCP. The curve used in this research and the UCP values in X, Y and Z direction, based on the value of stresses are presented in Figure 3-2. The reduced volumetric expansion through the function provided in equation (3-6) is then calculated in each principal direction based on the calculated percentages that are shown in Figure 3-3. To calculate the percentage of ASR expansion in each principal direction, first it is required to divide the UCP at each direction by the sum of the uniaxial confinement parameter in all directions. In this example, it is assumed that the reduced volumetric expansion by 3D confinement effect is 20 $\mu\varepsilon$/year. Finally, Table 3-1 shows the calculated value of ASR expansion in each principal direction according to this weighting technique.

Uniaxial expansion weighting ratio

| Parameter | Value | Unit |
|---|---|---|
| Stress XX | -5.4 | MPa |
| Stress YY | -2.0 | MPa |
| Stress ZZ | -4.6 | MPa |

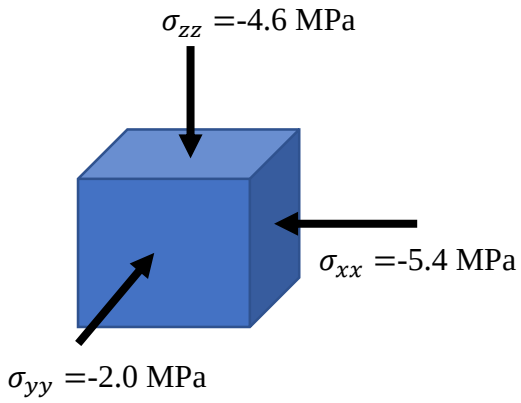


**Figure 3-1**. Stress state of a material point in finite element modelling.

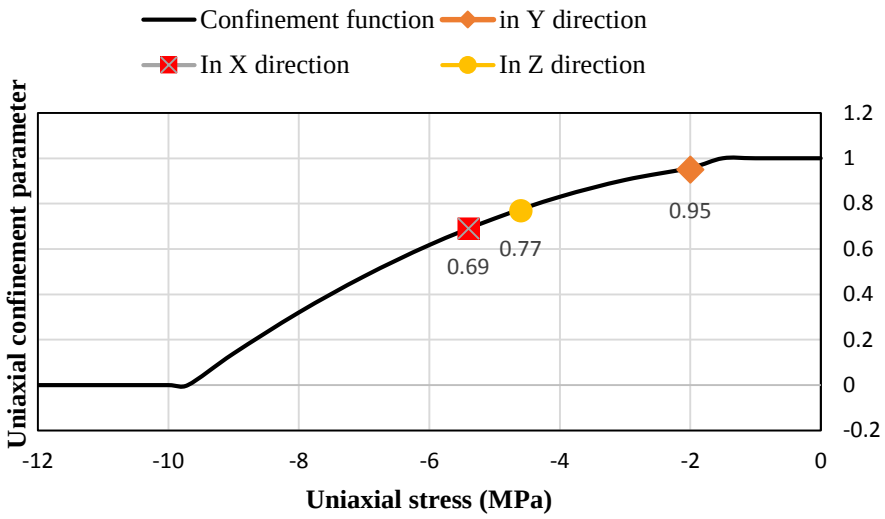


**Figure 3-2**. Determination of the uniaxial confinement parameter in principal directions.

| **Parameter** | Uniaxial confinement parameter | % of ASR expansion |
|---|---|---|
| Direction XX | 0.69 | 28 |
| Direction YY | 0.95 | 40 |
| Direction ZZ | 0.77 | 32 |
| Sum of parameters | 2.41 | |

Stress state data

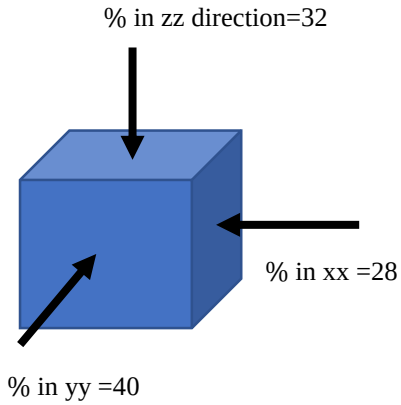


**Figure 3-3**. Percentage of ASR expansion in each principal direction.

**Table 3-1**.Percentage of ASR expansion for each principal direction.

| **Parameter** | % of ASR expansion | ASR expansion rate | |
|---|---|---|---|
| Direction XX | 28 | 5.6 | $\mu\varepsilon$/year |
| Direction YY | 40 | 8.0 | $\mu\varepsilon$/year |
| Direction ZZ | 32 | 6.4 | $\mu\varepsilon$/year |

## 3.4 Concrete material deterioration due to ASR

A further concern about the concrete material affected by ASR is that of concrete deterioration. Equation (3-7) uses an ASR damage factor which basically is a function of ASR expansion, to determine the deterioration of the concrete elastic stiffness (E-Modulus) and tensile strength $f_t$, which is a time-dependent function (Capra & Sellier, 2003):

$$E = E_0(1 - d_{asr})$$
$$f_t = f_{t0}(1 - d_{asr}) \tag{3-7}$$

where $E_0$ and $f_{t0}$ are the initial Young's modulus and tensile strength, respectively. During the ASR process, the swelling gels penetrate the concrete matrix and induce cracking of the aggregates and the surrounding cement paste. The damage of the material leads to elastic stiffness degradation. The ASR damage factor, $d_{asr}$ may be linked to the expansion strains from the experimental results as shown in Figure 3-4 (ISE, 1992). Furthermore, according to the experimental results, equation (2-8) is used to determine $d_{asr}$, using the maximum ASR expansion strain in principal direction (Capra & Bournazel, 1998):

$$d_{asr} = 1 - \frac{E}{E_0} = \frac{\max(\varepsilon_i^{asr})}{\max(\varepsilon_i^{asr}) + B} \tag{3-8}$$

here *B*, is a calibration parameter assumed to be 0.3 %.

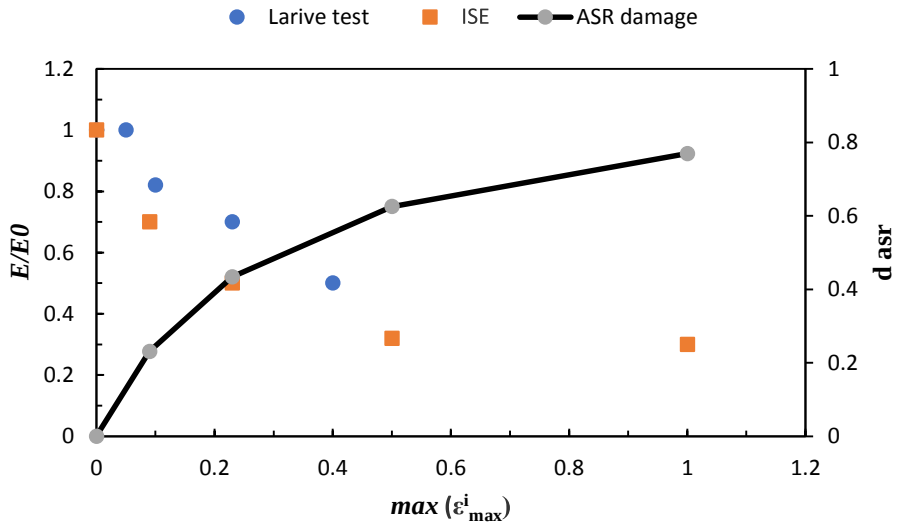


**Figure 3-4**. Degradation of the elastic modulus and evolution of ASR damage as a function of maximum ASR expansion in concrete (reproduced from Capra & Sellier (2003)).

## 3.5 Numerical model implementation

The coupled problem of heat diffusion and thermo-activated ASR kinetics is approached by initially doing transient thermal analysis with initial boundary conditions. This requires a number of parameters, among them: 1) the air temperature variation; 2) the spatial and temporal (at least 12 or 24 increments a year) variation of the water temperature which is required; 3) the dam reservoir level variation during a typical year; 4) the concrete thermal properties. For this analysis, and the subsequent stress analysis, an analysis time unit or time increment, must be defined. The flowchart in Figure 3-5 summarises the steps required to implement the numerical model. This model is implemented using the developed subroutines in a sequentially coupled multi-physics analysis technique in the Computational Structural Mechanics Unit at Stellenbosch University in the ABAQUS finite element package (Simulia, 2016). This model is now referred to as the SU-ASR model.

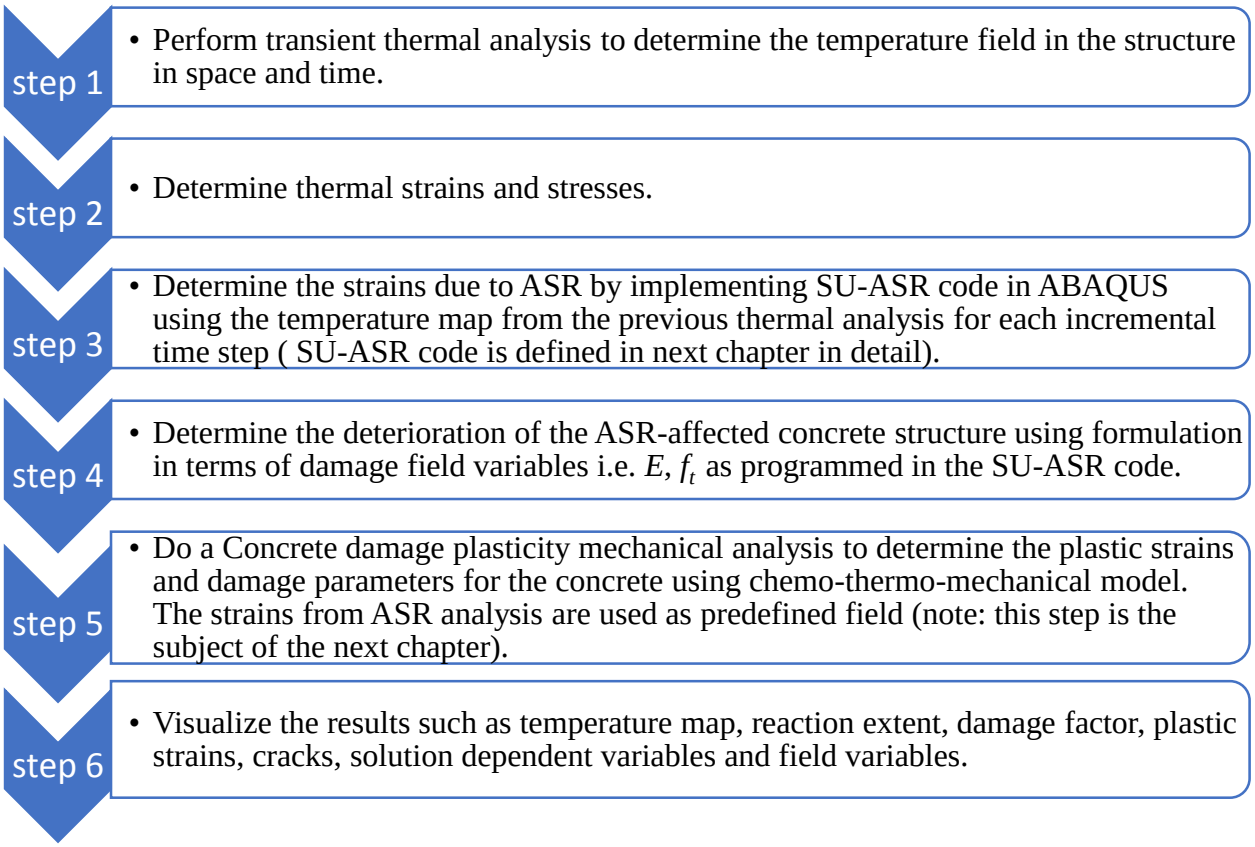


**Figure 3-5**. Flowchart of the SU-ASR model numerical implementation.

## 3.6 Summary

In this chapter the mathematical formulation of the ASR model proposed in this research is provided. Effective variables and parameters such as temperature history, kinetics of the reaction, gel absorption by micro cracking, confining effects from the 3D state of stress, anisotropic swelling in principal directions and non-uniform time dependent material degradation are taken into account. To capture the non-linear and inelastic behaviour of concrete associated with ASR in the next chapter a non-linear constitutive model of concrete is presented. Then the ASR strain constitutive equations presented in this chapter are combined by constitutive modelling of concrete to provide a loosely coupled chemo-thermo-mechanical finite element model. Finally, available published experimental results is used in the subsequent chapters to verify and validate the SU-ASR model and then to study the behaviour of some typical dams suffering from ASR.

# CHAPTER 4

# Nonlinear material behaviour and constitutive models of concrete

**Highlights:**

Constitutive modelling of concrete

ASR coupled with concrete damage plastic model

Numerical implementation of ASR model

## 4.1 Introduction

Concrete is a composite material including aggregates, cement paste, water, air and some other admixtures. Properties of the cement paste, aggregate and interfacial transition zone between these components are the key factors determining the physical and mechanical properties of concrete. Due to the different behaviour of concrete in compression and tension, it is important to get an insight for these types of behaviours.

The crushing and cracking mechanisms have a significant role on the non-linear behaviour of concrete material and response of the structures. In this chapter the concrete damage plasticity model for analysis of concrete material is provided and discussed. In the failure analysis of concrete structures, the modelling of crack initiation and propagation is one of the important aspects. The Concrete Damage Plasticity (CDP) model provides the capability to analyse non-linear response of concrete structures under cyclic and dynamic loading. Under low confining pressure, concrete behaves in a brittle manner. When the confining pressure is sufficiently large, the brittle behaviour of concrete abates and concrete behaves more like a ductile material. The ASR constitutive model was developed in chapter 3. In this this chapter, initially the nonlinear behaviour of concrete is addressed. Then, a technique based on finite element method to model cracking and crushing of concrete using a continuum damage mechanics approach

for modelling of nonlinear behaviour of concrete is presented. Finally, numerical mathematical models i.e. an ASR constitutive model and a CDP model coupled together are provided as the basis for the ASR modelling strategy adopted in this research.

## 4.2 Nonlinear behaviour of concrete

This section summarizes some typical mechanical properties of concrete under uniaxial, biaxial and multiaxial states of stress. Concrete is a material that contains a large number of micro cracks specifically at the interfaces between aggregate and cement paste even before the application of external load. This property has a significant role in the mechanical behaviour of concrete. The distribution of these micro cracks during loading contributes to the nonlinear behaviour of concrete at low stress level and causes dilatancy of the concrete near failure.

### 4.2.1 Concrete in uniaxial tension

Empirical observations on concrete specimens under uniaxial tension have indicated that the concrete is not a perfectly brittle material and the fracture process is not a sudden event, but rather a gradual release of stress along the crack surfaces. This process which was first introduced by Hillerborg *et al.* (1976) includes the initiation of micro crack, their gradual propagation and finally the formation of the localised macro crack and is illustrated in Figure 4-1.

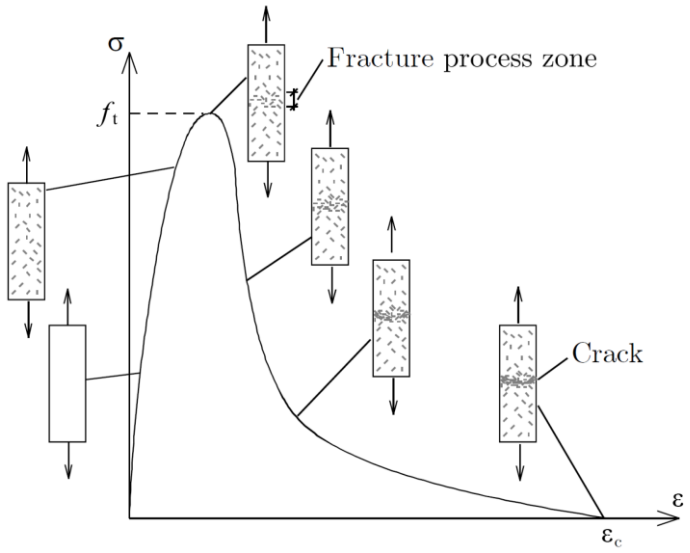


**Figure 4-1**. Typical tensile behaviour of concrete under uniaxial loading with micro cracks formation and formation of localised crack (after Hjalmarsson and Pettersson (2017)).

The behaviour of the concrete in the fracture process zone (FPZ) can be defined by a stress-Crack Opening Displacement. The stress-COD curve is derived by considering the unloading part of the stress-strain curve after maximum tensile stress has occurred as shown in Figure 4-2.

The area under the stress-COD curve is defined as the fracture energy $G_F$, which is an amount of energy dissipated per unit area as a crack develops. For the purpose of FE modelling a tension-softening law in the uniaxial direction is defined, hence the model can reproduce formation of the micro cracks and the evolution of the macro crack.

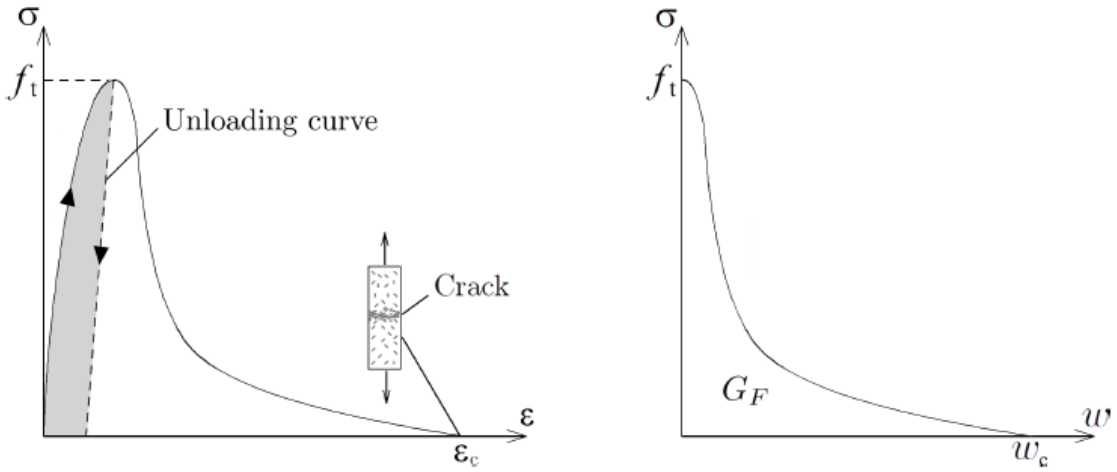


**Figure 4-2**. Developing the stress-COD curve from stress-strain in uniaxial tension.

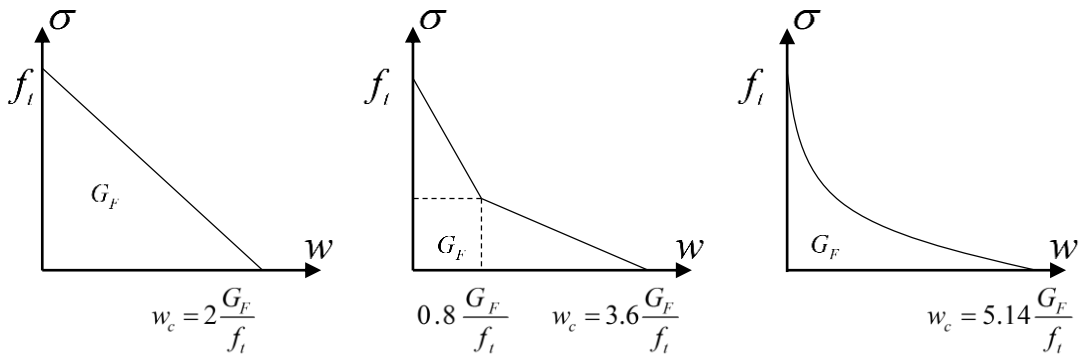


(a) Linear relation (b) Bi-linear (c) Exponential

**Figure 4-3**. Different approaches for describing the tensile stress-COD as a function of fracture energy, a) linear function, b) bi-linear function and c) exponential function.

The stress-COD relation can be derived using the fracture energy concept. Figure 4-3 Shows different approaches for defining the stress-COD in tension by assuming a linear, bi-linear and exponential softening.

Another softening model, an exponential model has been proposed by Cornelissen *et al.* (1986) expressed as:

$$\frac{\sigma}{f_t} = \left[1 + \left(c_1 . \frac{w}{w_0}\right)^3\right] . e^{-c_2 . \frac{w}{w_0}} - \frac{w}{w_0} . \left(1 + c_1^3\right) . e^{-c_2} \qquad (4\text{-}1)$$

where:

$w$ is the crack opening

$w_0$ is the crack opening at which stress can no longer be transferred.

$c_1$ is a material constant. $c_1$=3.0 for normal density concrete.

$c_2$ is a material constant. $c_2$=6.93 for normal density concrete.

The fracture energy is best determined by experiment. When there is no experimental data to determine this parameter, Model Code 2010 (CEB-fib, 2013) provides a way to determine the fracture energy given by:

$$G_F = 73 . f_{cm}^{0.18} \qquad (4\text{-}2)$$

where $f_{cm}$ is the mean cylindrical compressive strength of the concrete [MPa].

### 4.2.2 Concrete in uniaxial compression

A typical stress-strain curve for concrete in compression is shown in Figure 4-4. Concrete behaves highly nonlinear in uniaxial compression. The stress-strain curves for concrete in compression have a nearly linear elastic behaviour up to about 30 percent of the maximum compressive strength $f_{cm}$ as presented between point (a) and (b). From point (b) to approximately 75% of the ultimate compressive stress, at point (c), concrete shows non-linear behaviour and the elastic stiffness decline. Beyond (c) macro cracking of concrete is initiated.

After the peak compressive stress, $f_{cm}$, which corresponds with the failure strain $\varepsilon_f$, the concrete starts to soften and the stress-strain curve descends (Cornelissen *et al.*, 1986).

There are several material models available in the literature to define the stress-strain curve for the concrete in compression including compressive softening. De Borst (2002) introduced a fracture based stress-strain function to define the behaviour of concrete in compression and in the softening regime. Equation (4-3) and Figure 4-5 presents the detail of this model.

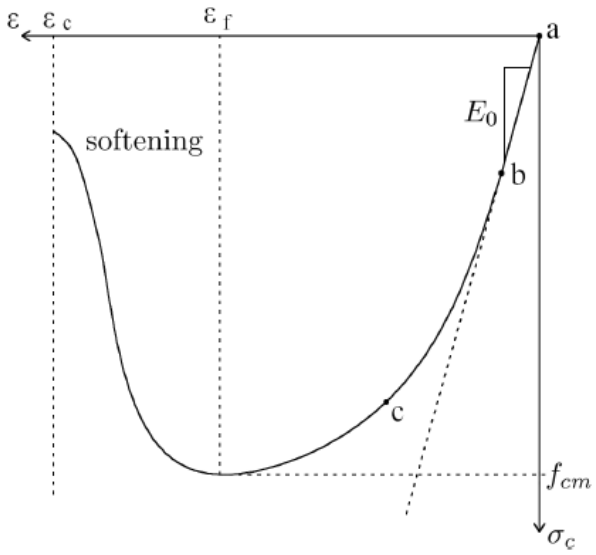


**Figure 4-4**. The Stress-strain curve for concrete under uniaxial compression.

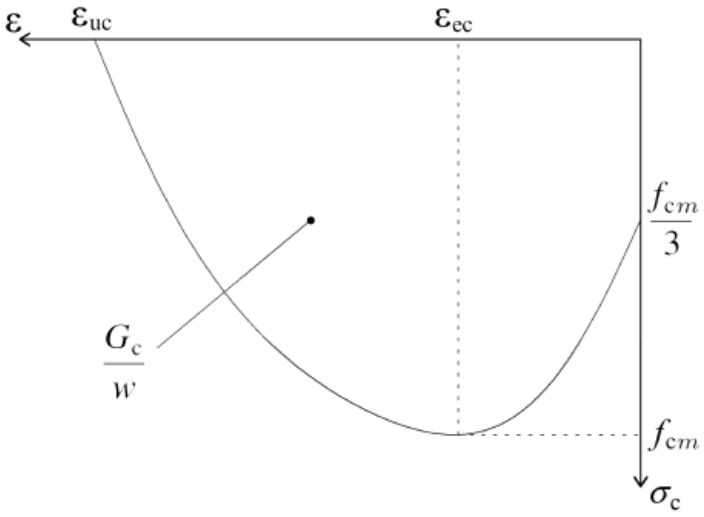


**Figure 4-5**. Relation between compressive stress and strain for concrete using the fracture energy concept (after De Borst (2002)).

$$\sigma_c(\varepsilon_q) = \begin{cases} \frac{f_{cm}}{3}\left(1+4\frac{\varepsilon_c}{\varepsilon_{ec}}-2\frac{\varepsilon_c^2}{\varepsilon_{ec}^2}\right) & if \quad \varepsilon_c < \varepsilon_{ec} \\ f_{cm}\left(1-\frac{(\varepsilon_c-\varepsilon_{ec})^2}{(\varepsilon_{uc}-\varepsilon_{ec})^2}\right) & if \quad \varepsilon_{ec} < \varepsilon_c < \varepsilon_{uc} \end{cases} \tag{4-3}$$

where:

$\varepsilon_c$ is concrete strain.

$\varepsilon_{ec}$ is the equivalent stain corresponding to the maximum compressive stress, $\varepsilon_{ec} = \frac{4}{3}\frac{f_{cm}}{E_0}$

$\varepsilon_{uc}$ is the fracture strain $\varepsilon_{uc} = \frac{3G_c}{2wf_{cm}}$

$G_c$ is the compressive fracture energy.

$w$ is the FE element mesh size.

### 4.2.3 Biaxial behaviour of concrete

The concrete behaves differently when it is loaded under a multiaxial state of stress. Concrete in uniaxial compression or tension shows brittle behaviour. However, when multiaxial compression or tension exists, concrete behaves similar to a ductile material. (Chen, 2007).

Figure 4-6 illustrates the biaxial crushing/failure evolution and cracking of concrete. An increase in the biaxial compressive strength up to 25% has been expected for the biaxial compression regime (Chen, 2007).

Concrete shows more ductile behaviour and an increase in compressive strength when it is under high triaxial state of stress. The concrete could act as quasi-brittle, strain hardening or strain softening material which basically depends on the level of confining stress. For higher confining stresses the cement paste is subject to a crushing mode of failure instead of localised cracking.

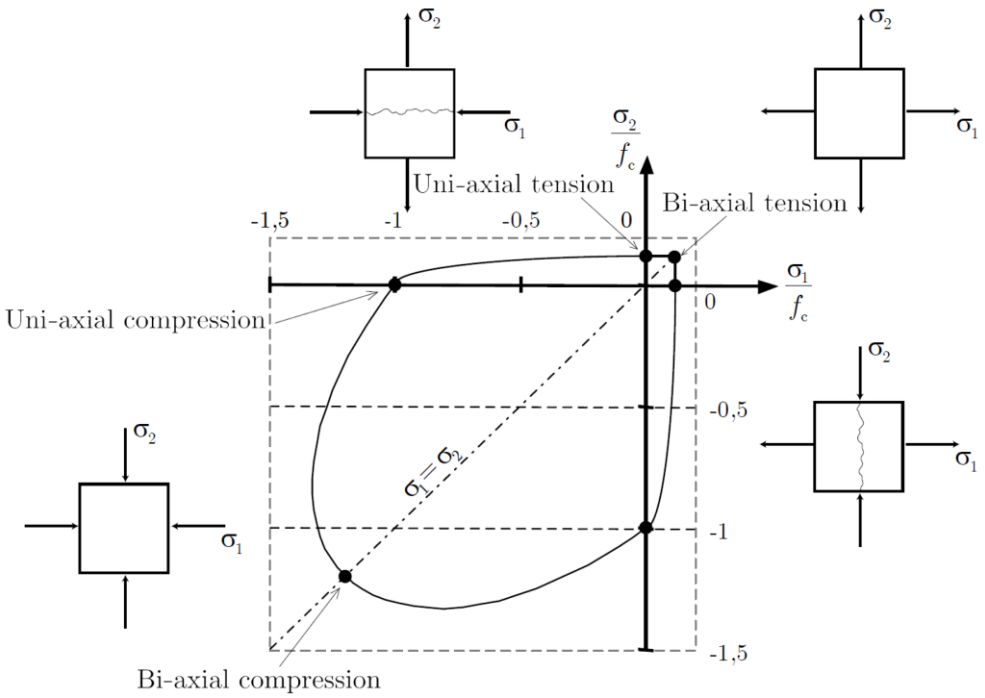


**Figure 4-6**. Failure mode of concrete under biaxial loading. Cracks are parallel to the compressive stress and in the transverse direction to the tensile stress (after Hjalmarsson and Pettersson, 2017).

## 4.3 Concrete damage-plasticity model

Extensive investigation by researchers over the years has led to a better understanding of the constitutive behaviour of concrete under various loading conditions. The material constitutive theory described in this section captures the effects of irreversible damage associated with the failure mechanisms that occur in concrete assuming low confinement effects from external loads (below than four or five times of uniaxial ultimate compressive stress). The following macroscopic properties must be defined to present these effects:

1. different yield strength in tension and compression,
2. initial hardening followed by softening in compression as opposed to softening behaviour in tension,
3. different deterioration mechanism of the elastic stiffness in tension and compression,
4. E-Modulus recovery for cyclic loading.

For developing the failure function for concrete a large number of methods are available. Therefore one must consider the condition of the problem in hand and then decide to select the appropriate type of failure or yield function for concrete (Chen & Saleeb, 1994). One parameter

models of independent pressure are only valid for low hydrostatic pressures state of stress. But for the problem with fairly large hydrostatic pressure two parameter models of the yield function should be used. In modelling of concrete affected by ASR, stresses usually fall into the intermediate range of stresses and therefore two parameter models such as Drucker-Prager might be adequate.

The behaviour of plastic deformation coupled with an elastic degradation is usually observed for concrete materials in the post-failure range and the combination of these two theories in modelling such behaviour is reasonable. The Concrete Damage Plasticity (CDP) model used here provides a means for combining these different theories. The CDP model is based on the model proposed by Lubliner *et al*. (1989) for monotonic loading and further developed by Lee and Fenves (1998) to consider the cyclic loading effects. The model is described as follows.

### 4.3.1 Strain rate decomposition

In continuum mechanics the total strain can be considered as a superposition of strains from different mechanisms involved in the medium. An additive strain rate decomposition is assumed for the rate-independent model:

$$\dot{\boldsymbol{\varepsilon}} = \dot{\boldsymbol{\varepsilon}}^{\boldsymbol{el}} + \dot{\boldsymbol{\varepsilon}}^{\boldsymbol{pl}} \tag{4-4}$$

where $\dot{\boldsymbol{\varepsilon}}$ is the total strain rate, $\dot{\boldsymbol{\varepsilon}}^{\boldsymbol{pl}}$ is plastic strain rate and $\dot{\boldsymbol{\varepsilon}}^{\boldsymbol{el}}$ is elastic strain rate.

### 4.3.2 Stress-strain relations

The stress-strain constitutive relations are governed by scalar damaged elasticity:

$$\boldsymbol{\sigma} = (1 - \mathrm{d})\overline{\boldsymbol{\sigma}} = (1 - d)\boldsymbol{D}_{\boldsymbol{0}}^{\boldsymbol{el}}(\boldsymbol{\varepsilon} - \boldsymbol{\varepsilon}^{pl}) \tag{4-5}$$

and

$$\boldsymbol{D}^{el} = (1-d)\boldsymbol{D}_0^{el} \tag{4-6}$$

where $\boldsymbol{D}_0^{el}$ is the initial (undamaged) elastic stiffness of the material; $\boldsymbol{D}^{el}$ is the deteriorated elastic stiffness; and $d$ is the scalar stiffness degradation variable, which the values are in the range from zero for undamaged material and one for fully damaged material. Following the

notions of scalar damage theory and continuum damage mechanics, the effective stress is defined as:

$$\bar{\boldsymbol{\sigma}} = \boldsymbol{D}_0^{el} : (\boldsymbol{\varepsilon} - \boldsymbol{\varepsilon}^{pl}) \tag{4-7}$$

In this equation the Cauchy stress is related to the effective stress through the scalar degradation relation: $\boldsymbol{\sigma} = (1-d)\bar{\boldsymbol{\sigma}}$ in equation (4-5).

The factor $(1-d)$ in above equation represents the ratio of the effective load-carrying area (i.e., the total area minus the damaged area) to the overall section area. Furthermore, it is convenient to formulate the plasticity problem in terms of the effective stress. When damage occurs, however, the effective stress $\bar{\boldsymbol{\sigma}}$ is a better representative of the stress state than the Cauchy stress, $\boldsymbol{\sigma}$ due to this fact that it is the effective stress area that is resisting the external loads. As discussed later the evolution of the degradation variable is governed by a set of hardening variables and the effective stress.

The stress-strain relationships in the CDP model under uniaxial tension and compression are given by using $E_0$ as the initial (undamaged) elastic stiffness of the material, defined as:

$$\sigma_t = (1-d_t)E_0(\varepsilon_t - \tilde{\varepsilon}_t^{pl})$$
$$\sigma_c = (1-d_c)E_0(\varepsilon_c - \tilde{\varepsilon}_c^{pl}) \tag{4-8}$$

where:

$\sigma_t$, $\sigma_c$ are the tensile and compressive stress.

$d_t$, $d_c$ are the damage variable in tension and compression.

$E_0$ is the initial Young's modulus.

$\tilde{\varepsilon}_t^{pl}$, $\tilde{\varepsilon}_c^{pl}$ are the equivalent plastic strain for tension and compression.

Figure 4-7 shows the loading\unloading curves for uniaxial tension and compression in the concrete damage plasticity model which are characterised by damage variables in tension and compression.

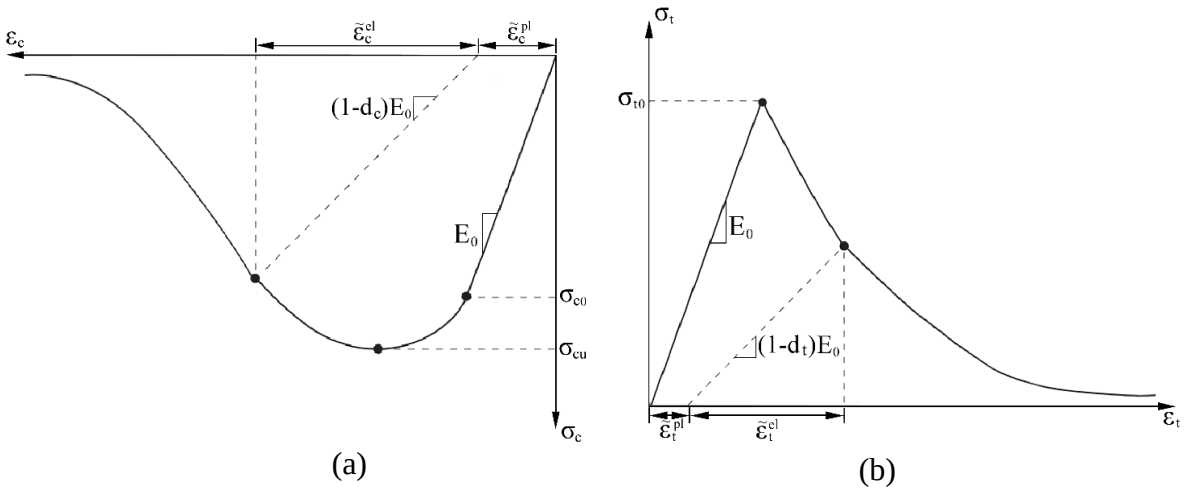


**Figure 4-7**. Response curve for uniaxial loading in concrete for compression and tension, a) curve show stress-plastic strain relation in compression, b) curve shows stress-strain relation in tension.

It is observed in Figure 4-7 a, for uniaxial compression the stress-strain response remains linear elastic before the initial yield $\sigma_{c0}$ is reached. From this point to the point of the ultimate stress $\sigma_{cu}$ the response curve exhibits a plastic regime behaviour which is characterized by stress hardening. After this point stress-strain curve enters the strain softening regime. While in Figure 4-7 b, it is shown that the stress-strain curve in uniaxial tension remains linear before the failure stress $\sigma_{t0}$ and after this point curve shows a softening regime associated with propagation of micro cracks and final localised cracking in the concrete material. In uniaxial tensile condition the cracks mainly develop in a perpendicular direction to the stress direction. The nucleation and evolution of cracks lead to an increase in the effective stress due to the reduction of the available load-carrying area. However, in compression cracks mainly propagate in a parallel direction to the applied load which result in the less pronounced effect on effective stress. In this condition, the effective load-carrying area is also reduced only after a significant amount of crushing occurs. Furthermore, the effective uniaxial cohesion stresses determine the size of the yield (or failure) surface.

### 4.3.3 Hardening variables

Two hardening variables are introduced to define the damage states in tension and compression $\tilde{\varepsilon}_t^{pl}$ and $\tilde{\varepsilon}_c^{pl}$, which represent equivalent plastic strains in tension and compression, respectively. The evolution of the hardening variables is given by an expression of the form:

$$\tilde{\varepsilon}^{pl} = \begin{bmatrix} \tilde{\varepsilon}_t^{pl} \\ \tilde{\varepsilon}_c^{pl} \end{bmatrix}; \quad \dot{\tilde{\varepsilon}}^{pl} = h(\bar{\boldsymbol{\sigma}}, \tilde{\varepsilon}^{pl}).\, \dot{\boldsymbol{\varepsilon}}^{pl} \tag{4-9}$$

where:

$$h(\bar{\boldsymbol{\sigma}}, \tilde{\varepsilon}^{pl}) = \begin{bmatrix} r(\bar{\boldsymbol{\sigma}})\, f_t(\tilde{\varepsilon}^{pl}) / g_t & 0 & 0 \\ 0 & 0 & -(1-r(\bar{\boldsymbol{\sigma}}))\, f_c(\tilde{\varepsilon}^{pl}) / g_c \end{bmatrix} \tag{4-10}$$

In this equation $r(\bar{\boldsymbol{\sigma}})$ is a stress weight factor that is equal to one if all principal stresses $\bar{\sigma}_i = (i = 1,2,3),$ are positive and equal to zero if they are negative. This weight function is defined as:

$$r(\bar{\boldsymbol{\sigma}}) = \frac{\sum_{i=1}^{3} \langle \bar{\boldsymbol{\sigma}}_i \rangle}{\sum_{i=1}^{3} |\bar{\boldsymbol{\sigma}}_i|}; \quad 0 \le r(\bar{\boldsymbol{\sigma}}) \le 1 \tag{4-11}$$

the Macaulay bracket $\langle \bullet \rangle$ is defined by $\langle x \rangle = \frac{1}{2}(|x| + x)$, and

$$\dot{\varepsilon}^{pl} = \begin{bmatrix} \dot{\varepsilon}_1 \\ \dot{\varepsilon}_2 \\ \dot{\varepsilon}_3 \end{bmatrix} \tag{4-12}$$

the eigenvalues of the plastic strain rate tensor $(\dot{\varepsilon}_i,\, i = 1,2,3)$ are ordered such that $\dot{\varepsilon}_{\max}^{pl} = \dot{\varepsilon}_1 \ge \dot{\varepsilon}_2 \ge \dot{\varepsilon}_3 = \dot{\varepsilon}_{\min}^{pl}$.

The quantity $g_{k=t,c}$ in this equation is defined as ratio between fracture energy $G_F$ and characteristic length $l_c$ of the finite element (FE) mesh and represents the dissipated energy density during the entire process of not only micro cracking, but localisation and softening until zero tensile resistance. Fracture energy can be used to define this dissipated energy per unit volume because $g_k$ cannot be given as a material property.

Furthermore, micro cracking and crushing in the concrete are represented by increasing values of the hardening variables. The evolution of the yield surface and stiffness degradation of the material are controlled by these variables. They are also related to the dissipated fracture energy required to produce micro cracks in the concrete.

### 4.3.4 Elastic stiffness degradation

The damage plasticity concrete model assumes that the elastic stiffness degradation is isotropic and characterized by a single scalar variable, *d* defined in equation (4-6).

In cyclic loading conditions the material damage variable *d* is governed by opening and closing of micro cracks formed from the initiation of the analysis as well as their interaction and is defined for multiaxial load conditions as:

$$(1-d)=(1-s_t d_c)(1-s_c d_t), \quad 0\le s_t, s_c \le 1 \tag{4-13}$$

in this equation only $s_t$ and $s_c$ are given in terms of the weight function $r(\hat{\bar{\sigma}})$ as:

$$s_t = 1 - w_t r(\hat{\bar{\sigma}}); \quad 0 \le w_t \le 1$$

$$s_c = 1 - w_c (1 - r(\hat{\bar{\sigma}})); \quad 0 \le w_c \le 1 \tag{4-14}$$

In CDP model it is assumed that in uniaxial load cycle as shown in Figure 4-8 only compressive stiffness is recovered when loading change from tension to compression. On the contrary, tensile stiffness is not recovered due to the developing of micro cracks and crushing in concrete material. This condition corresponds to $w_t$=0 and $w_c$=1 in above equation.

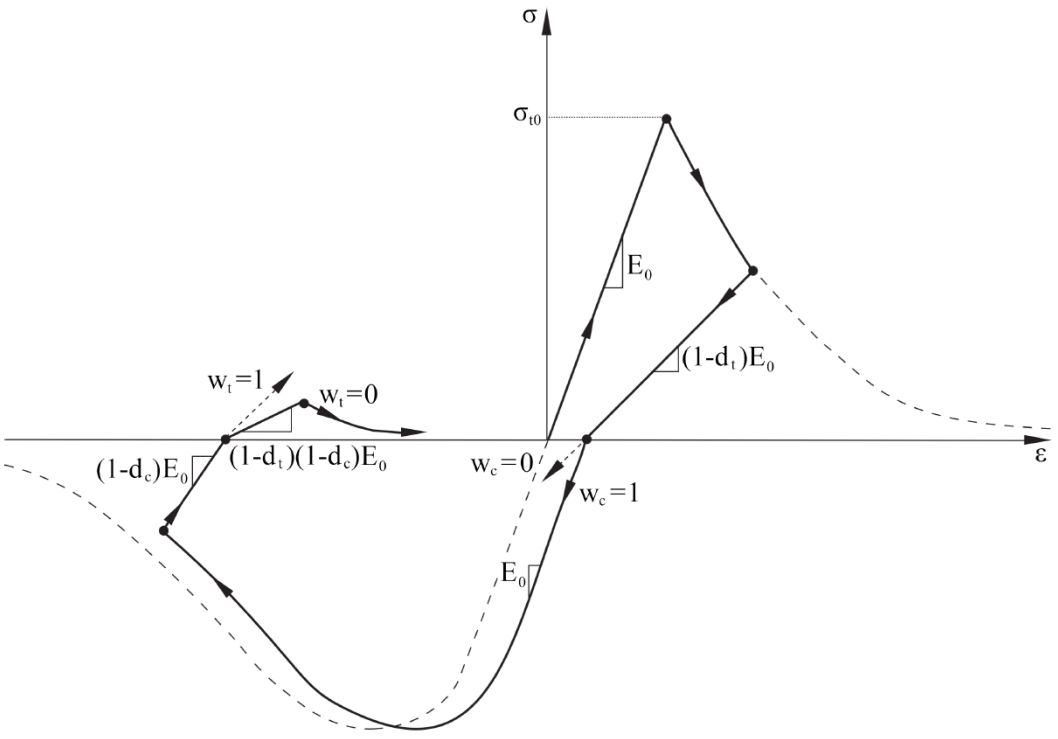


**Figure 4-8.** Uniaxial load cycle (Tension-compression-tension) (Simulia, 2016).

### 4.3.5 Yield function

In this section, the mechanical constitutive modelling of concrete using damage plasticity model which is initially proposed by Lubliner *et al.* (1989) and later modified by Lee and Fenves (1998) is presented. In effective stress space the yield function which is an isotropic, first degree homogenous scalar function with multi-hardening evolution, takes the form:

$$F(\bar{\boldsymbol{\sigma}}, \tilde{\varepsilon}^{pl}) = \frac{1}{1-\alpha}\left[\alpha I_1 + \sqrt{3J_2} + \beta(\tilde{\varepsilon}^{pl})\langle\hat{\bar{\sigma}}_{maz}\rangle - \gamma\langle-\hat{\bar{\sigma}}_{maz}\rangle\right] - \bar{\boldsymbol{\sigma}}_{\boldsymbol{c}}(\tilde{\varepsilon}^{pl}) \tag{4-15}$$

where

$\alpha$, $\beta$ and $\gamma$ are dimensionless material constants;

$I_1$ is the first stress invariant,

$J_2$ is the second deviatoric stress invariant,

$\bar{\sigma}_{\max}$ is the algebraically maximum eigenvalue of effective stress.

The function $\beta(\tilde{\varepsilon}^{pl})$ is given as:

$$\beta(\tilde{\varepsilon}^{pl}) = \frac{\bar{\sigma}_c\left(\tilde{\varepsilon}_c^{pl}\right)}{\bar{\sigma}_t\left(\tilde{\varepsilon}_t^{pl}\right)}(1-\alpha) - (1+\alpha) \tag{4-16}$$

where $\bar{\sigma}_t$ and $\bar{\sigma}_c$ are the effective tensile and compressive cohesion stresses, respectively. If the $\sigma_{\max} = 0$, i.e. biaxial compression condition then equation (4-15) is reduced to the well-known Drucker-Prager criterion. The coefficient $\alpha$ can be determined from the initial equi-biaxial and uniaxial compressive yield stresses, $\sigma_{b0}$ and $\sigma_{c0}$, as:

$$\alpha = \frac{\sigma_{b0} - \sigma_{c0}}{2\sigma_{b0} - \sigma_{c0}} \tag{4-17}$$

Typical experimental values of the ratio $\sigma_{b0}/\sigma_{c0}$ for concrete are in the range from 1.10 to 1.16, yielding values of $\alpha$ between 0.08 and 0.12.

The coefficient $\gamma$ enters the yield function only for stress states of triaxial compression, when $\bar{\sigma}_{\max} < 0$, and is defined as:

$$\gamma = \frac{3(1-K_c)}{2K_c - 1} \tag{4-18}$$

where $K_c$ is a parameter that defines the ratio of tensile meridian to the compressive meridian of second deviatoric stress invariant. A value of $K_c = 2/3$ which is typical for concrete, leads to $\gamma = 3$. Typical yield surfaces are shown in Figure 4-9 for the deviatoric plane and Figure 4-10 for the plane-stress condition.

In Figure 4-10, $\bar{p}$ is the hydrostatic pressure, which is a function of the first invariant $I_1$ ( $\bar{p} = -I_1/3$) and $\bar{q}$ is the von Mises equivalent effective stress ( $\bar{q} = \sqrt{\frac{3}{2} S:S} = \sqrt{3J_2}$ ).

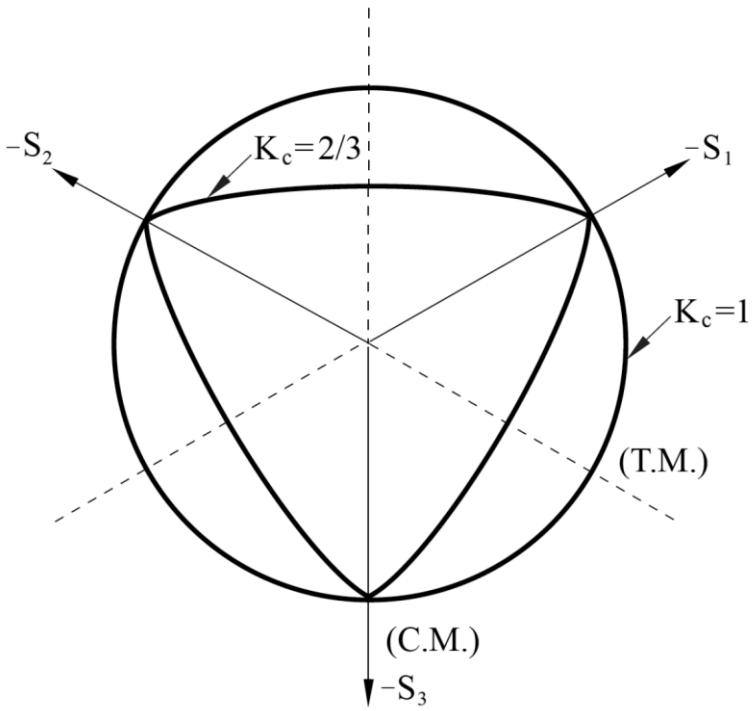


**Figure 4-9**. Deviatoric plane shows the yield surfaces in terms of different values of $K_c$.

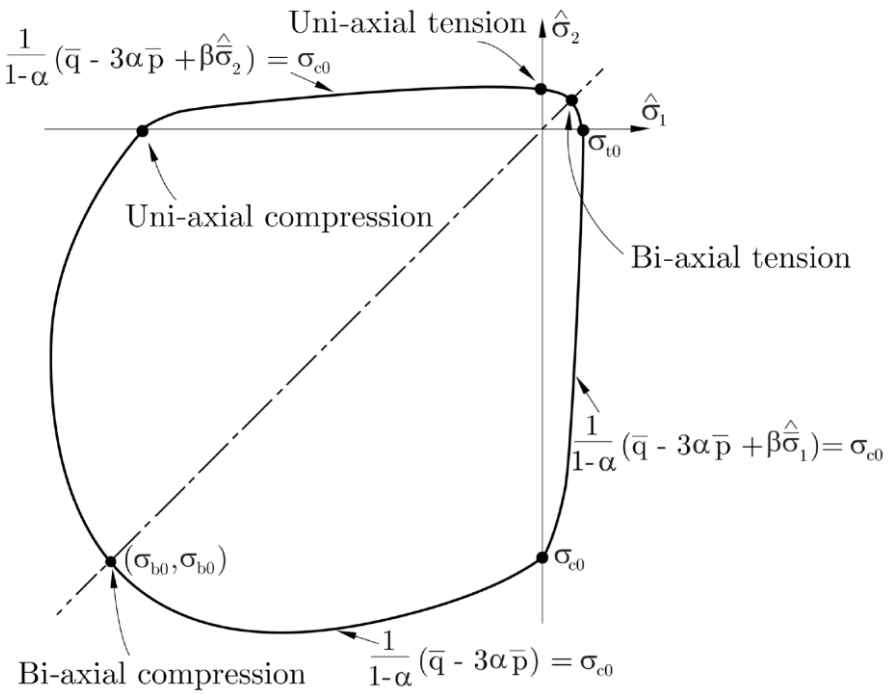


**Figure 4-10**. Yield surface for the in-plane stress condition. The formulation leads to an increase in compressive strength for biaxial compression.

### 4.3.6 Flow rule

The CDP model assumes non-associated potential flow for the plastic strain rate:

$$\dot{\varepsilon}^{pl} = \dot{\lambda}\frac{\partial Q(\bar{\boldsymbol{\sigma}})}{\partial \bar{\boldsymbol{\sigma}}} \tag{4-19}$$

where $\lambda$ is the nonnegative plastic multiplier. The flow potential $Q$ chosen for this model is the Drucker-Prager hyperbolic function:

$$Q = \sqrt{(\epsilon f_{t0}\tan\psi)^2 + q^2} - p\tan\psi \tag{4-20}$$

where $\psi$ is the dilation angle taken in the $p$-$q$ plane at high confining pressure; $f_{t0}$ is the uniaxial tensile stress as failure; $\epsilon$ is the eccentricity parameter which defines the rate at which the function approaches the asymptote (the flow potential becomes a straight line as the eccentricity approaches zero). The flow potential is continuous and smooth which ensures that the flow direction is uniquely defined. A family of these potential functions are shown in Figure 4-11.

In summary, the elastic-plastic response of the concrete damaged plasticity model is described in terms of the effective stress and the hardening variables:

$$\bar{\boldsymbol{\sigma}} = \boldsymbol{D}_0^{el}: (\boldsymbol{\varepsilon} - \boldsymbol{\varepsilon}^{pl}) \epsilon \{\bar{\boldsymbol{\sigma}} | F(\bar{\boldsymbol{\sigma}}, \tilde{\varepsilon}^{pl}) \leq 0\} \tag{4-21}$$

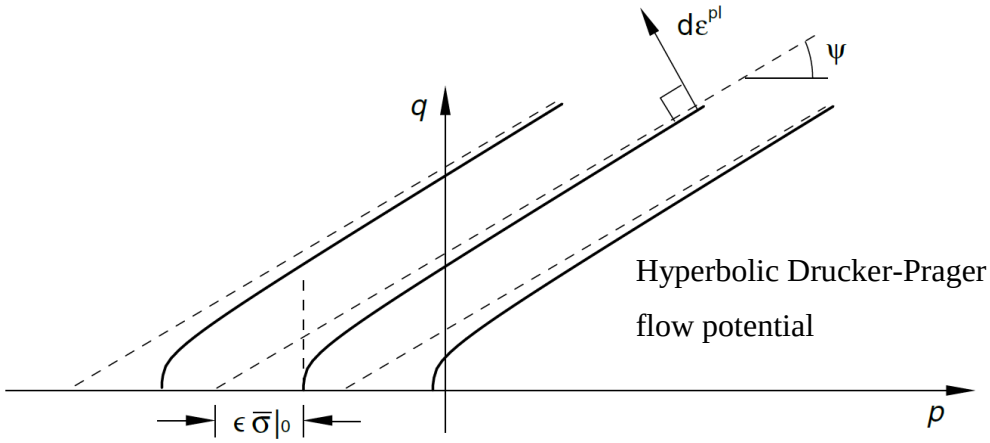


**Figure 4-11.** Family of Drucker-Prager hyperbolic flow potentials in the p-q plane.

In addition to the equation (4-21) the following relations from the Kuhn-Tucker complimentary conditions and the plasticity consistency conditions are applied, where $F$ in equation (4-15) and $\dot{\lambda}$ in equation (4-19) obey the following rules:

$$\dot{\lambda} F = 0; \dot{\lambda} \geq 0; F \leq 0 \tag{4-22}$$

This set of conditions insures the plasticity consistency conditions for loading/unloading. The Cauchy stress is calculated in terms of the stiffness degradation variable, $d(\bar{\boldsymbol{\sigma}}, \tilde{\varepsilon}^{pl})$ and the effective stress as $\boldsymbol{\sigma} = (1 - d)\bar{\boldsymbol{\sigma}}$ defined earlier in this chapter.

The constitutive relations for the elastic-plastic response, are decoupled from the stiffness degradation response, which makes the model attractive for an effective numerical FE implementation.

### 4.3.7 ASR concrete material modelling including damage plasticity constitutive model

In the elastic-plastic model of concrete involving the plastic strain, ASR strain and thermal strain, the total strain $\boldsymbol{\varepsilon}$ can be considered to be a sum of the elastic strain $\boldsymbol{\varepsilon}^{e}$, the plastic strain $\boldsymbol{\varepsilon}^{pl}$, the thermal strain $\boldsymbol{\varepsilon}^{th}$, and the strain due to ASR $\boldsymbol{\varepsilon}^{asr}$:

$$\boldsymbol{\varepsilon} = \boldsymbol{\varepsilon}^{e} + \boldsymbol{\varepsilon}^{pl} + \boldsymbol{\varepsilon}^{th} + \boldsymbol{\varepsilon}^{asr} \tag{4-23}$$

In the chemo-thermo-mechanical model, stress is given by:

$$\boldsymbol{\sigma} = (1 - \mathrm{d})\bar{\boldsymbol{\sigma}} = (1 - d)\boldsymbol{D}_{\boldsymbol{0}}^{\boldsymbol{e}}(\boldsymbol{\varepsilon} - \boldsymbol{\varepsilon}^{pl} - \boldsymbol{\varepsilon}^{th} - \boldsymbol{\varepsilon}^{asr}) \tag{4-24}$$

where $\alpha$, the concrete thermal coefficient and $\Delta\theta$ the temperature differences are used to define the thermal strains in this equation. The scalar degradation variable $d$ (total damage) is composed of ($d_{asr}$) the damage due to ASR and ($d_m$) due to mechanical loads, and is defined as:

$$d = 1 - (1 - d_{asr})(1 - d_m) \tag{4-25}$$

The nonlinear behaviour of concrete, rock and similar materials may be governed by stiffness degradation and not by permanent plastic deformation (Lubliner *et al.*, 1989). In concrete dams affected by ASR, however the nonlinearity from the stiffness degradation is important.

It is worth noting that the compressive stresses in most concrete structures are less than the compressive strength of the concrete, Hence the mechanical damage mainly occurs due to tensile stresses and equation (4-25) for damage is developed. The equation for computing $d_{asr}$ is already defined in section 3-4.

Finally, the implementation flowchart of the ASR model which is loosely coupled with the CDP constitutive modelling of concrete illustrated in Figure 4-12. This figure shows the relationships between variables in the SU-ASR code (**S**tellenbosch **U**niversity ASR FE-code) and explains the code input and output variables incorporated in the code.

## 4.4 Numerical implementation

ASR is a long term process and often continues for many years. As a result, a suitable time step size must be selected to insure sufficient accuracy of results and optimised computational time. The starting point of the analysis of the sequentially coupled problem of heat-diffusion and chemo-mechanical model is the solving of transient thermal analysis with initial boundary

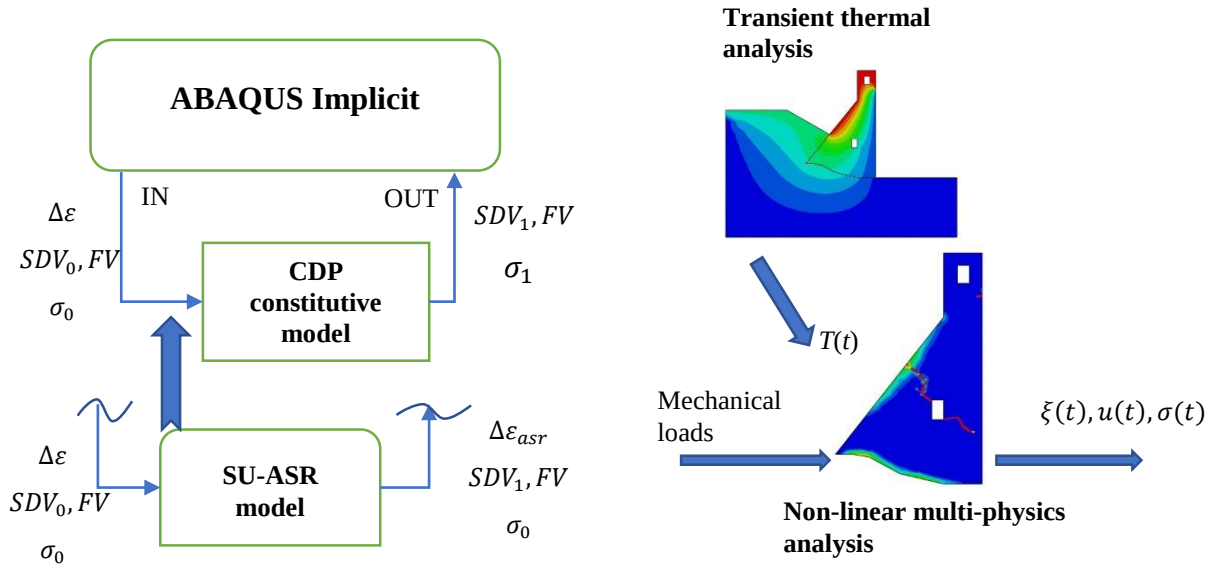


**Figure 4-12**. Numerical framework for the SU-ASR model coupled with CDP constitutive model for concrete material (SDV: Solution Dependent Variable, FV: Field Variable).

conditions. Then, the mechanical structural analysis is performed. This requires a number of parameters, among them: 1) the air temperature variations; 2) the spatial and temporal variation of the water temperature; 3) the concrete thermal properties and 4) mechanical properties of the concrete and damage-plasticity parameters such as the E-Modulus and Poisson's ratio, compressive and tensile nonlinear stress-strain/COD curves and damage variables in tension and compression. For thermal analysis, and the subsequent mechanical analysis, an appropriate analysis time unit or time increment, must be defined. The current code is implemented in an implicit framework in which Newtown's method as a numerical technique for solving nonlinear equations is used. Because, a non-associated plastic flow rule is used to develop the plastic strains, a non-symmetric numerical solver needs to be used in finite element modelling of concrete structures using the SU-ASR code.

## 4.5 Conclusion

In this chapter first, the nonlinear behaviour of concrete in tension and compression is discussed. The CDP model chosen in this research describe the cracking and crushing of concrete in different loading regimes. Material degradation is decoupled from the yield or failure mechanism which makes the model attractive for numerical modelling. The evolution of the degradation variable is governed by a set of hardening variables and the effective stress. The chemo-thermo-mechanical ASR model developed in chapter 3 is combined with CDP model of chapter 4 and a complete chemo-thermo-mechanical damage FE model is developed. In the next chapter, the model is validated by applying it to model and analyse typical problems on material and structural scale, the typical solutions of which are available in the literature.

# CHAPTER 5

# Verification and validation of the chemo-thermo-mechanical model

**Highlights:**

Validation of the Concrete Damage Plasticity (CDP) model on material level

Validation of Alkali Silica Reaction (ASR) model at a material scale

## 5.1 Introduction

This chapter presents the verification and validation of the proposed model to compute the effect of ASR in concrete dams. Two series of finite element models are developed. The first series aims to validate the CDP model in terms of mechanical loading and crack path detection in a three-point bending single-edge notched concrete beam. The second series presents the modelling of concrete specimens affected by ASR in the free stress state and the uniaxial stress state. Finally, a comparison of the results from numerical modelling and laboratory tests is presented and discussed. The results obtained with the numerical models based on this research compare well with the available results based on experimental research found in literature.

## 5.2 Concrete Damage-plasticity model validation

The application of CDP model to the selected experimental tests and the comparisons of the results (numerical computations and experiments) prove the usefulness of the CDP constitutive model to capture the nonlinear behaviour of concrete in particular softening and cracking. In this section results from laboratory tests on a single-edge notched concrete beam subjected to three-point bending are compared with the numerical results obtained for the model developed

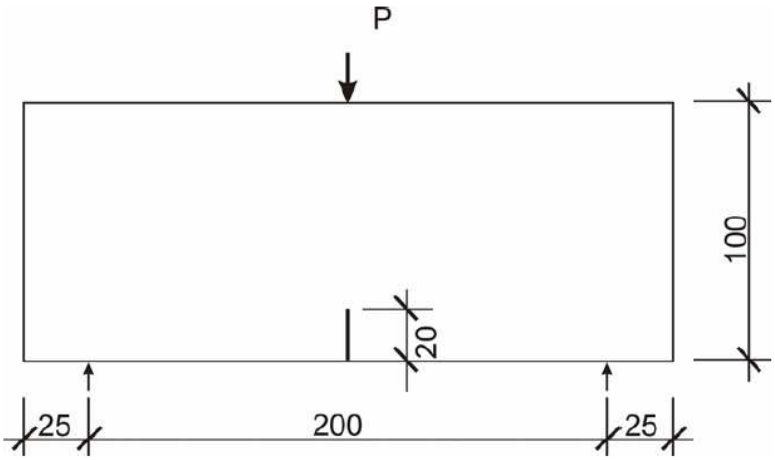


**Figure 5-1**. The geometry of three-point bending single-edge notched concrete beam (Davies, 1996).

in this research. The geometry of the three-point bending beam specimen is presented in Figure 5-1. All dimensions are given in millimetres. The thickness of the beam is 100 mm.

The mechanical behaviour of the material used for purpose of this modelling is shown in Figures 5-2 and 5-3 for tensile-COD and compression-strain, respectively. The concrete material behaviour in tension and compression shown in these figures is represented using the relations set out in chapter 4 i.e. the stress-strain relationships in tension and compression. In this experimental test concrete grade C30/37 is used. The elastic modulus and Poisson's ratio are considered as 33 GPa and 0.19, respectively. Table 5-1 summarises the CDP parameters used in the FE model of the three-point single edge notched beam in this experiment.

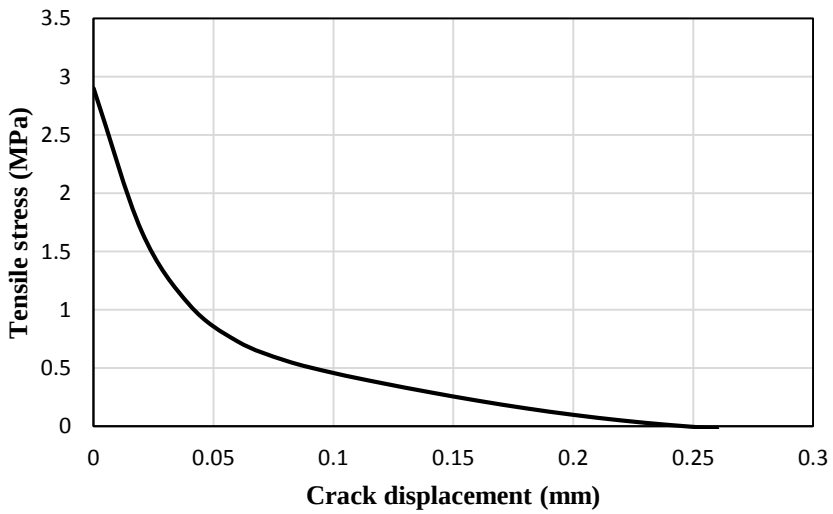


**Figure 5-2**. Tensile stress vs. crack opening displacement for concrete grade C30/37.

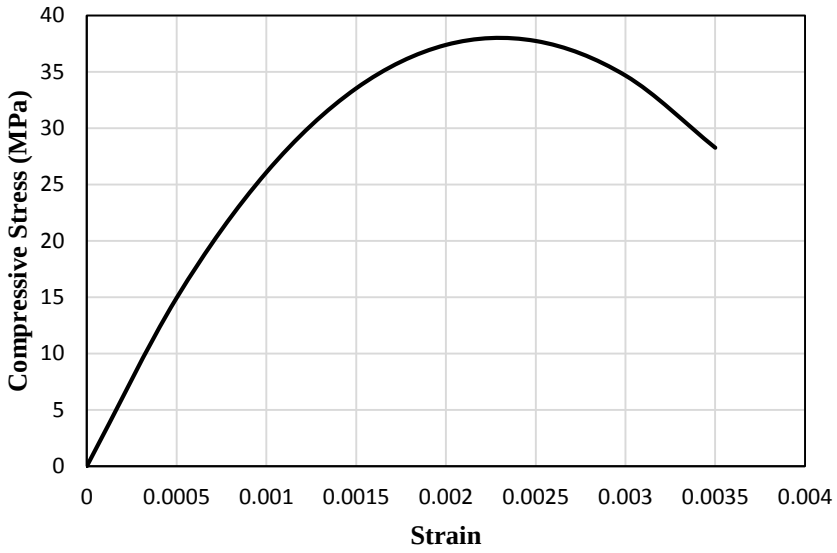


**Figure 5-3**. Compressive stress vs. strain for concrete grade C30/37.

**Table 5-1**. Parameters used to define the CDP model in ABAQUS.

| $\epsilon$ | $\psi$ | $f_{b0}/f_{c0}$ | $K_c$ |
|---|---|---|---|
| Eccentricity | Dilation angle | Stress ratio | - |
| 0.11 | 36.1 | 1.16 | 0.667 |

The FE model consists of 456 three-node linear plane stress elements. The finite element mesh used in the numerical modelling is shown in Figure 5-4. To analyse the effect of cracking in the vicinity of the notch-tip, a finer mesh (2X2 mm) is used. The size of the mesh is determined using the method introduced by Bazant and Oh (1983) to avoid finite element analysis mesh dependency. Equation (5-1) shows the maximum element length according to the fracture energy regularization method:

$$L_{max} < \frac{E.G_F}{f_t^2} \tag{5-1}$$

Using equation (4-2) to determine the fracture energy and tensile strength 2.9 MPa showed in Figure 5-2, the required maximum mesh size was computed to be less than 500 mm. Limiting the maximum size of element in the numerical FE model ensures that a sufficient amount of energy is dissipated in each finite element before cracking occurs and the snap-back problem is avoided. The total length of the specimen in this example is 250 mm and elements that are below the maximum element length are naturally selected.

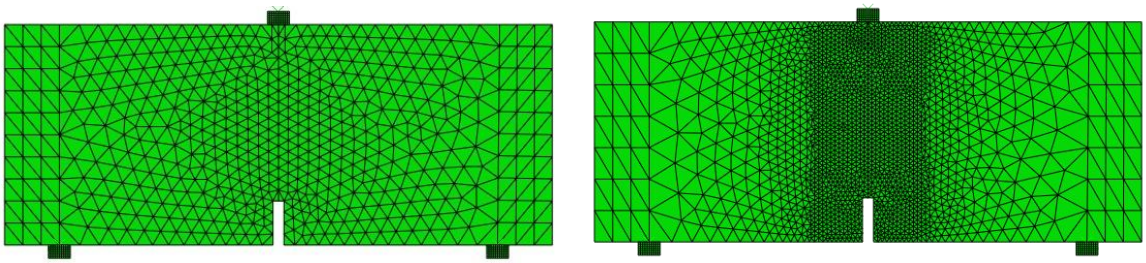

(a) (b)

**Figure 5-4**. Finite element mesh used for the analysis, a) FE mesh with 5X5 mm mesh size, b) FE model with fine mesh 2X2 mm.

### 5.2.1 Results and discussion

Figure 5-5 presents the load-displacement curve comparison of the two different meshes used in this analysis. In this figure both meshes result in an ultimate force about 5.27 kN which demonstrates an equal force-deflection response in this modelling.

The results of the FE modelling of the three-point notched beam problem are illustrated in Figure 5-6. In this figure, tensile damage is presented at four time steps during the load application. The numerically computed crack pattern is similar to that observed in the experimental model (Davies, 1996). A single dominant crack appears in the three-point bending concrete beam specimen. The experimental pattern of the fracture zone is shown in Figure 5-7 for the same instances. In addition to the main crack, a small region in the top corner of the notch shows approximately 25% of tensile damage. This rather represents the initiation of micro cracking in this region but not opening. The tensile damage contours for fine mesh are shown in Figure 5-8. The computed crack path is similar to the curved from experimental analysis.

Typically, smaller elements will produce a more brittle response if the crack band approach is used. Crack band is related to the element size, so that the actual fracture energy is dissipated in the element ($G_F = g_f \times l_c$). For crack band theory to correctly regularize the computed cracking path, a single row/column of elements must become plastic and dissipate fracture energy. In a physical notched beam test, there is a single crack, therefore a double row of (smeared) cracks is not physically encountered.

In larger structures such as dam wall, it might be multiple cracks arise, leading to unrealistic, unphysical high energy dissipation. Hence, single elements along the crack path becoming plastic would indicate a reasonable computed crack path. However, the other issue of crack orientation is not completely solved with crack band theory. The refined regularization methods such as XFEM (Extended Finite Element Method) and rate-dependent material models fall outside the scope of this research. Finally, in the next chapters the ASR model is coupled with concrete damage plasticity constitutive law and is used to model and analyse the actual dams, the crack paths are scrutinized and generally only a single row of elements become plastic.

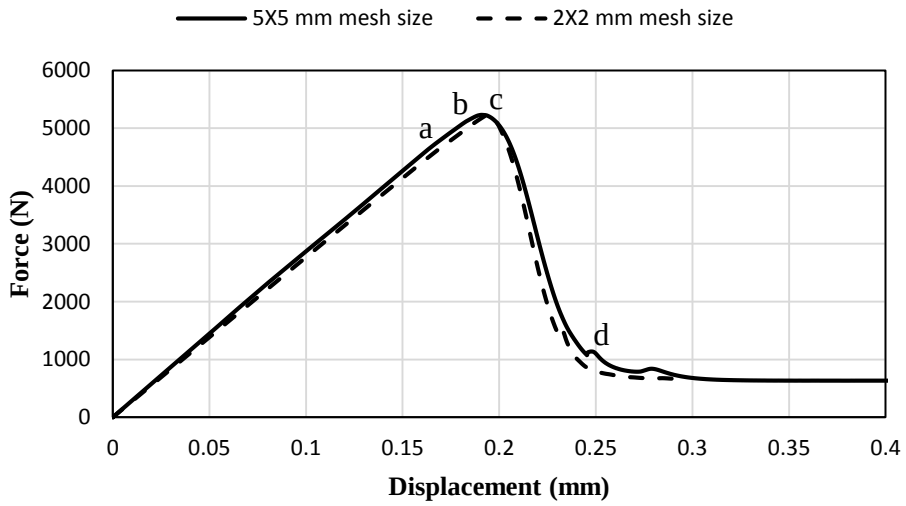


**Figure 5-5**. Load vs. displacement for the numerical modelling of the beam with notch for two set of mesh, 5X5 mm mesh size and 2X2 mm mesh size.

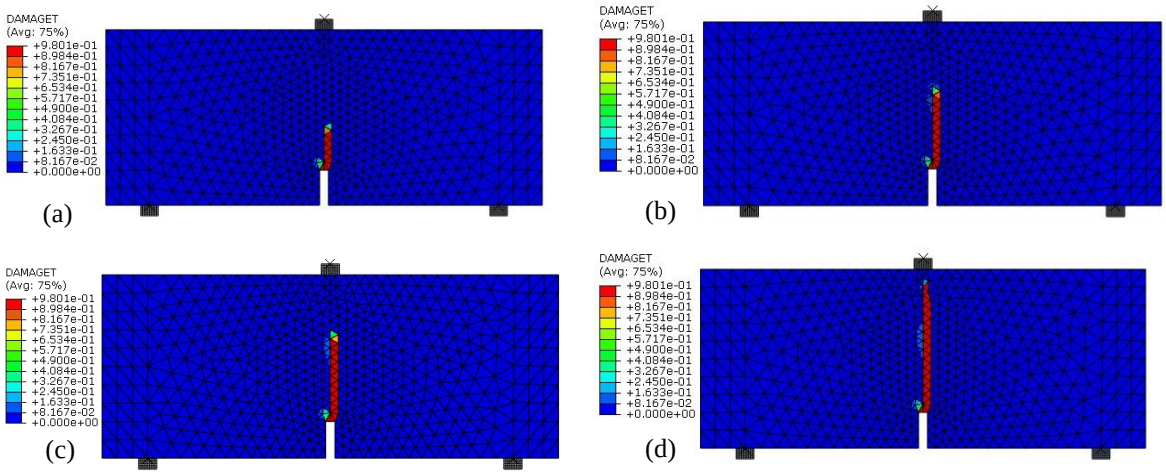


**Figure 5-6**. Results of tensile damage variable for mesh size 5X5 mm of the FE analysis of a notched beam at different stages.

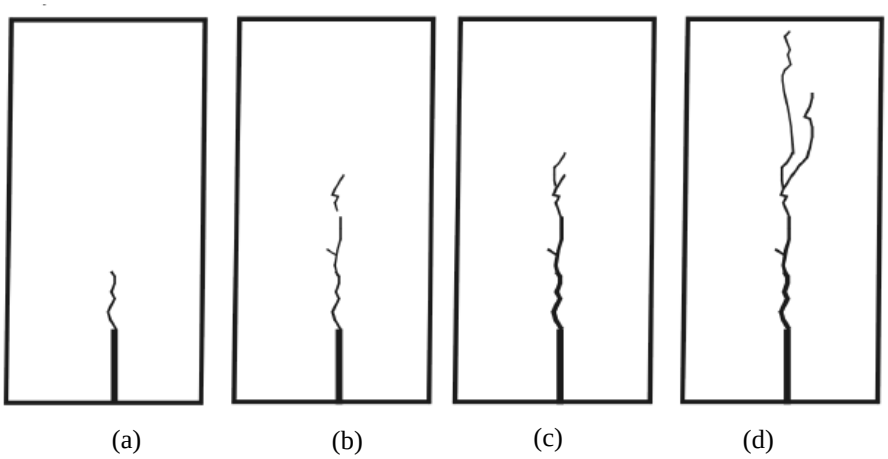


**Figure 5-7**. Fracture path according to the experiment at various time steps (Davies, 1996).

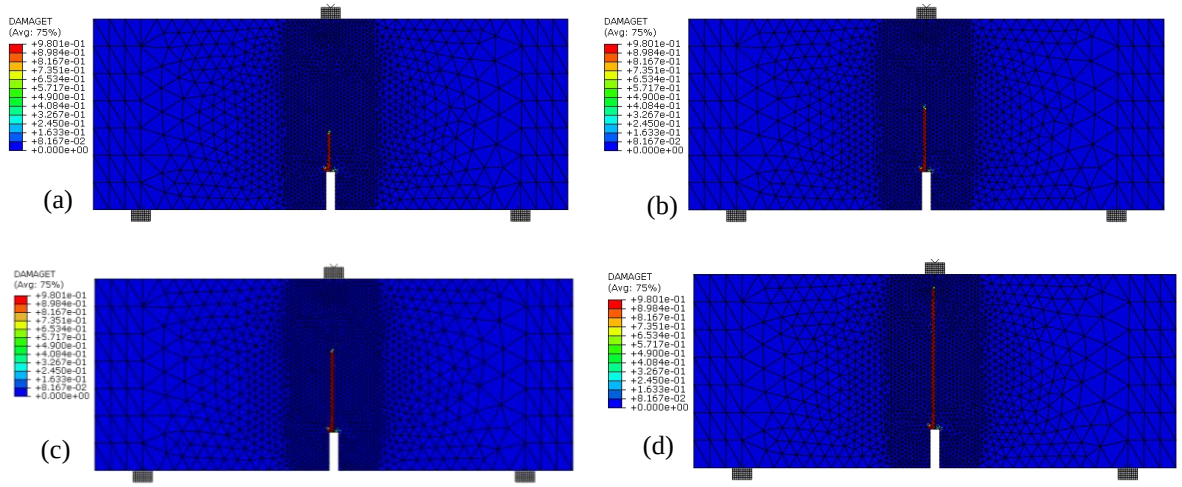


**Figure 5-8**. Results of the tensile damage variable for mesh size 2X2 mm of FE model for the notched beam at various stages.

Finally, Figure 5-9 shows the load-displacement curve for the beam without a notch in three-point bending. The ultimate load is equal to 12.98 kN which is in agreement with the experimental peak obtained by Davies (1998), as summarised in Table 5-2.

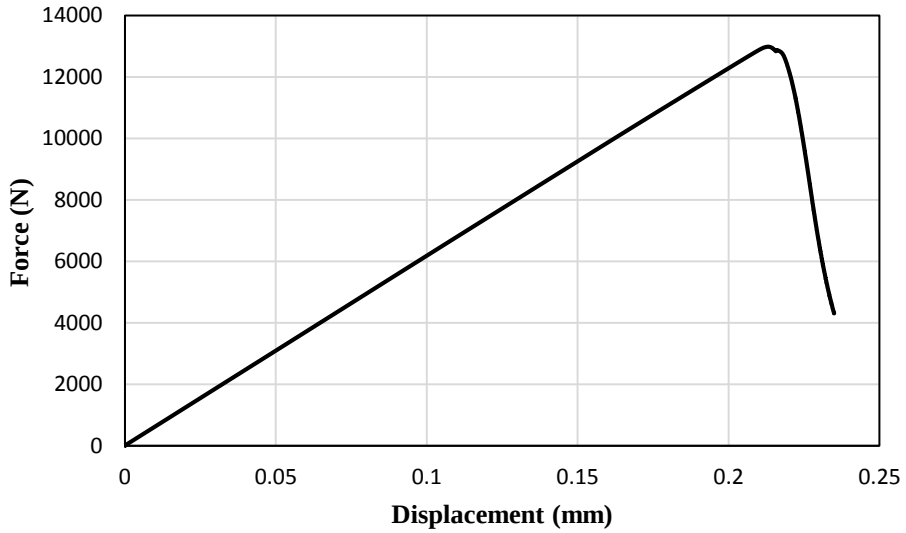


**Figure 5-9**. Load vs. displacement for the numerical modelling of the beam without a notch.

**Table 5-2**. Comparison of the numerical results with experimental tests.

| | Beam model with notch | | Beam model without notch | |
|---|---|---|---|---|
| Results | Maximum Force (kN) | Displacement (mm) | Maximum Force (kN) | Displacement (mm) |
| Numerical modelling | 5.27 | 0.19 | 12.98 | 0.25 |
| Experiment (Davies, 1996) | 5.48 | 0.20 | 13.28 | 0.26 |

## 5.3 ASR model validation on the material level

In order to calibrate and validate the proposed model, references have been made to the experimental tests carried out on small concrete samples by Multon and Toutlemonde (2006). These tests were performed using accelerated methods. The experimental values of Young's modulus and Poisson's ratio given in (Multon & Toutlemonde, 2006), namely $E$=37300 MPa and $v$=0.22. Figure 5-10 shows the loading conditions and the 3D finite element mesh. These cylindrical specimens are 130 mm in diameter and 240 mm in height. They behave anisotropically and have different experimental axial and radial strains under the stress-free condition. These differences are mainly caused by the casting procedure (Multon *et al.*, 2005). According to the authors of the experimental programme, the main source of the inhomogeneities in the samples is due to the vertically pouring direction of the concrete which caused an alignment of the aggregates along planes perpendicular to the longitudinal axis. Similar anisotropic behaviour is reported by Larive (1998). This material anisotropy is not

considered in the proposed model. The duration of the tests were 450 days and the temperature was $\bar{\theta}_0 = 38^{\circ}C$. Also, the strains of the samples are measured using an ad-hoc device which is developed for the experiment. Applied stress and resulting strain were measured separately. The sensors are installed on the surface of the concrete at 3 levels of cylinder (bottom, middle, top) and at 10 regularly spaced angular locations to extract the mean radial strain based on the diameter variations. Also, vertical strains are measured between two metallic targets glued to the top and bottom of the specimens.

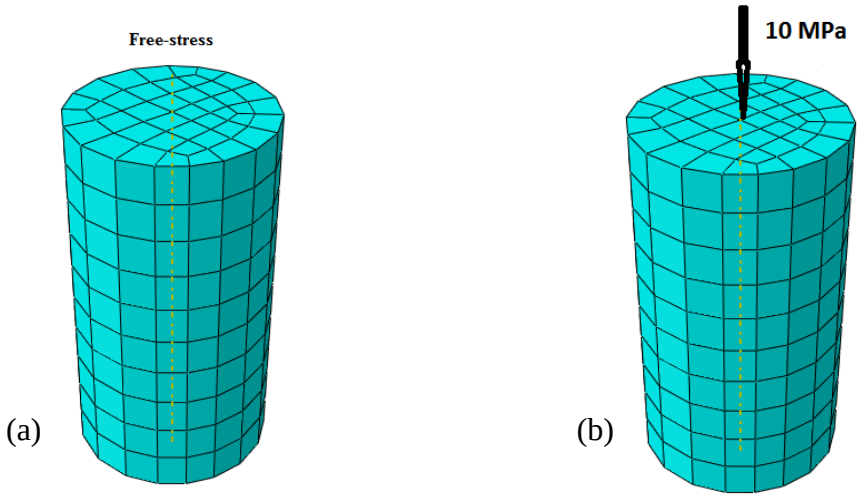


**Figure 5-10**. Multon's samples used for model calibration in free expansion and computing axial and radial strains showing specimens for a) free expansion b) 10 MPa axial compression.

The strains from the experiment without and with axial loading condition versus time duration of the tests are shown in Figures 5-11 and 5-12. The computed strains are compared with the experimental results. It is worth noting that the strains in axial and radial directions show different final values mainly because of the casting procedure (Note: The specimens are casted in axial direction).

Furthermore, Figure 5-11 shows a comparison of computed strains of the samples under free axial loads. In this curve the strain form creep is extracted in the experimental results. The volumetric strain for cylindrical sample is computed according to $\varepsilon^{vol} = \varepsilon^{axial} + 2\varepsilon^{radial}$ (Pourbehi *et al.*, 2018) and the parameters of ASR kinetics are estimated by inverse analysis based on the mean volumetric strain measured and from a stress-free experiment. These parameters are shown in Table 5-3. The result is compared with the mean volumetric strain measured from the experiment (dashed line in Figure 5-11 corresponds to $\varepsilon^{vol}/3$). As it is

expected the computed mean volumetric strain lays between the axial and radial strain curves and shows a good agreement with the measured data. Then, the model is used to capture the axial and radial strain using the same $\tau_l$ and $\tau_c$ reported in Table 5-3, but different values for $\beta$, each one fitting data along the radial and the axial direction. These values of beta are $\beta = 0.24$ % and $\beta = 0.31$ % for radial and axial respectively. The radial and axial strains are in a good agreement with the experimental results as shown in Figure 5-11. The axial strain from free-stress test after 400 days is 0.09% while radial is 0.06%.

**Table 5-3**. Parameters governing ASR volumetric expansion determined by inverse analysis at $\overline{\theta}_0 = 38^{\circ}C$.

| Parameter | value |
|---|---|
| $\tau_l$ (days) | 120 |
| $\tau_c$ (days) | 70 |
| $\beta$ (%) | 0.28 |

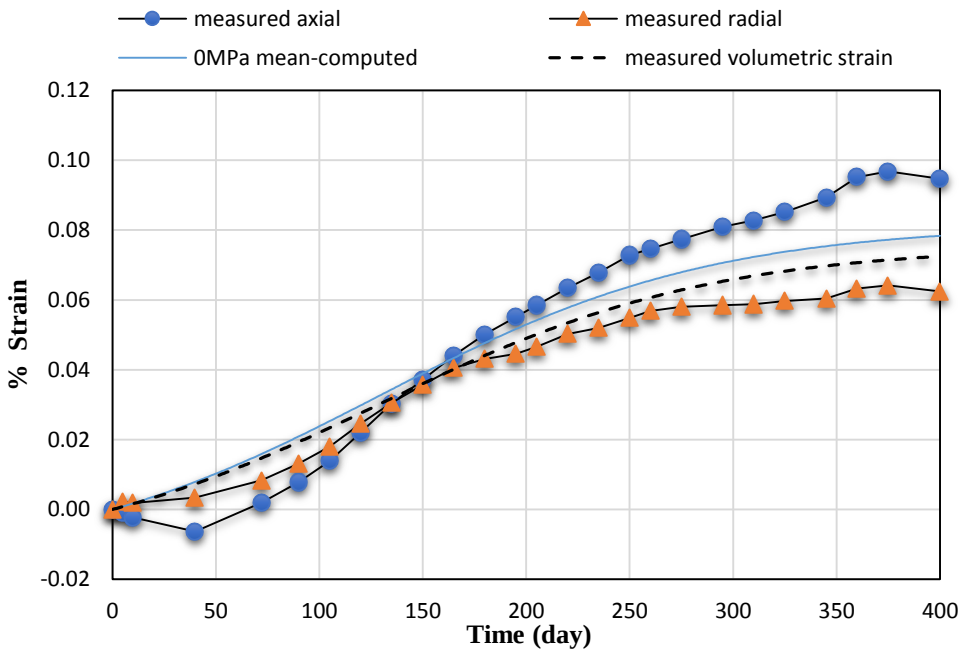


**Figure 5-11**. Experimental axial, radial and mean volumetric strains and computed mean volumetric strain for the expansion tests without stress.

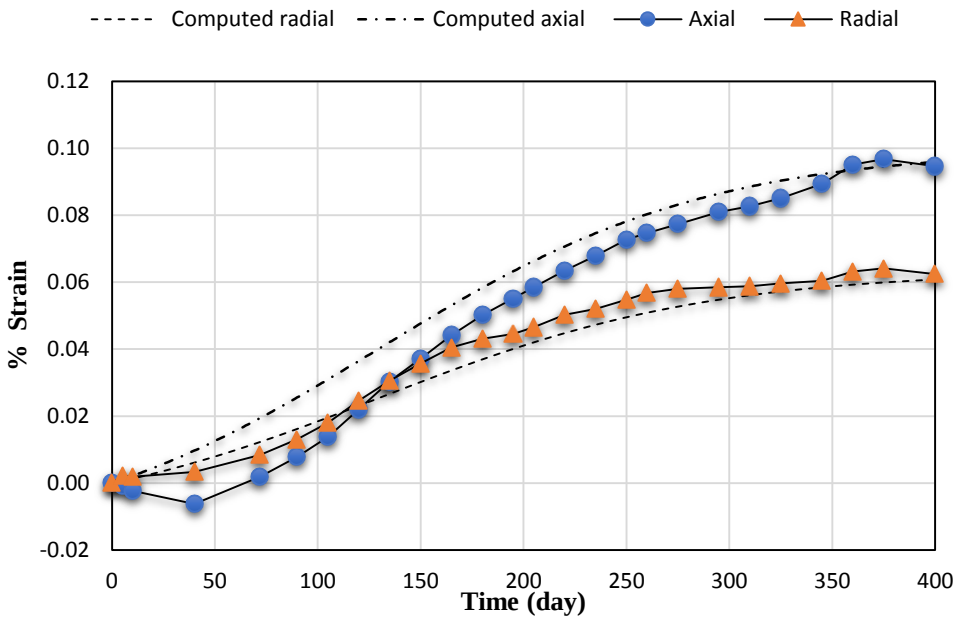


**Figure 5-12**. Computed and experimental axial and radial strains for the expansion tests without stress.

One of the major effects confirmed in this test is the effect of stress state in axial direction in comparison with free stress tests. For the modelling of the test with axial stress which implies a confining stress in vertical direction, use will be made of the ASR parameters in Table 5-3, calibrated on the mean volumetric strain as shown in Figure 5-12. Accordingly, when 10 MPa axial load is applied the axial strain is reduced to 0.02% while the radial strain is increased to 0.09% confirming that the volumetric strain is transferred to the less compressed direction. See Figure 5-13.

It is worth noting that, in both specimens the volumetric strain is about $\varepsilon^{vol} = 0.21$ %, which is in good agreement with the assumption that ASR strain is volumetric and transfers to the less compressed direction. Finally, as shown in Figures 5-11, 5-12 and 5-13 the model reproduces the expansion strains in all cases to a reasonable level and thus validates it on the material scale.

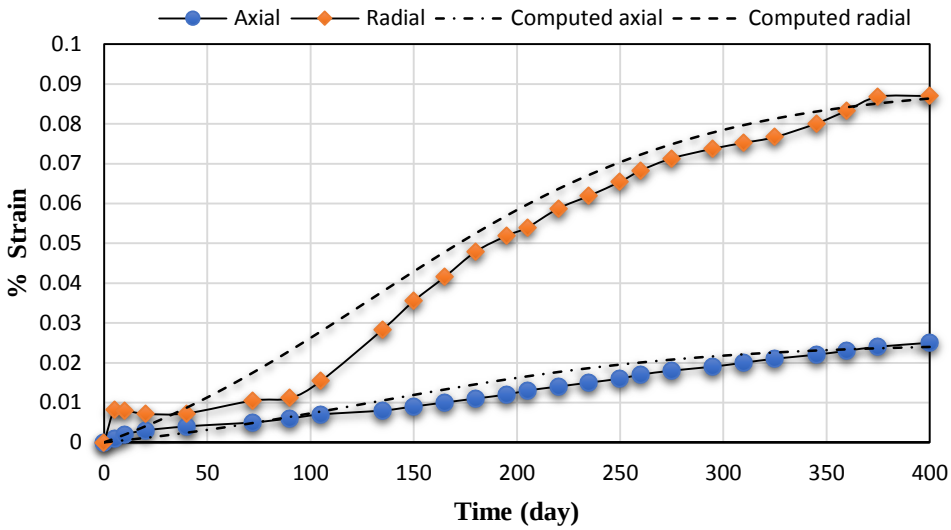


**Figure 5-13**. Computed and experimental axial and radial strains for the 10 MPa axial compression tests.

## 5.4 Summary

This chapter is devoted to validation of the proposed model both in mechanical and ASR analysis. First the mechanical model using concrete damage plasticity (CDP) model is validated by performing a three-point bending of single-edge notched of concrete beam. The FE model could predict the crack path and the load-displacement curve in good agreement with the experiment. Second, the SU-ASR model was validated on the material scale by considering the effect of confinement from external stress. The model could successfully predict the anisotropy associated with the samples developed in the laboratory. In addition, it is confirmed in this chapter that ASR could be considered as a volumetric strain which transfers to the less confined direction when the samples are under external stresses.

# CHAPTER 6

# Analysis of the concrete dam structures affected by ASR

**Highlights:**

Transient thermal analysis

Fontana dam

Kleinplaas dam

ASR and service loads (gravity and hydrostatic loads)

## 6.1 Introduction

In this chapter the modelling of two well-known concrete dams affected by concrete expansion due to ASR is undertaken. The chemo-thermo-mechanical damage model is used to analyse the cracking behaviour of these dams due to ASR. Firstly, numerical modelling of the Fontana dam is considered. Then, Kleinplaas dam which is located in the Jonkershoek River in Stellenbosch municipal area and affected by ASR is analysed. Both analyses are performed to validate the SU-ASR model.

## 6.2 ASR analysis of Fontana dam

The Fontana dam, is a concrete gravity dam with a height 147 m, crest length of 720 m and a thickness at the basis of the wall of 114 m. Its construction was completed in 1944, and it is located in the Tennessee River in North Carolina, United States. Only 4 years later, in 1948, a pattern of map cracking together with upstream movements were observed in the parapets and this continued to develop over a number of years.

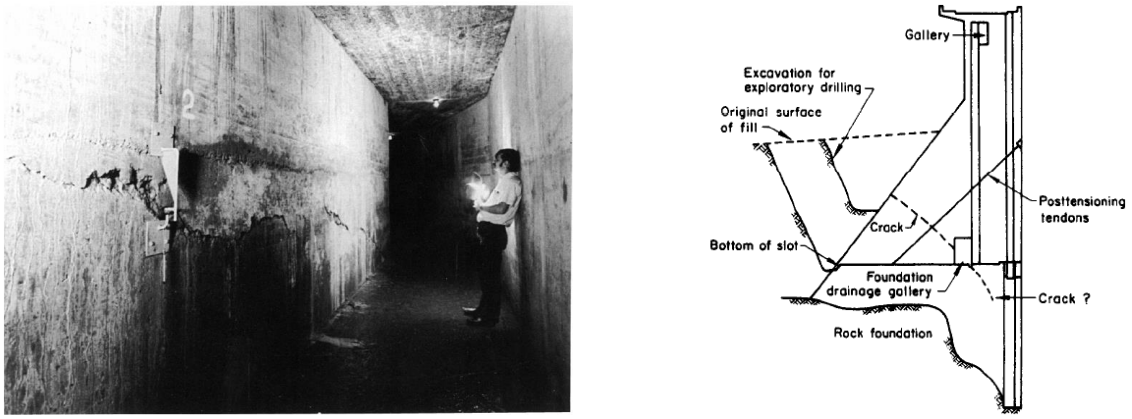


(a) (b)

**Figure 6-1**. Fontana dam a) crack inside gallery in left flank b) predicted crack (after Ingraffea, (1990)).

During the structural inspection that was performed due to increasing concerns about the safety of the dam by 1972, cracking was found inside the foundation gallery near the left flank as shown in Figure 6-1 a (Ingraffea, 1990). In addition, the petrographic analysis revealed symptoms of ASR and micro cracks in the dam aggregates with deposits of gels from alkali silica reaction. The chemo-thermo-mechanical model (SU-ASR) is used to simulate and interpret the ASR phenomenon in the Fontana dam. The dam wall section is analysed using the numerical model proposed in this study, in order to evaluate the pattern generated by mechanical loads plus strains from ASR.

### 6.2.1 Thermal analysis of Fontana dam

Temperature history is the key factor driving the ASR in massive structures such as dams (Ulm *et al.*, 2000). Therefore, before performing mechanical analysis it is necessary to determine the temperature field in space and time. By assuming an initial condition for temperature $\theta_0$ at time $t_0$ at each integration point of the FE model of the dam, the computer code is used to solve the transient thermal analysis problem:

$$\frac{\partial(\theta-\theta_0)}{\partial t} = D_\theta \frac{\partial^2(\theta-\theta_0)}{\partial x^2} \tag{6-1}$$

where $D_\theta = k/C$ denotes the thermal diffusivity (i.e., conductivity $k$ divided by the volumetric heat capacity $C$). In order to determine the initial temperature, a steady-state analysis considering the average temperature during one cycle is performed. The results, from this analysis are used as the boundary condition for the subsequent transient analysis. The results from thermal analysis are used in chemo-thermo-mechanical analysis through defining a predefined field temperature variation in space and time during the mechanical analysis. The SU-ASR Abaqus code uses the temperature value at each integration point of the FEM model to compute the reaction extent and consequent ASR strains.

Sloan and Abraham (1978) have investigated three different gravity blocks of the Fontana dam. One of the main blocks that suffered from severe ASR is Block 35 with a height of 36 m. See Figure 6-2. It is worth noting that the crack which was observed during the inspection is mainly located in this block. This block is near the left flank of the dam. In this analysis, the downstream filled-soil and the rock foundation are also considered in the thermal analysis as they have different conductivity and thermal diffusion properties compared to concrete material. The thermal and mechanical properties of the dam-filled soil-foundation system are listed in Table 6-1. A preliminary heat diffusion analysis is performed including the downstream soilfill, rock foundation and concrete domains. Seasonal temperature variations for the upstream and downstream surfaces of the dam are incorporated in the transient thermal analysis and are shown in Figure 6-2.

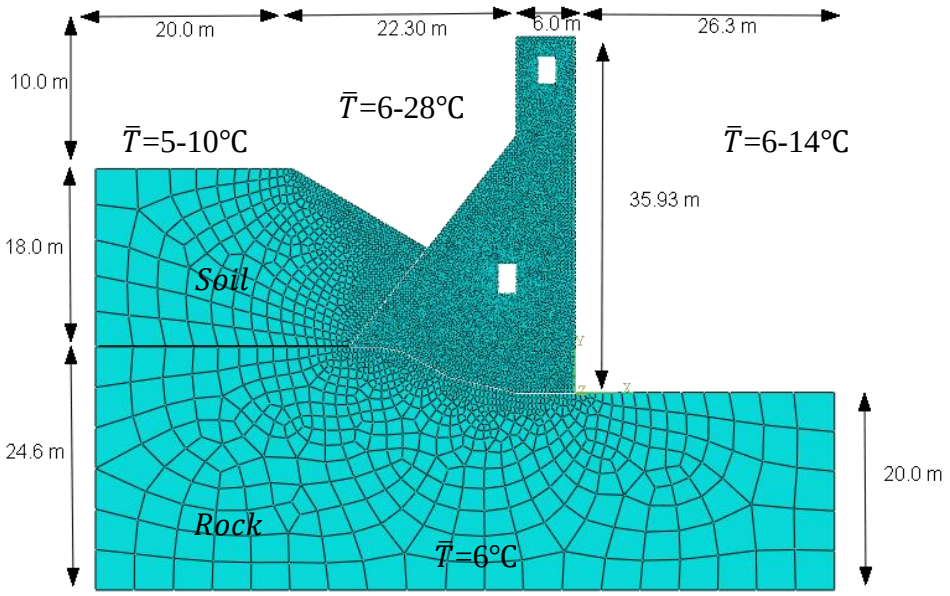


**Figure 6-2**. Geometry and FE model of Fontana dam and temperature values used for the thermal analysis.

**Table 6-1**. Material properties of the Fontana dam structure, foundation and soil fill.

| | Young's modulus $E_0$ (GPa) | Poisson's ratio $\nu$ - | Tensile strength $f_t$ MPa | Fracture energy $G_F$ (N/m) | Thermal conductivity $\kappa$ (W/(m K)) | Specific heat $c$ (KJ/ (kg K) | Thermal expansion coefficient $\alpha$ ($10^{-5}$) |
|---|---|---|---|---|---|---|---|
| **Concrete** | 22.0 | 0.17 | 2.1 | 200.0 | 1.75 | 0.75 | 1.0 |
| **Rock** | 20.0 | 0.25 | - | - | 0.75 | 0.85 | 0.5 |
| **Soil fill** | 0.15 | 0.2 | - | - | 0.55 | 1.00 | 0.5 |

In typical commercial FE codes such as Abaqus (Simulia, 2016) the solution for the steady-periodic heat diffusion problem is not available and a time consuming transient analysis needs to be performed until the temperature oscillations reach stable level over the whole FE model. Instead of this, according to the procedure which is mentioned in section 6.2.1, the initial temperature field $\theta_0$ is sought using an average temperature during one season for upstream and downstream faces of the dam. See Figure 6-2. Then this initial temperature field in the dam is used to find seasonal temperature variations in space and time by performing a transient analysis for 10 years, using seasonal temperature data shown in Figure 6-3. The initial temperature field is shown in Figure 6-4 and is obtained using an average temperature for the upstream, downstream, filled-soil material and foundation boundary surface areas.

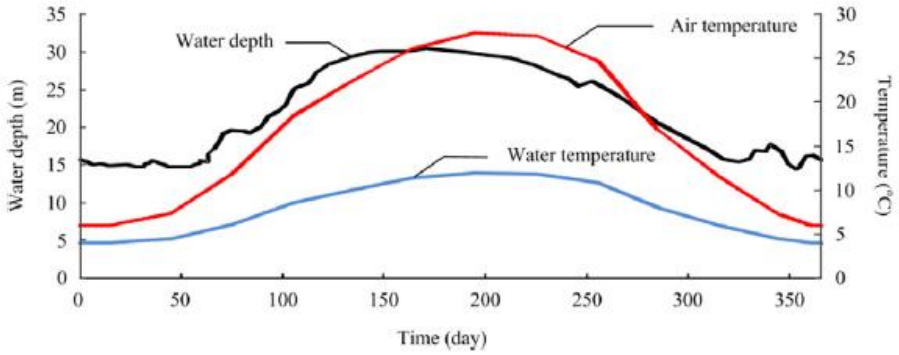


**Figure 6-3**. Seasonal variation of air and water temperature for performing the transient thermal analysis.

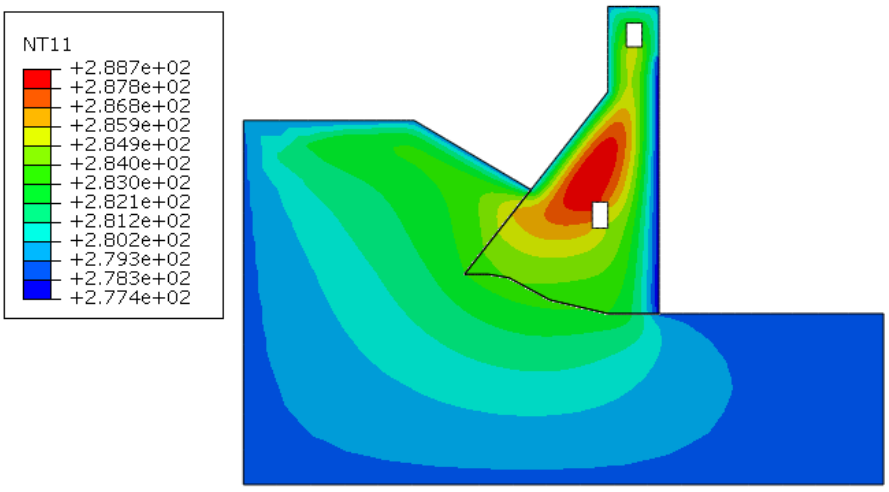


**Figure 6-4**. Computed initial temperature field in Kelvin for the Fontana dam. This temperature is used as an initial condition for transient thermal analysis.

### 6.2.2 Chemo-mechanical analysis

For the mechanical analysis, 4500 4-node quadrilateral plain strain elements of type CPE4R are used with reduced integration. Service loading namely the gravity load, seasonal temperature variations and hydrostatic pressure are applied. For purpose of simplicity and reducing the cost of analysis, only the dam structure is modelled in the mechanical analysis and the soilfill and foundation are not modelled. A fixed boundary condition is applied along the dam foundation.

No monitored values of the displacements of the ASR affected dam are available to determine the ASR kinetics parameters for use in the models used for this research. Hence, the cracking patterns which are available in the literature are considered to identify these parameters using an inverse analysis. They are taken as: (i) the latency time $\tau_l(\theta_0)=170$ days (ii) the characteristic time $\tau_c(\theta_0)=70$ days and (iii) and the maximum volumetric expansion strain $\beta$=0.3%.

Figures 6-5 illustrates the development of ASR kinetics and associated tensile damage within the considered dam; spatial variation of the kinetics (first column) and tensile damage (second column) are shown at different instants along the study period of about 10 years. At the beginning, the temperature increases through a thin layer from downstream and gradually diffuses into the dam body. The temperature activates the kinetics of the reaction and associated

strains purely from chemo physical activation of ASR appear. Because of the available constraints such as stress state from gravity and hydrostatic loads and also natural boundary conditions, these expansive strains increase the compressive stresses along a narrow band which gradually moves into the dam body. As a consequence of strain compatibility, the internal core of the dam must release the fracture energy through the increase in tensile strains and subsequent crack opening as shown in Figure 6-5a. Furthermore, when kinetics of the reaction at this band reaches the asymptotic value, these strains exceed the tensile strength of the concrete and therefore cracks open. The ASR progresses further, and after 8 years, another crack zone appears on the lower right side of the gallery and initially propagates at a similar slope as the first cracks but soon after turns toward the rock foundation upstream of the dam. See Figure 6-5b. It is worth noting that in the model this crack remains stable during next phases of the analysis. This mechanism is likely due to the fact that the upstream side of the dam is not exposed to a high temperature gradient and kinetics of the ASR is not activated during these years. From Figure 6-5c, it can be observed that the model predicts initiation of another localized zone with a crack opening in the downstream face of the dam. These findings are in good agreement with observed cracks inside the gallery as shown in Figure 6-1b. This crack propagates toward the internal gallery and finally intersects with the older crack. One can interpret that after 8 years, the ASR concentration reaches the gallery and causes high compressive stresses inside the dam. Irreversible plastic strains and cracks in the downstream face are basically due to strain compatibility with high constraining stresses around the gallery.

In order to evaluate the global behaviour of the dam structure, it is also important to assess the strain rate and displacements of the dam at the crest level. Figures. 6-6 and 6-7 illustrate the strain rate, horizontal and vertical displacements at this level. From these figures it is evident that the dam crest has experienced a constant crest displacement in the downstream direction of about 4.5 mm/year.

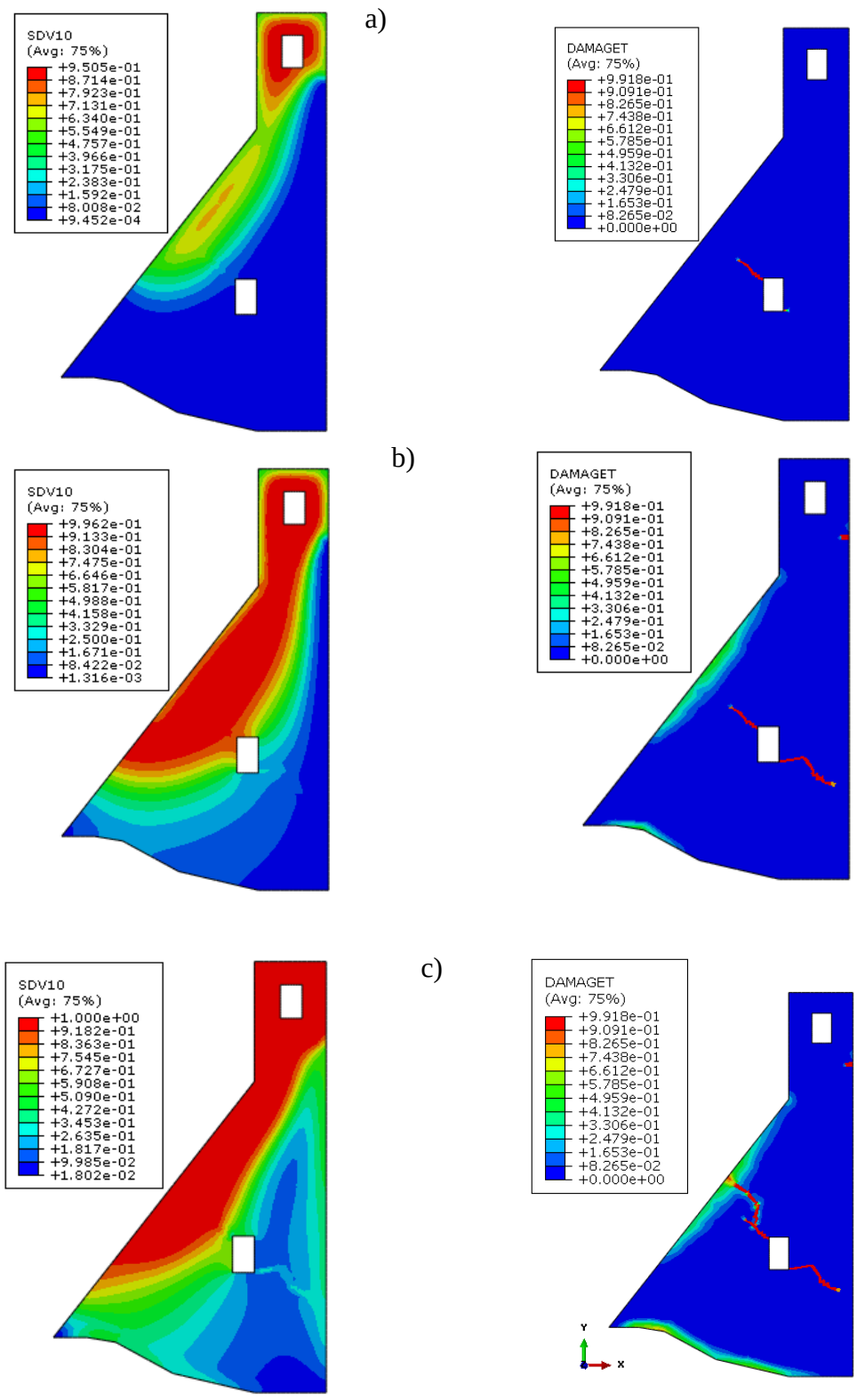


**Figure 6-5**. Contour of the reaction extent and tensile damage, a) after 4 years, b) after 8 years, c) after 10 years, (note:SDV10 represents a solution dependent variable which considered in SU-ASR FE code to present the reaction extent).

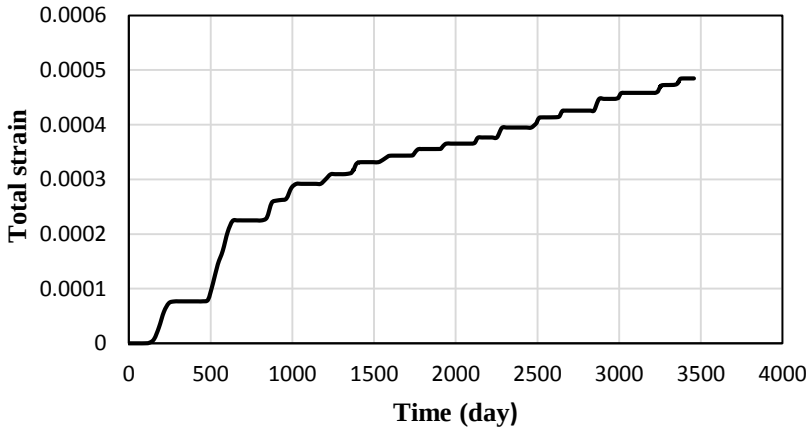


**Figure 6-6**. Horizontal strain vs. time at the crest level.

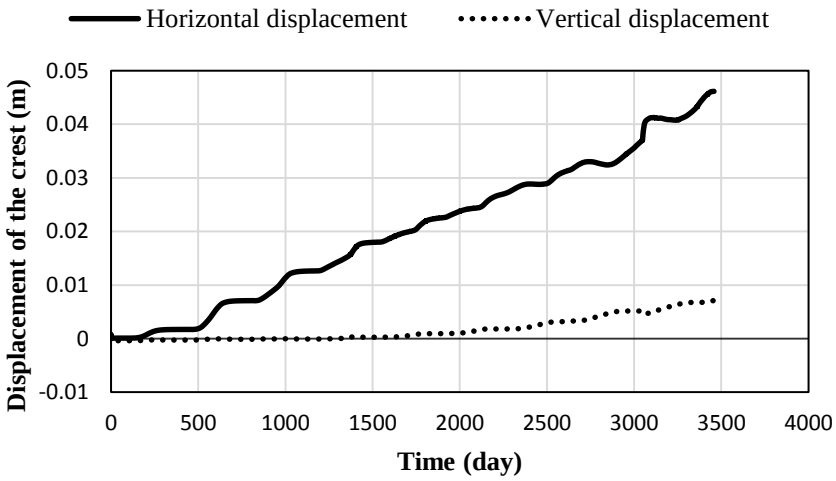


**Figure 6-7**. Vertical and horizontal displacement vs. time at the crest level.

## 6.3 ASR analysis of the Kleinplaas dam on the Jonkershoek River in South Africa

Kleinplaas dam is located in the Jonkershoek River near Stellenbosch in the Western Cape province of South Africa. This balancing concrete gravity dam was designed and constructed in 1982 and consists of a 25.5 m high uncontrolled ogee spillway (see Figure 6-8) in the river section with a 36 m length and blocks of concrete gravity dam supported by a rock fill embankment with a clay core in left flank. The gravity section has a downstream slope of 1V:0.8H and is vertical on the upstream side. A gallery along the entire length of the gravity section provides pressure relief as well as drainage and access to the inside of the structure for regular inspections. The foundation of the concrete gravity wall has also been grouted from the gallery. Vertical construction joints, 12 m apart, have been provided and a dual system of

rubber as well as UPVC water-stops has been installed on the upstream side. See Figure 6-8. A concrete stilling basin has been provided on the downstream side of the spillway. The rock fill embankments on both sides of the concrete section comprise of a central impervious core bordered by rock fill on both sides. Close to the concrete wall on the left flank the embankment is founded on solid granite or residual soils of granite origin. Further to the left flank it is mainly founded on the alluvial layer. Seepage is controlled by narrow clay blankets.

The first dam safety inspection was done in 1994 and the results from the stability and stress analysis indicated no problems with the global stability of the dam as reported in the safety inspection by Department of Water and Sanitation of South Africa (*DWS*, 2009). However, about 9 years after the completion of the dam, evidence of swelling was observed including pronounced cracking and opening of the horizontal construction joints of the concrete section. Greywacke aggregate of the Malmesbury Group (from quarry in the Western Cape area) which is intrinsically alkali-reactive (Alaud & van Zijl, 2017) was used in the manufacture of concrete for the dam. This is possibly the main contributing factor to the ASR encountered in this dam. Since 1996 monitoring of the swelling has been carried out with 3D-crack gauges and since 2000 with a geodic survey system on the crest level. Vertical movement in the range of 20 to 42 micro strain per year has been measured since 2000.

**Figure 6-8**. A perspective view of the Kleinplaas dam in the Jonkershoek River near Stellenbosch.

In 2014 an accumulated value of vertical strain of approximately 850 micro strain was measured. Some decrease in vertical swelling is evident since 2009. Currently, continued monitoring of the expansion behaviour is taking place (Sellier *et al.*, 2017).

For the purpose of this research the Kleinplaas dam is chosen to perform a finite element analysis based on the developed SU-ASR FE code to predict the ASR expansion and other effects on the dam wall. Due to the difficulties to provide cores from the dam in order to perform standard accelerated laboratory tests to estimate the ASR parameters and calibrate the model, calibration of the SU-ASR model using the data available in the literature such as strain rates and current displacement at the Kleinplaas dam is performed. In the following sections the detail analysis and interpretation of the results are presented.

### 6.3.1 Site investigation of Kleinplaas dam

A permit for a site inspection was obtained from the Department of Water and Sanitation of South Africa. During the inspection and investigation carried out, signs and symptoms of major ASR effects on various levels and of extensive spatial extent were observed in the dam wall. Following are some of the issues about Kleinplaas dam:

1. Map pattern cracking in the downstream wall,
2. Extensive cracks inside the gallery,
3. Swelling of the crest and vertical movements,
4. Seepage of water from the upstream wall of the dam inside the gallery,
5. Pop outs of the aggregates in downstream wall of the dam,
6. And joints movements in horizontal and vertical direction.

Figures 6-9 and 6-10 show the downstream wall of the dam that is partially covered from embankment dam in the left flank. Extensive micro cracks, leaching of the reacted material plus joint opening are observed at various locations on the dam wall. These micro cracks are possibly due to the strains from ASR that initially appeared in the downstream face of the dam due to the higher thermal gradient. Furthermore, pop out of the aggregates and spalling of concrete material are evident in the vicinity of the parapet wall of the dam on the downstream side. This phenomenon is possibly due to the increase in plane compressive stresses parallel to

**Figure 6-9**. Perspective view from the downstream wall of the dam. Symptoms of leached reaction material through the micro cracks and joints are shown.

the wall that cause perpendicular irreversible plastic strains taking place on the exposed face of this surface layer.

Figures 6-10 shows the symptoms of permanent deformation, cracking and pop out of concrete material in downstream wall of the Kleinplaas dam.

(a) (b)

**Figure 6-10**. Symptoms of permanent deformations, cracking and pop out of aggregates in parapet wall of the dam in downstream face, a) localised crack in downstream wall of the dam, b) pop out of the aggregate in downstream wall.

The Kleinplaas dam has only one gallery that extends from the left flank of the concrete gravity dam to the right side and passes through the spillway. Figure 6-11 shows photos taken during the inspection done for the purpose of this research. Various cracks and openings joints were observed at different location of the upstream face of the wall of the gallery. In addition, an abnormal amount of seepage and leaking of the water were seen on this face of the dam. The extensive cracks and opening of the concrete construction lift joints from the upstream wall in the distance between this wall and the galley could possibly explain this harmful problem.

Figure 6-12 shows the crack in the roof of the gallery in the left flank of the dam. This crack could be due to large compressive stresses in downstream wall of the dam and to satisfy the compatibility of the strains around the galley structure.

The vertical movement of the concrete Block 9 in the vicinity of the embankment dam in the left flank is shown in Figure 6-13. It is mentioned in the introduction of this section that measurements which have been done since 2000 show approximately 850 micro strain for this

(a) 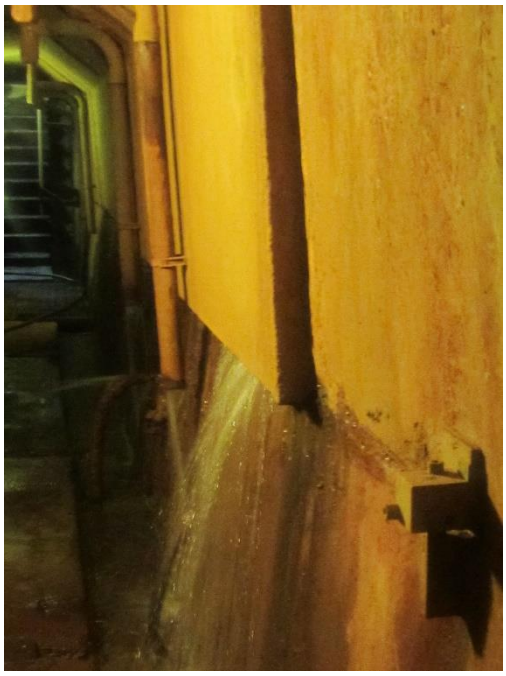 (b) 

**Figure 6-11**. Sign of severe seepage of water in gallery in the upstream wall.

(a)  (b) 

**Figure 6-12**. Cracking in the roof of the gallery in the left flank of the dam, a) crack in the left flank, b) a close up view of the crack in the left flank of the dam.

expansion. The technical inspection and measurement which have been done by the author confirms the finding about the vertical displacement of this block. This information is used to calibrate the FE model developed for Kleinplaas dam.

### 6.3.2 Geometry and material properties of the dam

Geometry and layout of the dam are shown in Figures 6-14 and 6-15. During the extensive site investigation that has been done by the author, the Block 9 of the concrete gravity dam located in the left flank has been identified as the one with most significant swelling and damage. This

 

**Figure 6-13**. Displacement and cracking in the crest of the dam, a) sign of cracking in the upstream wall and b) vertical movements of the construction joint at crest at left flank.

block is shown in Figures 6-14 and 6-15. Material properties and the thermal data to perform the preliminary thermal analysis are shown in Table 6-2.

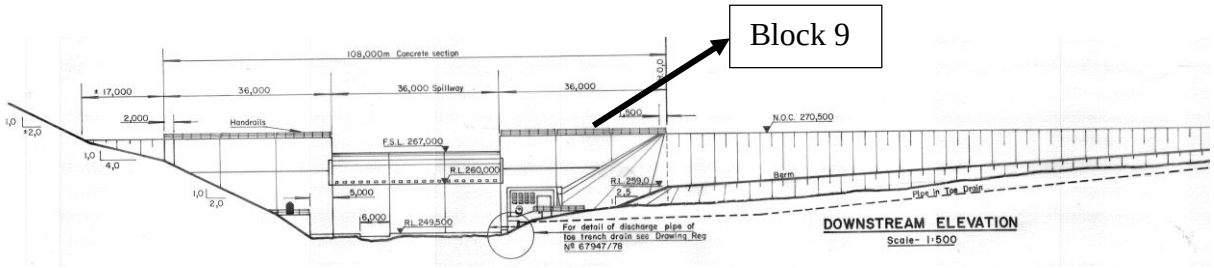


**Figure 6-14**. Kleinplaas dam layout and dimension.

**Table 6-2**. Material properties and thermal data used in the numerical modelling of Kleinplaas dam.

| | Young's modulus $E_0$ GPa | Poisson's ratio $\nu$ - | Tensile strength $f_t$ MPa | Fracture energy $G_F$ N/m | Thermal conductivity $k$ W/(m K) | Specific heat $c$ KJ/ (kg K) | Thermal expansion coefficient $\alpha$ $(10^{-5})$ |
|---|---|---|---|---|---|---|---|
| **Concrete** | 27.0 | 0.19 | 2.9 | 140.0 | 1.75 | 0.75 | 1.0 |
| **Rock** | 20.0 | 0.25 | - | - | 0.75 | 0.85 | 0.5 |
| **Soil fill** | 0.15 | 0.2 | - | - | 0.55 | 1.00 | 0.5 |

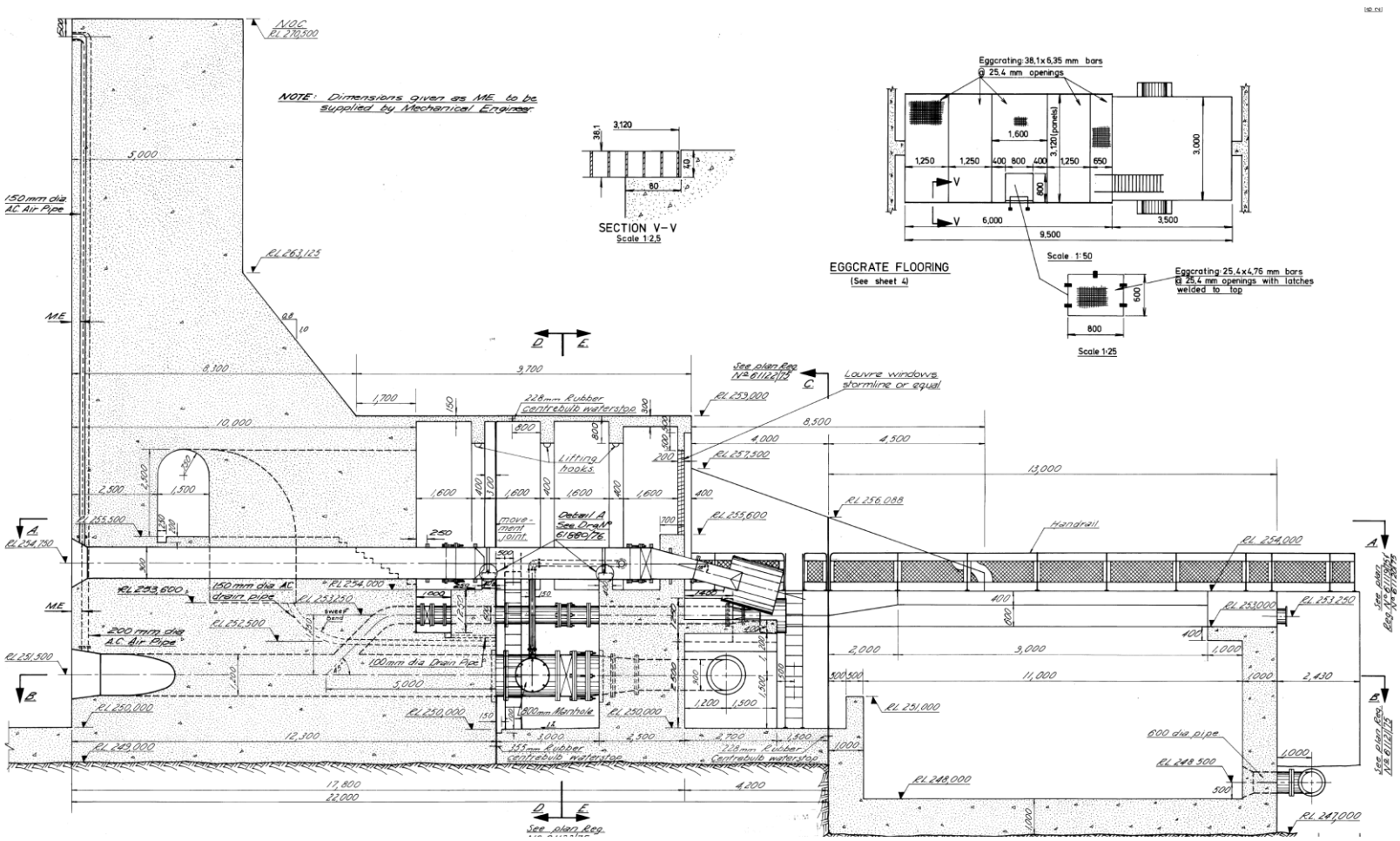


**Figure 6-15**. Section through the dam in the left flank.

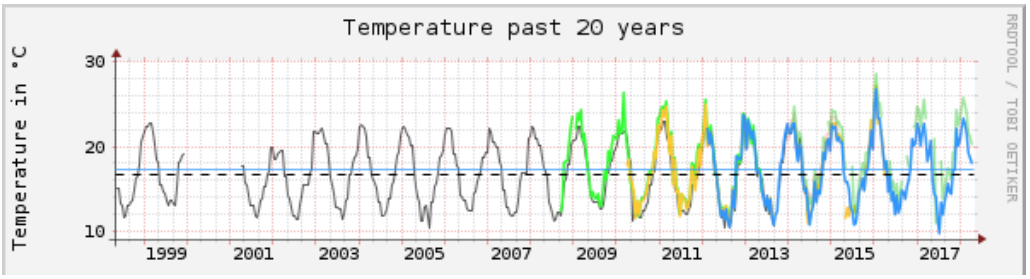


**Figure 6-16**. Temperature history for Stellenbosch area for past 20 years (Meijers, 2018).

For the estimation of extent of swelling occurring in concrete dams, environmental conditions using data available from weather observation stations near the structure, are required. Figure 6-16 shows the temperature history that is used in the thermal analysis of the dam. This information was collected from a climate station installed at Stellenbosch University, 8.2 km from the dam structure (Meijers, 2018).

### 6.3.3 Numerical analysis

In order to analyse the dam to predict the swelling behaviour, first an initial thermal analysis is performed. Because the thermal properties of concrete, soil and rock are different, all these mediums are considered in the transient thermal analysis. The thermal interaction between soil, dam and foundation is considered by defining appropriate interface gap elements at the interactive boundaries. 2D heat transfer elements are used for the thermal analysis and a finer FE mesh is applied in the interfaces and corners to avoid mesh dependency. It is worth noting that this mesh was used for the ASR and stress analysis as well.

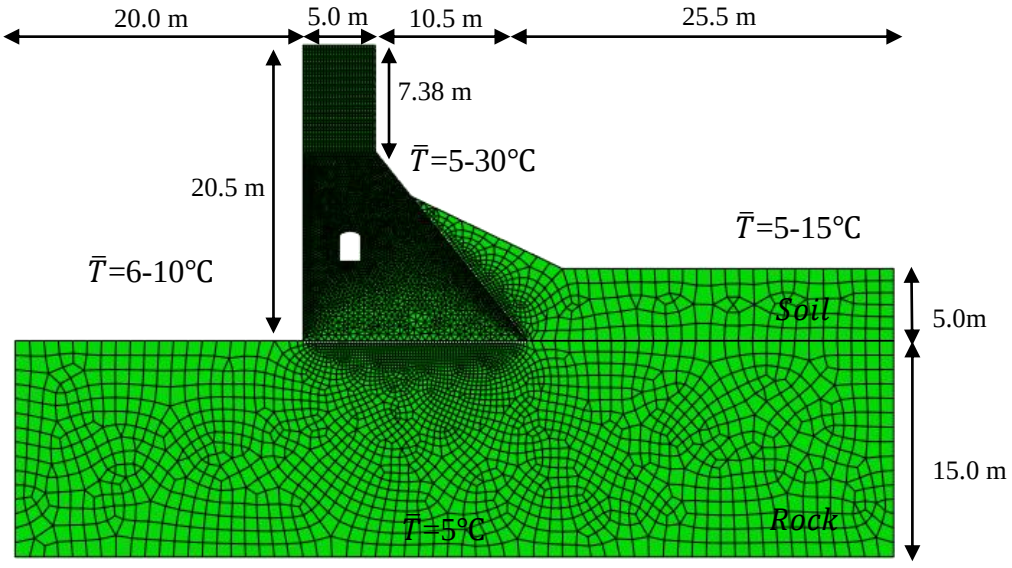


**Figure 6-17**. Geometry, configuration and finite element mesh of block 9 of Kleinplaas dam.

The thermal analysis for the dam is performed using the same method which was used for the Fontana dam. Seasonal temperature variations for the upstream and downstream surfaces of the dam incorporated in the transient thermal analysis are shown in Figure 6-18. These figures show the thermal variation from 1982 to 2014. The thermal analysis performed here, is used for the subsequent stress analysis by introducing the temperature as a predefined field in the mechanical FE modelling of dam. It is evident that the thermal gradient is higher in the downstream face of the dam mainly because of the more exposure to direct sunlight.

For the subsequent ASR and mechanical analysis, 3780 4-node quadrilateral plain strain elements of type CPE4R are used with reduced integration. Service loading namely the gravity load, seasonal temperature variations and hydrostatic pressure are considered for the preliminary steps in the modelling. The free board level of the water in the reservoir is assumed to be 3 m below the crest level of the dam.

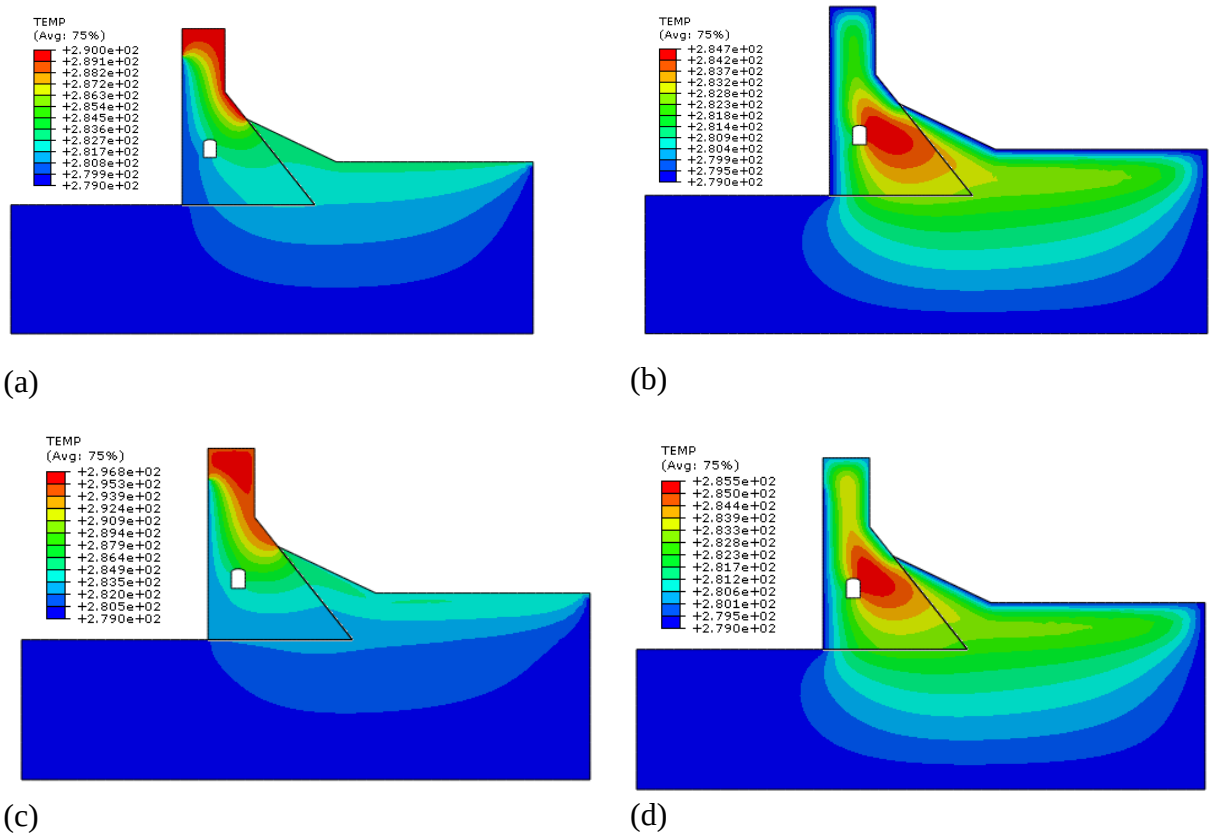


**Figure 6-18**. Results of the transient thermal analysis of the Kleinplaas dam for 32 years a) after 5 years, b) after 10 years, c) after 20 years and d) after 32 years (temperature values given in Kelvin).

### 6.3.4 Results and discussion

The results of the FE modelling of the Kleinplaas dam using SU-ASR code are presented in this section. The finite element analysis which is performed aims to capture the most prominent issues of the dam and compare the results with technical field investigations and the data that are available for the dam in the literature. In addition, this dam is modelled from 1982 (year of construction) to 2014 for a period of 32 years.

#### *6.3.4.1 Model calibration*

Initially, it is important to calibrate the model with the expansion and displacement data that are reported for this dam. Monitoring gives a possible access to different criteria quantifying the expansive reaction. Unfortunately, the complete set of data is not available for this dam. Hence, for the purpose of this research some information about the strain rate from year 2000 to 2014 which is reported in the literature is used to calibrate the model (Sellier *et al.*, 2017).

Figure 6-19 shows the total strain for the crest of the dam in the left flank in bock number 9. The measured data presented in this figure are used to calibrate the model. Actually, the calibration is a try and error analysis, hence the code is run several times to estimate the ASR parameters that predict the measured strain with adequate accuracy. Based on the performed analysis, the ASR model parameters are determined and reported in Table 6-3. The characteristic and latency time are the parameters that present in the calculation of the kinetics of the reaction. The free volumetric asymptotic expansion $\beta$ is estimated to be 0.2 %.

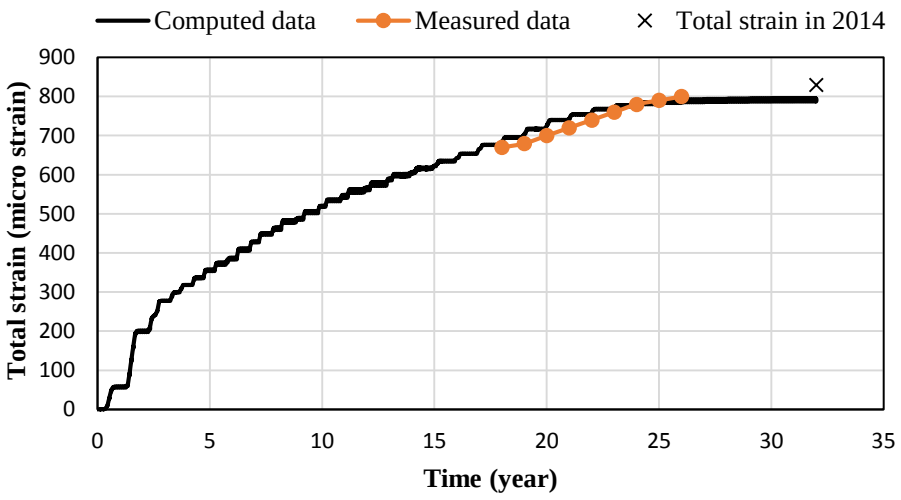


**Figure 6-19**. Results of the total strain vs. time at crest level for 32 years. The measured data is used to calibrate the model.

**Table 6-3**. ASR parameter model calibrated using measured data from the Kleinplaas dam.

| Parameter | Value |
|---|---|
| Latency time $\tau_l$ | 200 days |
| Characteristic time $\tau_c$ | 80 days |
| ASR material dilatancy $\beta$ | 0.2 % |

Figures 6-20 and 6-21 present the vertical displacement of the dam. It is evident that the dam has experienced gradual vertical movement for many years after its construction. The maximum value of the displacement is about 25 mm which is in good agreement with the current value of the displacement that is measured during the inspection by the author. The analysing of the Kleinplaas dam shows that the dam has experienced a complex displacement regime. The results show that ASR vertical strain at the crest level is reduced after 27 years from the construction time in 2009. The report by Sellier *et al.* (2017) also confirms this finding.

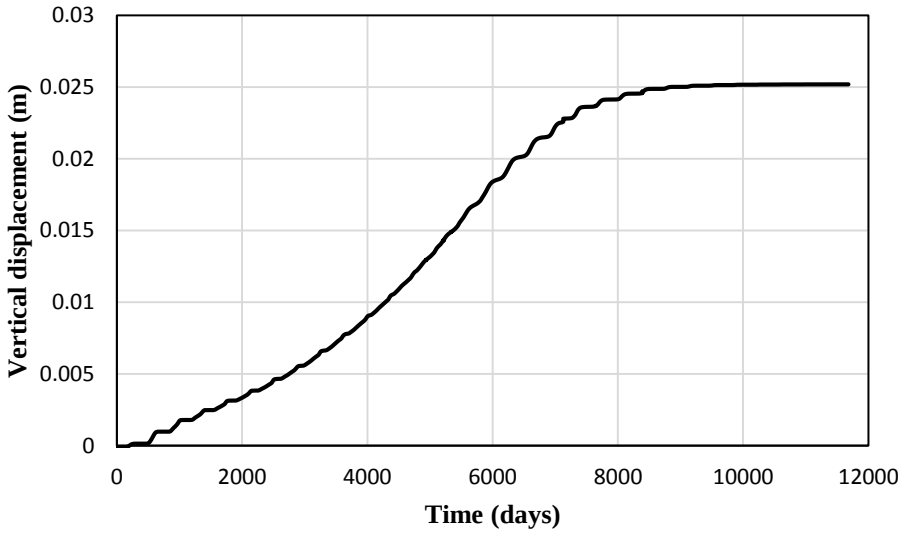


**Figure 6-20**. Modelled vertical displacement of the crest for the duration of 32 years from 1982 to 2014.

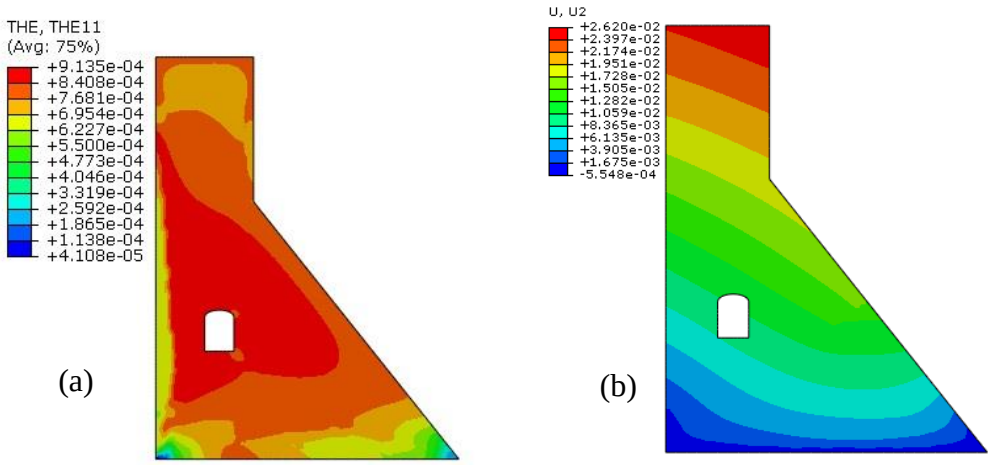


**Figure 6-21**. ASR strains and vertical displacement contour of the Kleinplaas dam after 32 years, a) total strain at 2014 after 32 years of modelling, b) contour of the total vertical displacement.

### *6.3.4.2 Kinetics of the reaction*

Variations of the reaction extent during the service life of the structure are shown in Figure 6-22. These figures show the extent of the ASR development in the dam wall and the whole dam was subject to ASR after 23 years by the year 2005. The ASR process was complete and can be deemed to have stopped in 2005. The report on this dam (Sellier *et al.*, 2017) also confirms this hypothesis.

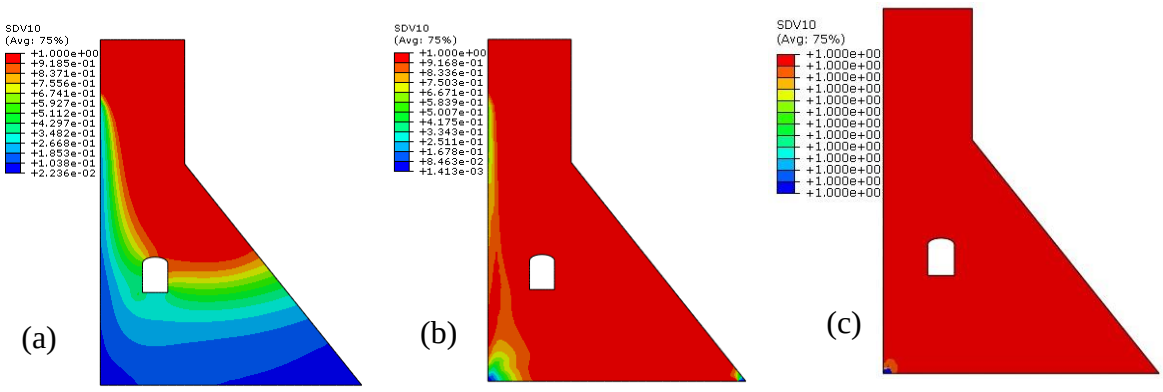


**Figure 6-22**. Variations of the kinetics of the reaction for 32 years, a) reaction extent after 10 years, b) reaction extent after 20 years and c) reaction extent after 32 years.

### *6.3.4.3 Material degradation*

Figure 6-23 shows the material damage variable history after 10, 20 and 32 years respectively. It is evident that the concrete material is highly degraded since construction time. Figure 6-23 c, illustrates that the extent of the ASR damage, $d_{asr}$ is about 24.4 % after 32 years. The Young's modulus of concrete in this study is 27 GPa which is presented in Table 6-1. By assuming the current maximum damage from ASR, approximately 6.6 GPa reduction in E-Modulus likely has been experienced by the dam. Therefore, the material degradation could affect the global behaviour of the dam specifically in seismic events.

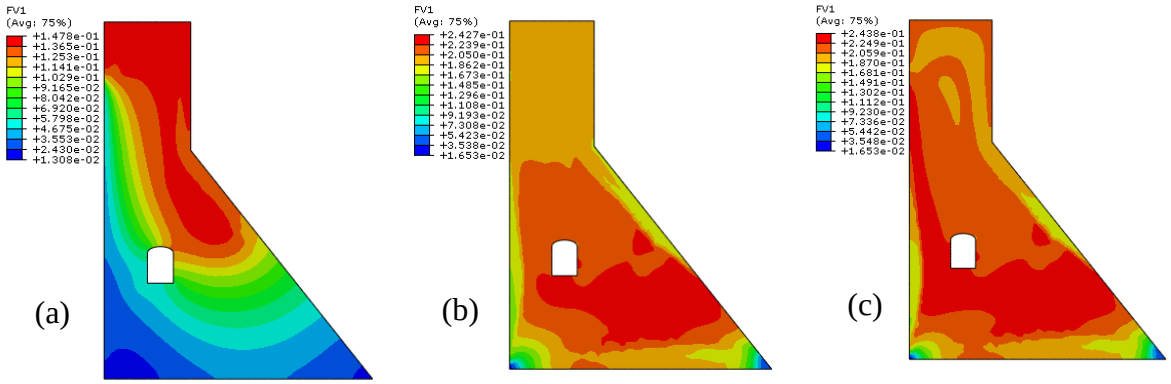


**Figure 6-23**. Stiffness degradation since 1982 to 2014, a) after 10 years, b) after 20 years c) after 32 years.

### *6.3.4.4 Damage and cracking in Kleinplaas dam*

In massive hydraulic structures, the ASR process often results in a network of map pattern cracking due to the low steel reinforcement ratio. Map cracks are usually harmless, except for ingress of gas and water. Localised cracks are the ones that can lead to instability. Figure 6-24 illustrates the result of FE modelling of the downstream wall of the dam. The crucial issues in this side of the dam have been already investigated and discussed. The construction of the embankment dam close to the downstream side of the dam could help to hamper the thermal gradient and subsequent expansion from ASR. The FE element modelling shows that approximately after 12 years in 1994 the irreversible plastic stains caused map cracking and opening of the joints. Figure 6-24 b shows a compatible result between finite element modelling and actual crack in the downstream wall of the dam. It can be concluded that, although several cracks observed in the structure of the dam, but these cracks are not very deep and have occurred in the area close to the surface of the dam. This hypothesis could be verified by taking cores from the downstream side of the dam especially in the cracked area.

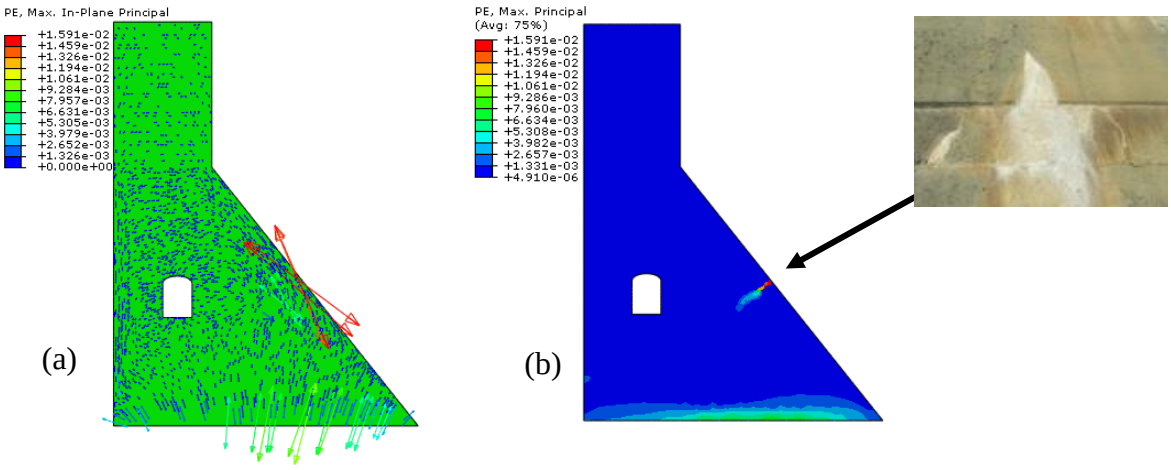


**Figure 6-24**. Maximum principal plastic strain at upstream and downstream of the dam, a) contour of maximum principal strains, b) crack detection in downstream wall of the Kleinplaas dam and comparison with actual crack in this face.

Figure 6-25 is a close up view of the maximum principal plastic strain in the vicinity of the gallery. The irreversible maximum principal plastic strains around gallery are evident. The concentration of plastic strains in this area, confirms that an extensive number of cracks and opening in several positions of the upstream wall of gallery should have formed. It is mentioned that abnormal seepage was observed from the upstream wall of the gallery in the concrete block 9 in the left flank. The extensive irreversible plastic strains could possibly explain the reason of this seepage. The micro cracks and voids which developed during the service life of the dam due to the effects from mechanical and chemical processes in the left and top side of

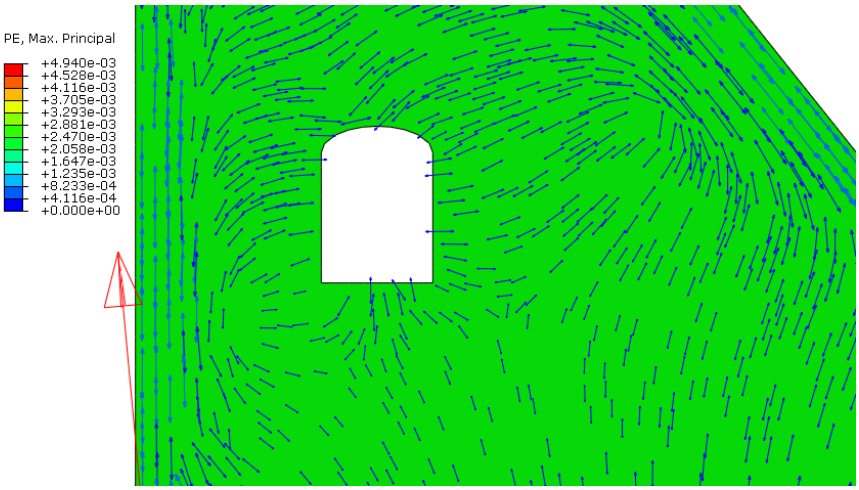


**Figure 6-25**. Maximum Principal plastic strain around galleries and upstream wall of the dam.

the gallery could possibly join and create a narrow passage through the gallery, therefore water can easily flow from the upstream wall to the gallery.

It is shown in Figure 6-2 that a crack is observed in the roof of the gallery in Block 9 which is located in the left flank. Although, this crack is not predicted using the damage tensile variable, but according to the maximum principal plastic strain contours which are shown in Figure 6-25, it can be concluded that large plastic strains in the roof of the gallery ranging from 100 to 400 με have developed during the several years. By drawing a continuous line along the centre of the arrows that represent the maximum plastic strains, a single crack can be detected which propagates to the top of the gallery and the main body of the dam. Furthermore, comparison of the structural behaviour of Fontana dam and Kleinplaas dam shows that the crack detected in this gallery (Kleinplaas dam) can only be a superficial crack.

## 6.4 Summary

In this chapter the SU-ASR model is further validated by numerical modelling of dams that are suffering from ASR. Fontana dam which is located in United State of America and Kleinplaas dam in South Africa. For both cases, the chemo-thermo-mechanical analysis of the dams considering various parameters and variables including thermal history, kinetics of the reaction, confining stresses and non-uniform time dependent material degradation is performed and the results are presented.

The results show good agreement with the current state and damage mechanisms of the both dams. These studies reveal that ASR is a chemical reaction that strongly is coupled with some environmental conditions such as temperature and humidity that could affect the kinetics of the reaction. Other remarkable variable which has strong influence on the ASR evolution is confining stresses. Experimental investigation has been performed on 3D stress effects on ASR strain evolution reveals that ASR could be considered as a volumetric strain and transferred to the less confined direction. Concrete material degradation is correlated to ASR expansion and implemented in the SU-ASR model. The results from Kleinplaas dam show that over 24 % of the ASR induced damage has occurred in the dam cross section during the years from 1982 to 2014.

# CHAPTER 7

# Combined action of ASR and Seismic loads

**Highlights:**

Fundamentals of Fluid-Structure Interaction analysis.

Added mass technique by Westergard.

Seismic analysis of the Koyna dam.

Combined ASR and seismic analysis of Koyna dam.

## 7.1 Introduction

Dams are important infrastructure components and an asset for any country. Past earthquakes have highlighted their vulnerability to damage and even failure which can have major socio-economic consequences, losses and other cascading effects (e.g. water supply, power generation and irrigation). Hence, considerable efforts have been devoted to evaluating the safety of aged dams and in some cases to pursue a suitable remedial action and rehabilitation strategies.

In this chapter the numerical simulations using the SU-ASR finite element analysis approach are used to assess and predict the dynamic stability of a dam structure considering fluid-structure interaction and are also used to investigate the evolution of damage associated with inception and development of macro cracks in the dam structures due to the combined effect of the ASR and seismic loading on the dam.

## 7.2 Fluid and structure interaction

While the mechanical performance of ASR affected structures under monotonic and quasi-static loading has been extensively investigated over the last decades, limited research has addressed dynamic loading. The combined action of old and new cracks under dynamic excitation may cause dam failure. Considering the predicted interaction between ASR and seismic loads, remedial measures can be adopted at the right time to safeguard the dam in the event of an earthquake. Fluid-Foundation-Structure Interaction (FFSI) also has received much attention in Finite Element Analysis (FEA) of dams. These techniques include the effects of hydrodynamic pressure on the dam-water interface, and assumed boundary conditions on the fluid domain, such as far-field non-reflective and the admittance boundary condition for modelling the sediments in the reservoir bed.

The hydrodynamic pressure induced in the reservoir which exceeds the hydrostatic pressure during motions of small amplitude is governed by the Helmholtz equation (Zienkiewicz, 2006):

$$\nabla^2 P = \frac{1}{C_0}\frac{\partial^2 P}{\partial t^2} \tag{7-1}$$

with $P$ the hydrodynamic pressure, $t$ the time and $C_0$ the acoustic wave speed in water. The FFSI system with boundary conditions for the upstream dam face, non-reflecting radiating boundary, admittance (sediment layer) and free surface boundary condition is shown in Figure 7-1.

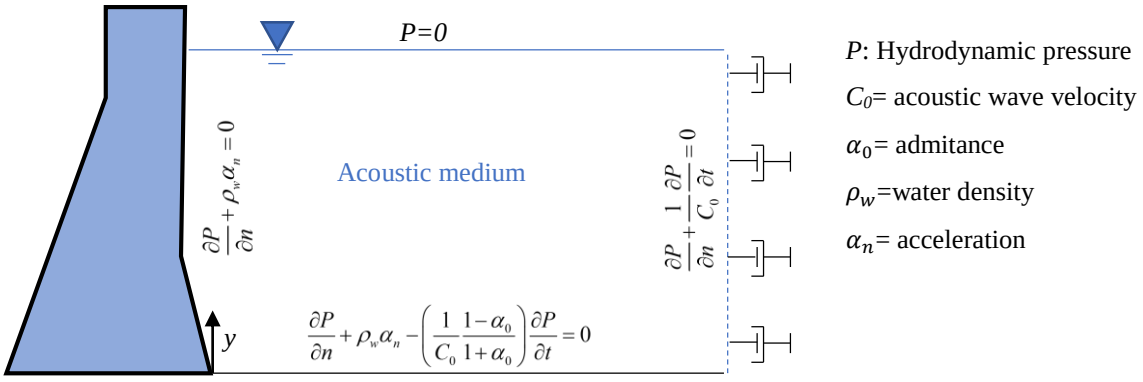


**Figure 7-1**. Dam-reservoir-foundation system and boundary conditions

The added-mass technique with expression $M_{add} = \frac{7}{8}\rho_w\sqrt{h_w(h_w - y)}$ for $y \le h_w$, is used to model the incompressible fluid assumption (Tan & Chopra, 1995). In this equation, $h_w$ is the water level in the reservoir and $y$ is the vertical coordinate of the upstream face. This technique implies that the hydrodynamic pressures of the water on the dam upstream face during an earthquake are the same as that when a certain body of water moves back and forth with the dam while the remainder of the reservoir is left inactive. This equation is implemented in an Abaqus FEM code user subroutine that adds the mass of the water to the upstream dam face. Infinite elements are used for far-field rock boundaries and seismic waves are not allowed to reflect into the rock field when they pass across the boundaries of the rock domain.

## 7.3 Combined action of ASR and dynamic excitation

The Koyna dam, completed in 1964 in the region of Maharashtra (India), developed cracks on one of the non-overflow monoliths in a devastating earthquake of magnitude 6.5 $M_w$ on 11 December 1967. See Figure 7-2. The model developed here is used to predict the long term behaviour of the dam due to synthetic ASR, and then the current state of the structure is used as an initial state for the seismic analysis. The response of the dam is validated by analysing the Koyna dam under seismic loads with three different assumptions, empty reservoir, added-mass technique and FFSI and comparing the results with experimental research performed on this dam. Then, combined action of ASR and seismic loads is studied to evaluate the long term behaviour.

## 7.4 ASR modelling of Koyna dam

The Koyna dam geometry is shown in Figure 7-3. The material properties of the dam in the present study are: modulus of elasticity of the dam, $E_0$=31500 MPa; Poisson's ratio=0.20 and mass density=2643 kg/m$^3$. ASR damage is defined as a field variable in the code that shows the material deterioration during the service life of the structure in terms of E-Modulus and tensile strength. Non-uniform degradation of concrete material is considered. Figure 7-4 shows the result of the ASR analysis of Koyna dam. ASR kinetics parameters are assumed to be $\tau_l = 200$ days, $\tau_c = 80$ days and $\beta = 0.3\%$. The upstream and downstream average temperatures are assumed as: $T = 5℃$ and $T = 25℃$, respectively. Extent of the reaction, ASR damage and tensile damage contours are plotted after 10 years. It is observed that the dam experiences a

tensile damage mainly in the downstream face due to exposure to the larger thermal gradient. Figure 7-4 b shows the non-uniform material degradation that is used for the subsequent seismic analysis as an initial state. Figure 7-5 shows the crest displacement versus time for the Koyna dam including the service loads e.g. gravity and hydrostatic loads without considering the seismic excitation. The maximum displacement after 10 years is -195.5 mm in horizontal direction which implies an average rate of 19.55 mm/year.

(a)

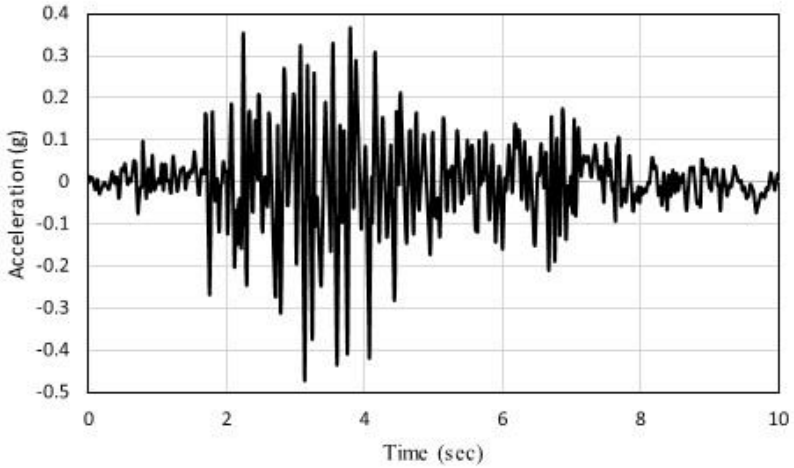


(b)

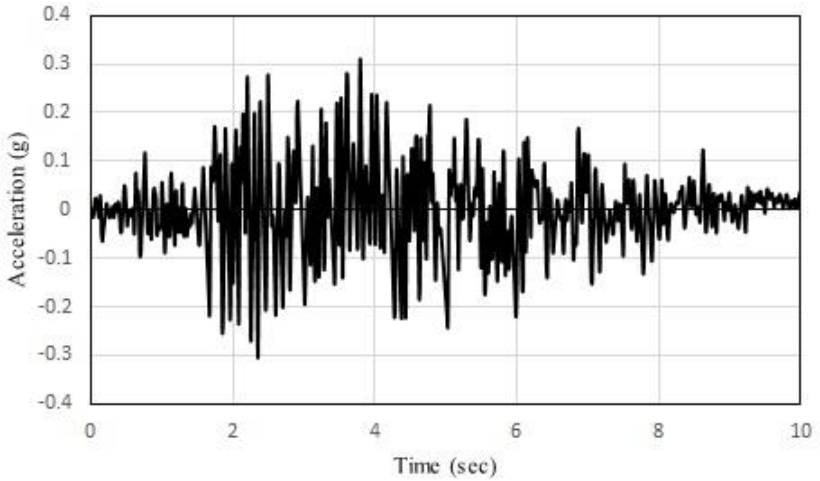


**Figure 7-2**. Seismic acceleration histories for the Koyna dam vs. time, a) horizontal and b) vertical earthquake.

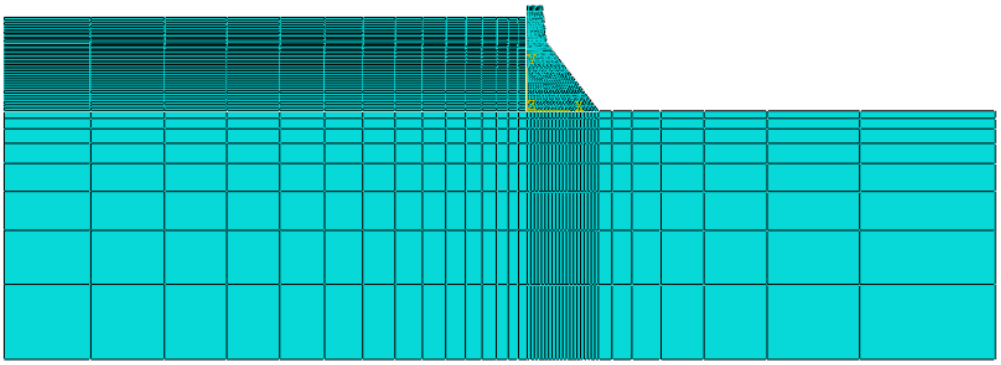

(a)

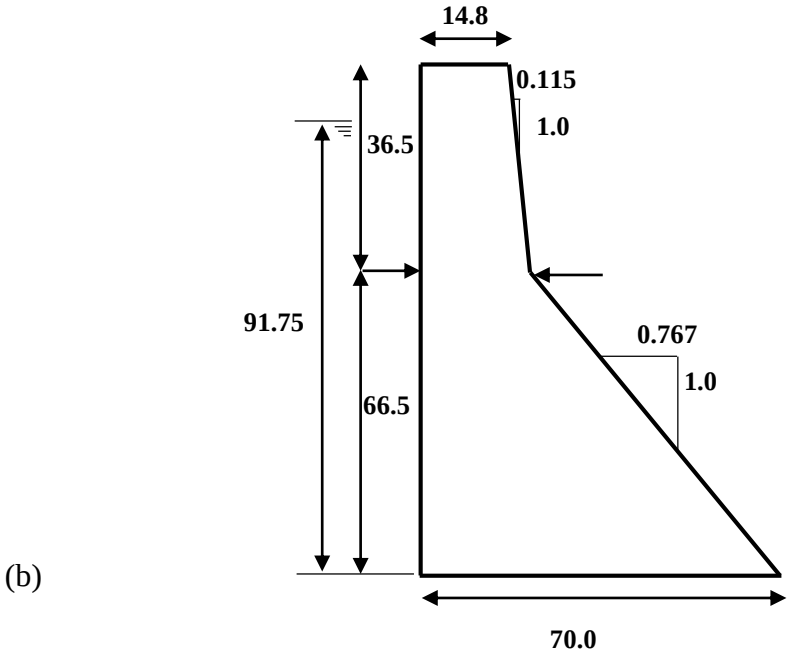


(b)

**Figure 7-3**. Finite element model and the geometry of the Koyna dam, a) finite element mesh of the dam-water-foundation system, b) geometry of the dam, (units are in meter).

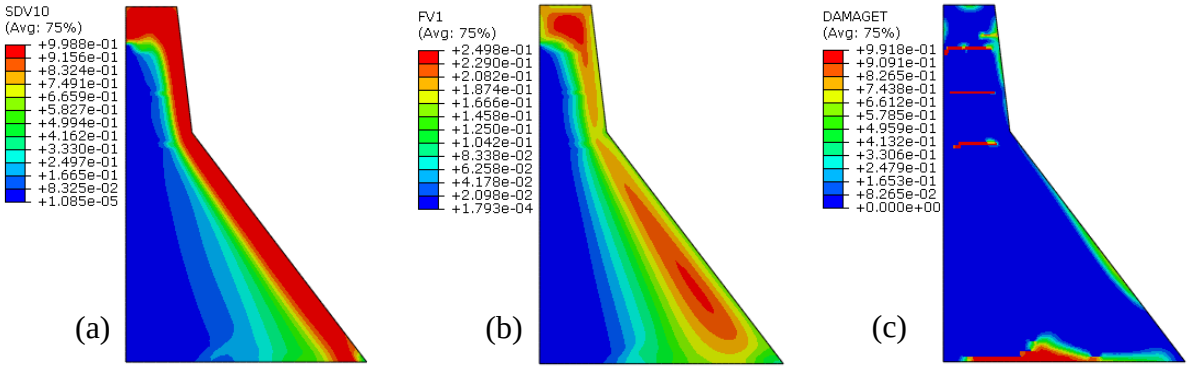


(a) (b) (c)

**Figure 7-4**. FE results of the Koyna dam a) reaction extent, b) ASR damage and c) tensile damage after a period of 10 years.

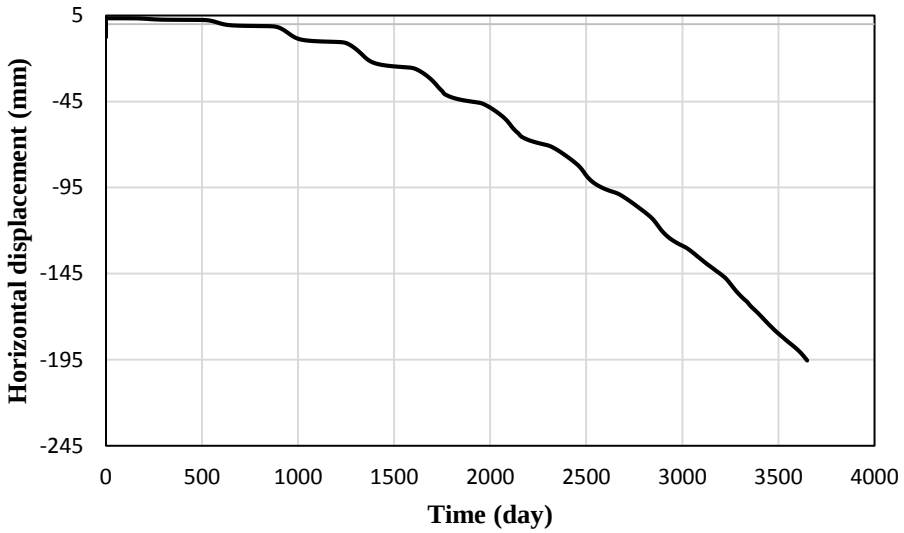


**Figure 7-5**. Horizontal displacement at crest of the Koyna dam for a duration of 10 years affected by ASR.

## 7.5 Combined action of ASR and seismic load

From forced vibration tests on dams (Clough & Penzien, 2003), damping ratios in the range 2-5% have been determined. In implicit dynamic analysis, dissipation mechanisms such as dashpots or inelastic material behaviour can be applied. In this study damping ratio used is $\zeta_1$ =3% fraction of critical damping for the first mode of vibration of the dam. From a natural frequency extraction analysis, the first mode of vibration of the dam is found to be $\omega_1 = 18.61\, rad/sec$. By assuming Rayleigh stiffness-proportional damping, $\eta = \frac{2\zeta_1}{\omega_1}$ is computed to be $3.23 \times 10^{-3}$ sec. The acoustic wave velocity of water, $C_0$, used is 1438.5 m/s. The loading consists of self-weight of the dam, hydrostatic and hydrodynamic effects of the reservoir and the transverse and vertical components of earthquake loading. The hydrodynamic loading is modelled by applying two assumptions of the reservoir modelling: incompressible fluid using added-mass technique and compressible, inviscid, small amplitude motion, irrotational fluid with the Helmholtz equation and appropriate boundary conditions as mentioned in the previous section. The dam is analysed in the time domain using Newton's method as a numerical technique for solving non-symmetrical nonlinear equilibrium equations using a time step of 0.02 second. The numerical analyses are carried out for two cases, without ASR, and with ASR deterioration for 10 years. Before analysing the dam for combined action of synthetic ASR and actual seismic load, the model is validated in seismic analysis for three different reservoir modelling strategies of a) empty reservoir; b) added mass technique; 3) FFSI with compressible

fluid. Structural responses and damage parameters are obtained for both cases to evaluate the seismic performance of the dam considering effects from ASR. Figure 7-6 shows the result of the analysis for Koyna dam without the ASR for a) empty reservoir; b) added mass technique and c) FFSI modelling. The results for added-mass technique and FFSI are in good agreement with experimental modelling. Figure 7-7 illustrates the comparison of tensile damage for both experiment and numerical model at the end of the seismic loading. It is observed that the computed crack pattern is in reasonable agreement with the crack pattern in the experiment. The result of the combined analysis of the ASR and seismic load for tensile damage is shown in Figure 7-8. This figure shows that severe damage in the body of the dam mainly due to reduction in stiffness has occurred. The dam experiences several localised cracks in downstream parapet wall which these cracks propagate mainly through the interior body of the structure and change the dynamic behaviour of the dam. The thermal gradient is at a maximum on the downstream surface of the dam wall which leads to the higher ASR strains in comparison to the upstream wall surface, where the temperature is lower due to the contact of this surface with water in the reservoir.

Furthermore, Figures 7-9 and 7-10 show the time histories of horizontal displacement at the dam crest for modelling without ASR and combined action of ASR and seismic load, respectively. The displacement of the ASR affected dam is larger than the case when ASR is not considered. This is due to the decrease in the material stiffness of the concrete and inelastic behaviour and damage in the dam with crack opening. The maximum crest displacement for the combined action of ASR and seismic load for FFSI modelling strategy is 302.2 mm, which is significantly larger than the crest displacement when only ASR effect is considered and is equal to 195.5 mm (see Figure 7-5). It is worth noting that due to the combined action of seismic load and ASR an irreversible horizontal displacement of 106.7 mm is added to the dam horizontal displacement when only ASR effect is considered.

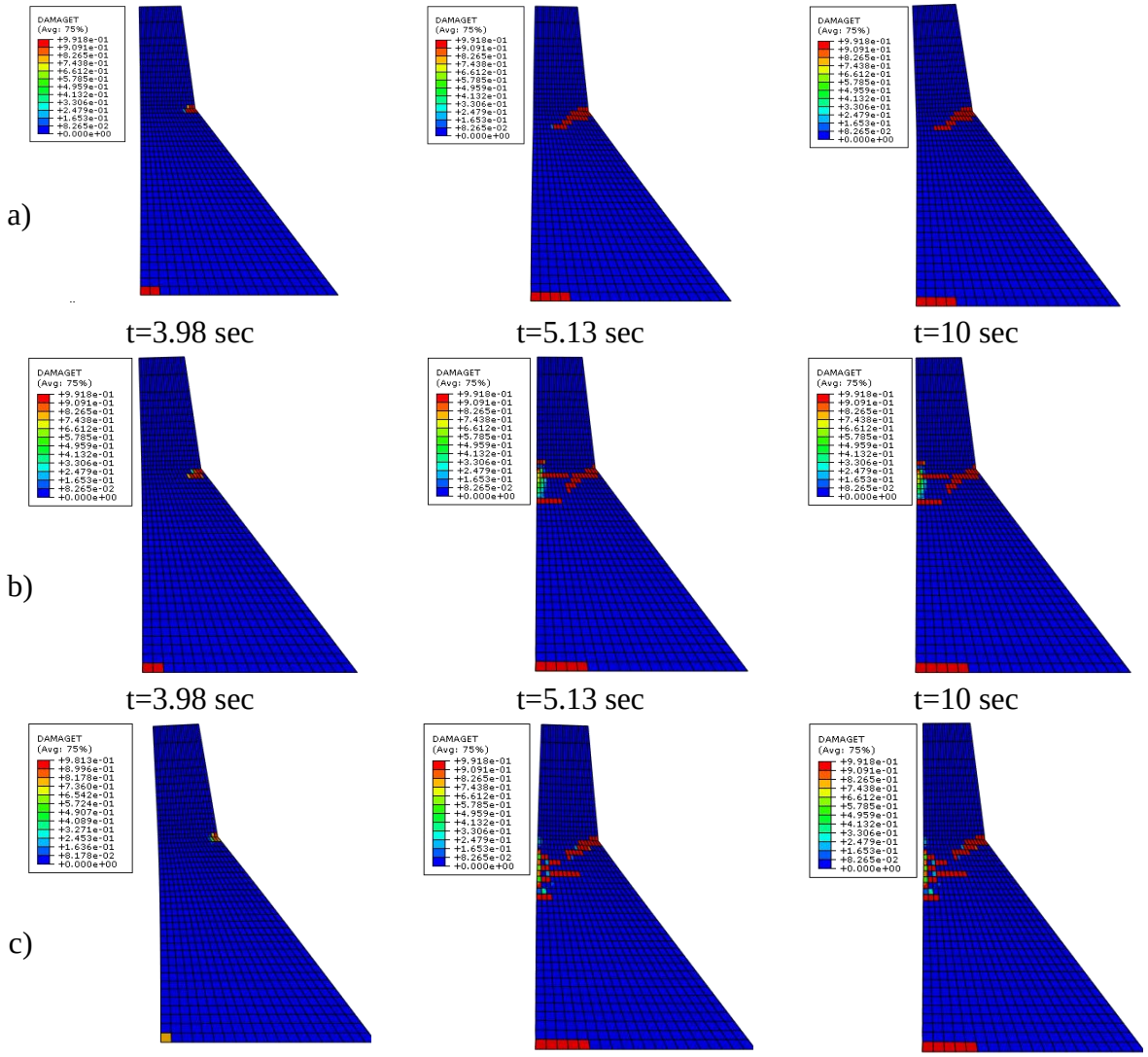


**Figure 7-6**. Results of Koyna dam due to seismic loading at given times and without ASR. The contours show tensile damage variable in the dam wall a) empty reservoir b) added mass technique c) FFSI modelling

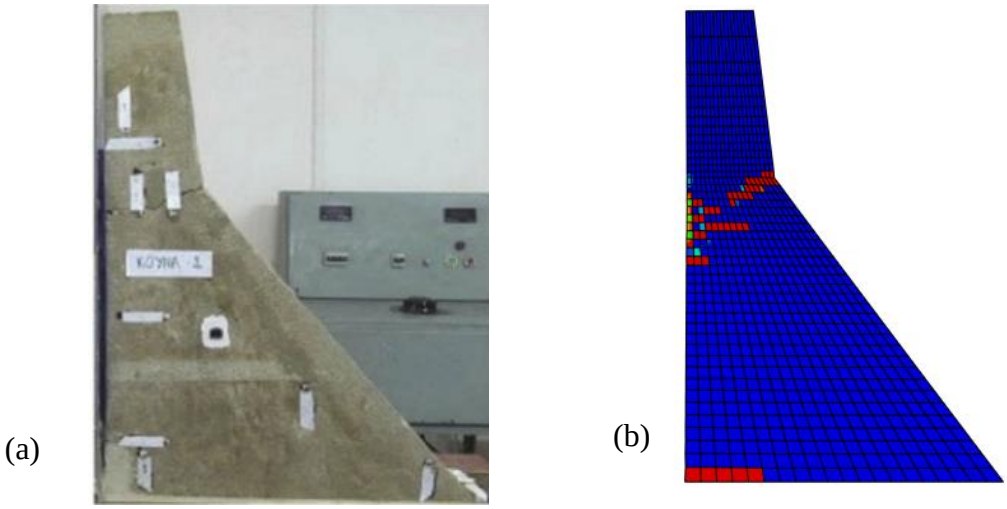


**Figure 7-7**. Numerical and experimental (Wang *et al.*, 2015) modelling of Koyna dam due to an earthquake. a) Experiment result, b) computed result with FFSI after 10 sec.

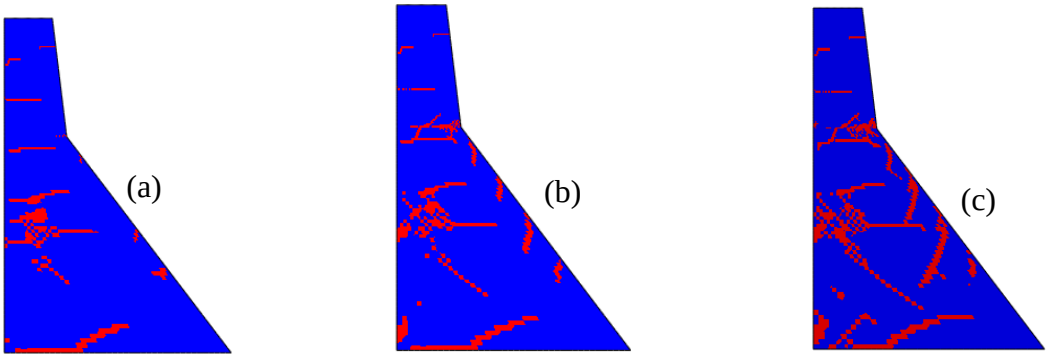


**Figure 7-8**. Contours show the tensile damage of combined action of ASR and seismic analysis of the Koyna dam using the FFSI strategy to model the reservoir, a) after 5 sec., b) after 7 sec. and c) after 10 sec., (note that this analysis is done after 10 years of ASR induced degradation in the dam).

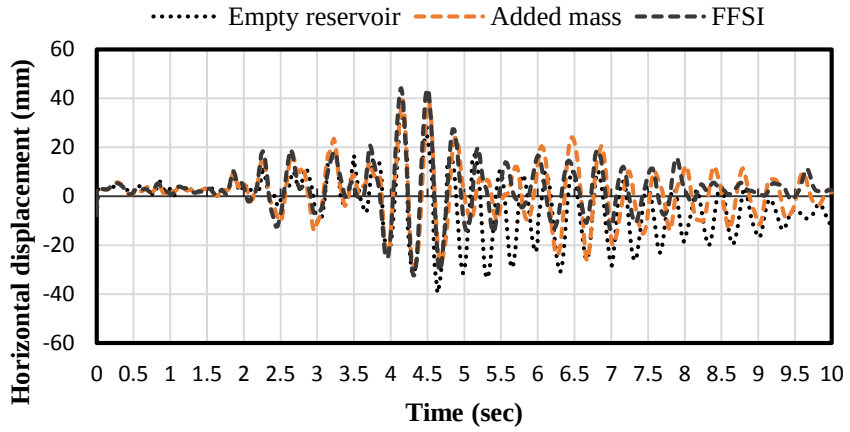


**Figure 7-9**. Comparison of the horizontal displacement of the crest of a dam not affected by ASR.

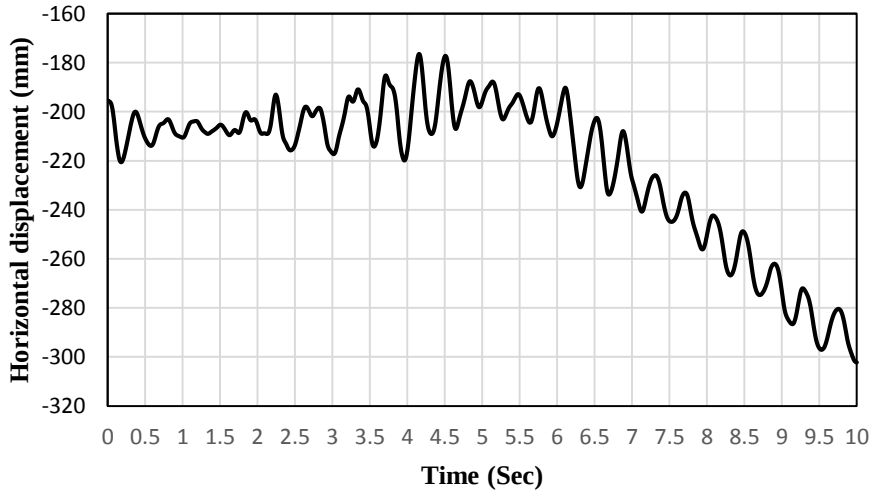


**Figure 7-10**. Horizontal displacement of the dam at crest level for the combined action of ASR and seismic excitation.

## 7.6 Summary

This chapter presented the nonlinear response of an ASR affected concrete gravity dam (the Konyna dam) after long term operation followed by a subsequent seismic event using the code developed in this research. In the chemo-thermo-mechanical model, ASR kinetics is combined with a damage plasticity model using a finite element approach which takes the ASR expansion with the effects of temperature, humidity, confinement from 3D stress state and non-uniform time dependent material degradation, into account.

The model is applied to the Koyna dam to predict the long term behaviour of the dam wall due to the ASR. Subsequently, a seismic analysis considering the state of the structure at the end of the ASR analysis as an initial state for the analysis is performed. Three assumptions are used for modelling the water-dam interaction i.e.: i) empty reservoir, ii) added-mass technique and iii) FFSI using the Helmholtz wave equation. It is shown that the FFSI modelling strategy predicts the damage pattern better than the other approaches by comparing the crack pattern and crest displacement. It can be concluded that there is a difference in displacement response between ASR affected and non-affected concrete dam indicating that the vibration characteristic of the dam is significantly changed due to crack opening and non-uniform material degradation caused by the ASR. The seismic displacement response of the ASR affected dam is larger than that from the non-affected dam. Cracks propagate through the upper face of the dam during the earthquake which may cause collapse of the dam.

In this research, long term strains such as creep, relaxation and shrinkage are not considered, and future research and modelling should be conducted to include these phenomena. Also, FE modelling of a rehabilitated dam to assess the effectiveness of the remedial actions is another topic for future research. In the next chapter, the SU-ASR code is used to model and analyse the effects of the slot cutting remedial technique on a synthetic dam.

# CHAPTER 8

# Towards repair and rehabilitation of dams affected by ASR

**Highlights:**

ASR rehabilitation, repair and remedial strategies

Numerical modelling of slot cutting technique

## 8.1 Introduction

During the two last decades research has been done in the field of dams suffering from ASR, resulting in practical advancements in the study of relevant areas of the effect of expansive chemical reactions. An increasing number of affected dam cases have been documented, whereas in some of them rehabilitation and repair provisions were implemented and a small number of them were decommissioned (Sellier *et al.*, 2017). These studies emphasise that the ASR effects depend on the type of the dam and its geographic location which lead to the specific risk related to the dam under investigation. A variety of parameters such as rate and magnitude of the expansion, local environmental conditions, long term viscoelastic behaviour such as creep and relaxation, type of the dam, equipment and foundation geological configuration could determine the appropriateness and effectiveness of remedial actions.

In this chapter, first the strategies for repair and rehabilitation of the typical dams suffering from ASR are reviewed and presented. Well-known dams on the African continent and other locations which have experienced severe damage related to ASR are addressed. The SU-ASR code is used to demonstrate the applicability of the FE model to predict the behaviour of a synthetic dam affected by ASR and then rehabilitated using the slot cutting technique. This is

a strategy which is applicable to rehabilitation, repair and remedial action of concrete dams suffering from ASR.

## 8.2 Critical zones identification in an ASR affected dam

According to the numerical analysis performed in previous sections and through a comprehensive literature review, critical zones in a generic ASR affected gravity dam are identified. The zones shown in Figure 8-1 are distinguished based on the region of manifestation of the ASR, issues identified for and impacts resulting from the ASR expansion. In general, these zones are Zone I, where spillway and measuring instruments are installed at the crest, Zone II, where galleries are located, Zone III where the drainage system, piping and foundation are located, and Zone IV the downstream face of the dam.

In Zone I, there is not any natural boundary condition against ASR expansion and often strain from ASR leads to vertical and horizontal movements during the service life of the structure. Extensive cracks are observed during gallery inspection. The numerical analysis performed in chapter 6 supports this finding. If spillways are equipped with sluice gates, possible misalignments of the gates and pendulums are expected. The Kariba dam in the Zambezi river is a representative case in this category. In this arch dam, the concrete expansion is affecting the spillway sluice geometry and has damaged the upstream stop-log roller path. The remedial

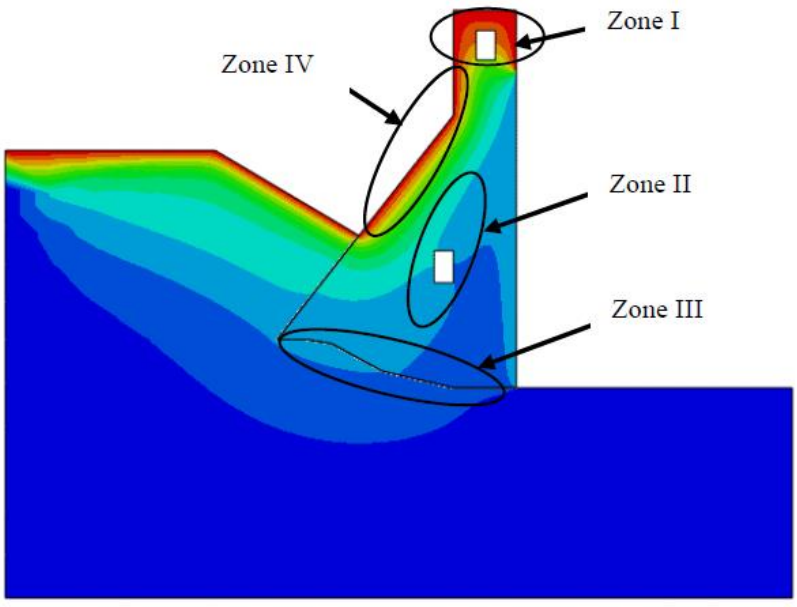


**Figure 8-1**. Recognised damage zones in a typical gravity dam.

measures for this dam include refurbishment of the stop-log roller path and installation of the new upstream set of stop-beams in combination with an emergency gate (Mhalanga, 2014).

Zone II, represents the major body of the dam and most of the inspection galleries and penstocks are in this area. In this zone, cracks along gallery wall and potential leakage from upstream through these cracks, causing penstock equipment misalignments are detected. The Fontana dam and Kleinplaas dam, which are evaluated in this research contain examples of problems encountered in this zone. Figure 8-2 shows the rehabilitation of the Fontana dam using post-tensioned tendons. The effectiveness of this remedial action was shown by Ingraffea some years later (1990). Foundation and drainage systems are critical parts of the dam and are mainly located in Zone III. The concerns in this zone are mainly vulnerability of these parts to the increase of the pore pressure from right or left flanks or abutments, uplift from upstream heel and stress concentration at the toe of the dam due to large constraints causing by foundation structure and slope instability of the foundation as a result of liquefaction of the soil. The ASR may lead to worsening all of these unfavourable mechanisms. Finally, in Zone IV, the downstream face is exposed to the temperature gradient represents a potential region of the dam where the alkali silica reaction will commence. Here, this can also lead to opening of the horizontal and vertical construction joints and failure of the water tightness elements in this zone.

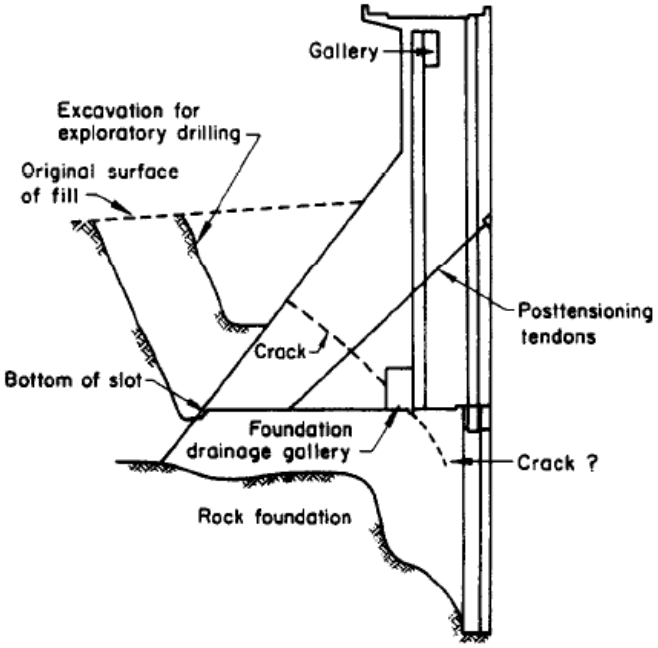


**Figure 8-2**. Rehabilitation of Fontana dam using Post tensioning tendons and slot cut method (Ingraffea,1990).

In summary, examples of effects of swelling from ASR in dams and hydraulic structures which are identified from reports in literature (Sellier *et al.*, 2017; Blight & Alexander, 2011; Sims & Poole, 2017; Souma, 2014) and this research are considered for planning the monitoring and surveillance programmes of dams are addressed in Table 8-1.

**Table 8-1**. Pathologies of the dam affected by ASR based on dam type.

| Dam type | Pathology | Example |
|---|---|---|
| Concrete gravity dam | Vertical and horizontal movements at crest | Kleinplaas dam, Fontana dam |
| | Opening at lift joints | |
| | Excessive cracks inside the galleries | |
| | leaching at openings and excessive uplift pressure due to seepage | |
| | Horizontal movements in structural and lift joints | |
| Arch dam | "m" shape movement of the crest | Kouga dam, Kariba dam, Mactaquac dam |
| | Stability problems due to changes in thrust block at abutments | |
| | Localized and structural cracks in galleries | |
| | Major cracks at dam/abutment contact | |
| | Symptoms of slip in lift joints | |
| | Excessive seepage due to ingress of water through openings and cracks | |
| Buttress dam | Lateral displacements of end piers | Poglia dam, Pracana dam |
| | Significant map pattern cracking in piers | |
| | Cracking and degradation of buttress with possible consequence of deteriorating reinforcing steel | |
| Spillways | Problem in gate tolerances and clearances may cause to clamp the gates | Kariba dam, Cahora Bassa, Chambon dam |
| | Transverse displacement of piers | |
| | Signs of cracking in fluid passage close to the piers | |
| | Increase in stress surrounding concrete leading to exert excessive pressure on the structure and equipment | |

## 8.3 Numerical study on slot cutting in a simplified dam

The relief of compressive stresses by the slot cutting technique has already been applied successfully to various dams and a growing demand could be expected due to the large number of dams affected by ASR (Metalssi *et al.*, 2014). However, still more research must be done regarding its efficiency and the proper design of its technical detail. In some cases, to efficiently release the compressive stresses and minimize the stress build-up at the supports, several distinct cuts have been created along the length of the affected dam. In others, strategies used to make cuts in a localized area of stress concentration, seems to have been successful (Sims & Poole, 2017). The demand for distributed slots might increase with higher concentrated swelling strains. Although, modelling of such rehabilitation and repairs strategies for a real dam are not within the scope of this research, the capabilities of the model are demonstrated in an analysis of slot cutting for a synthetic dam affected by ASR.

### 8.3.1 Problem description

The configuration and dimensions of the assumed dam are shown in Figure 8-3. A slot cut with a thickness $e_{sc} = 10\ mm$ is used in this study. Metalssi *et al.* (2014) pointed out that the current range of the slot cuts used in industrial applications varies between 10 to 20 mm. A constant initial temperature of $8\,℃$ is assumed anywhere inside the dam and the upstream and downstream temperature are $8\,℃$ and $20\,℃$, respectively. In addition, the gravity and hydrostatic loads due to the water in the reservoir are considered in the modelling. The main goals of this modelling are to demonstrate the capabilities of the SU-ASR FE code to analyse and predict the ASR effects on a synthetic dam which is rehabilitated using a slot cutting technique and to assess the stress behaviour in the dam wall under continuous ASR swelling before and after the sawing of the slot.

The material properties of the concrete and ASR model parameters are presented in Table 8-2. In this study a linear analysis of the dam is performed and concrete damage plasticity (CDP) constitutive model is not active in this simulation.

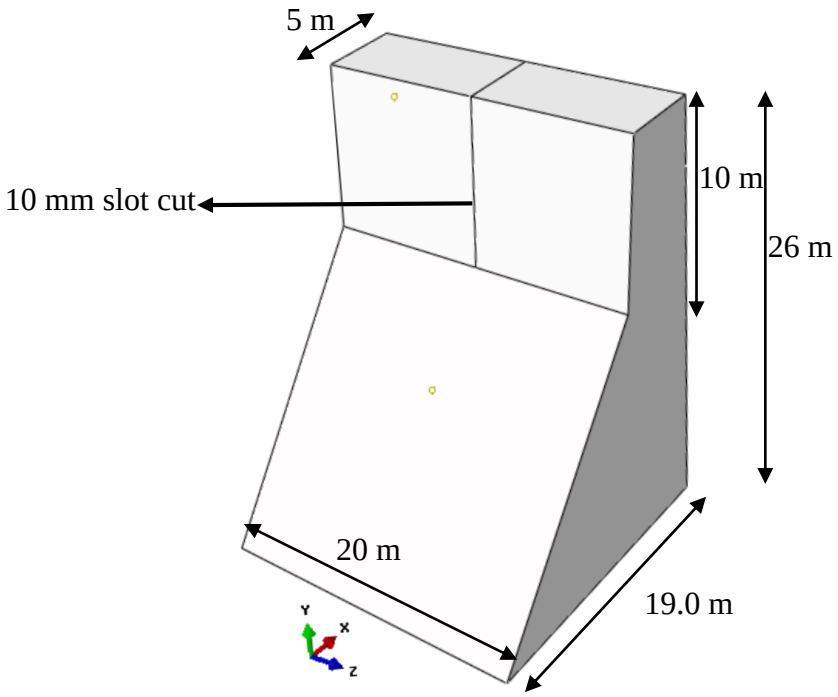


**Figure 8-3**. Layout and dimension of the assumed dam with 10 mm slot cut.

### 8.3.2 Finite element modelling of the dam

A preliminary transient thermal analysis for a duration of 20 years is performed to determine the thermal gradient incorporated in the subsequent ASR analysis. For the transient thermal diffusion analysis 37611 3-node (DC3D4) tetrahedral heat transfer elements are used. A surface to surface contact region using gap elements is defined to model the contact problem during the closure of the slot-cut. The finite element mesh and location of point A are shown in Figure 8-4. The results of the analysis such as ASR strain, displacement and stress are illustrated at the Point A.

**Table 8-2**. Properties of the concrete material and ASR kinetics parameter used in FE modelling.

| $E_c$ (GPa) | $\nu$ | $\rho$ (kg/m$^3$) | $\tau_l$ (day) | $\tau_c$ (day) | $\beta$ (%) |
|---|---|---|---|---|---|
| 30 | 0.2 | 2400 | 200 | 80 | 0.20 |

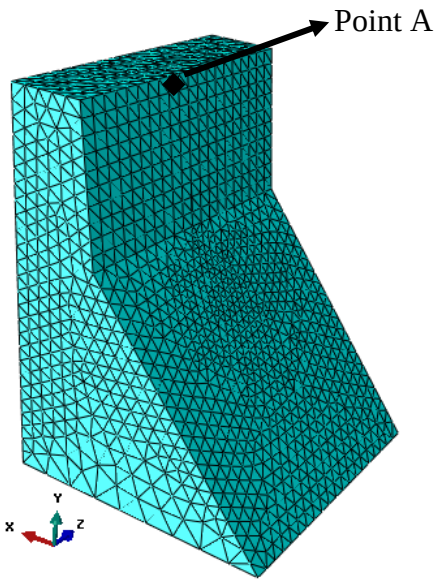


**Figure 8-4**. Finite element mesh used in the ASR modelling of the dam with slot cut (note to the global coordinate system. The global Z direction is along the transverse direction of the dam).

### 8.3.3 Results and discussion

The FE results of the transient thermal analysis are presented in Figure 8-5 for two different time steps i.e. 5 and 20 years after start of the analysis, respectively. The results show the gradual increase of the surface heat diffusion from the downstream side of the dam into the body of the dam. As mentioned in previous chapters the ASR model is strongly coupled with the temperature, hence the time and spatial variations of the temperature in the dam result in different levels of activation of the ASR mechanism occurs i.e. the higher temperature the faster the ASR proceeds.

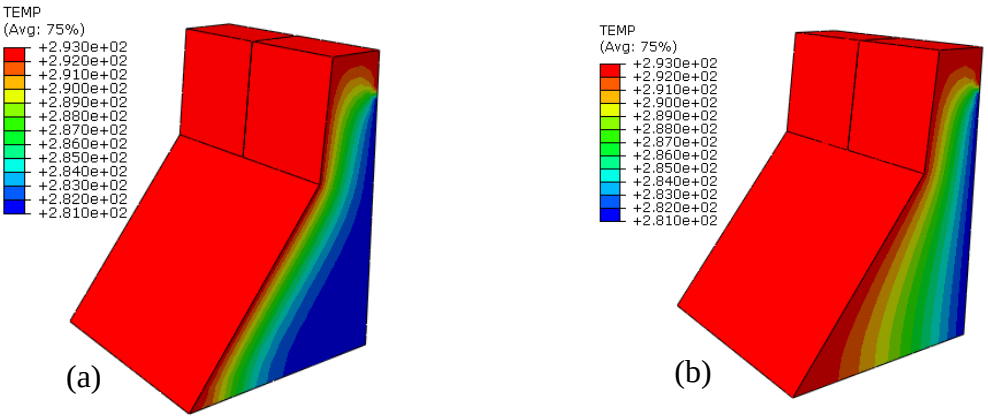


**Figure 8-5**.Temperature variation along the dam body in Kelvin, a) after 5 years b) after 20 years.

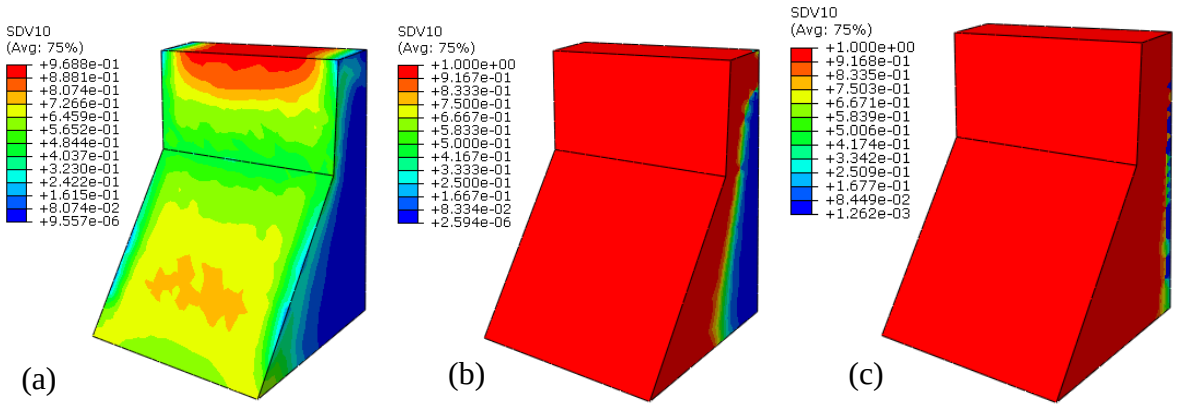


**Figure 8-6**.Variations of the reaction extent in the dam wall without slot cutting, a) after 5 years, b) after 10 years and c) after 20 years.

Figure 8-6 shows the contours of the reaction extent after 5, 10 and 20 years, respectively. It is observed that the extent of the kinetics of the reaction is about 96.8 % at point A after 5 years. Also, Figure 8-6 c shows that after 20 years the extent of the reaction reaches the maximum value in the whole dam.

The vertical strain and vertical displacement of the point A for the dam model without the slot cutting are shown in Figures 8-7 and 8-8 respectively. It can be observed that the ASR strain reaches its maximum value of 0.08 % after 6 years and stays constant during the rest of the analysis. Also, Figure 8-8 shows that the vertical displacement of the dam is 5 mm after 5 years and the maximum displacement is 11.5 mm after 20 years of the suffering from ASR.

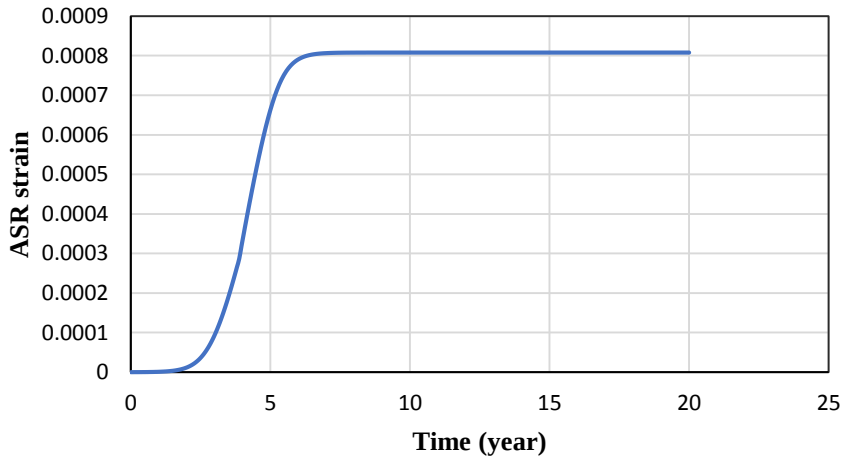


**Figure 8-7**.Vertical ASR strain of Point A without slot cutting during 20 years.

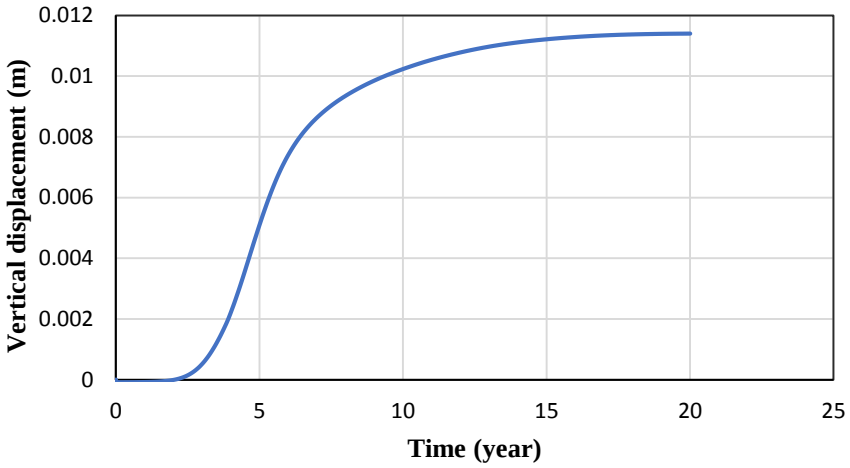


**Figure 8-8** .Vertical displacement of the Point A without slot cutting for a period of 20 years.

Material degradation is also considered in the model using a damage variable (FV1) and the result is presented in Figure 8-9 after 20 years. This figure shows that the current value of the ASR damage variable is 26.4% which implies that concrete material in the dam wall has experienced 26.4% reduction in its initial E-Modulus. The value of the Young's modulus is estimated to have reduced to 22.1 GPa after 20 years.

Figure 8-10 illustrates the displacement (U3) of the point A in global Z direction for a duration of 20 years. The slot cut is drilled after 4.8 years to study the effect of stress state in ASR behaviour of the dam. In this figure the constant displacement of 5 mm after 4.8 years is depicted. It can be interpreted that the slot closes due to the quick release of the initial

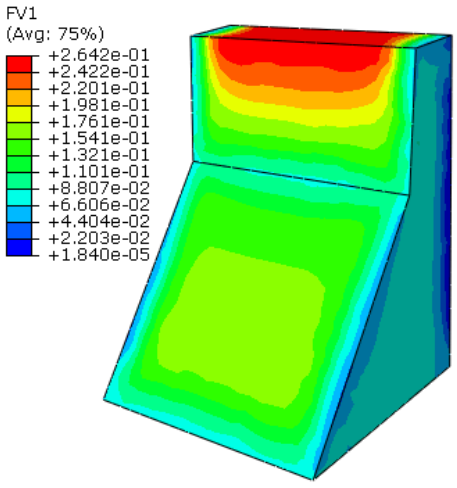


**Figure 8-9**. Contours of the ASR damage variable in the dam wall after 20 years.

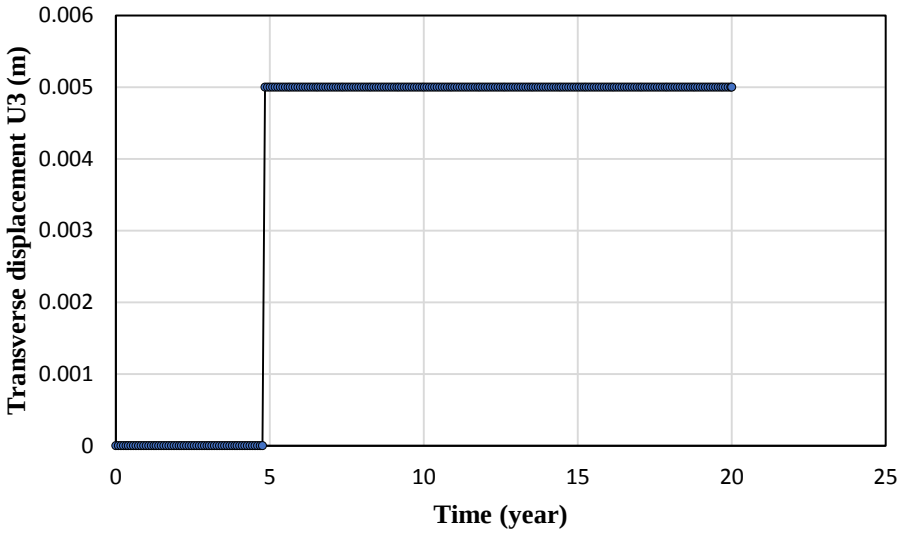


**Figure 8-10**. Transverse displacement (U3) in global Z direction of Point A vs. time before and after slot cutting. The slot is drilled after 4.8 years.

compressive stresses when the cut is created. For performing this analysis an import analysis phasing type technique which is available in Abaqus FE software (Simulia, 2016) is used. Figure 8-11 shows the contour of the transverse displacement (U3) of the dam 15.2 years after slot cut is drilled which confirms that the slot cut remains closed after sawing. Because of the symmetry, other side of the slot also has 5 mm displacement.

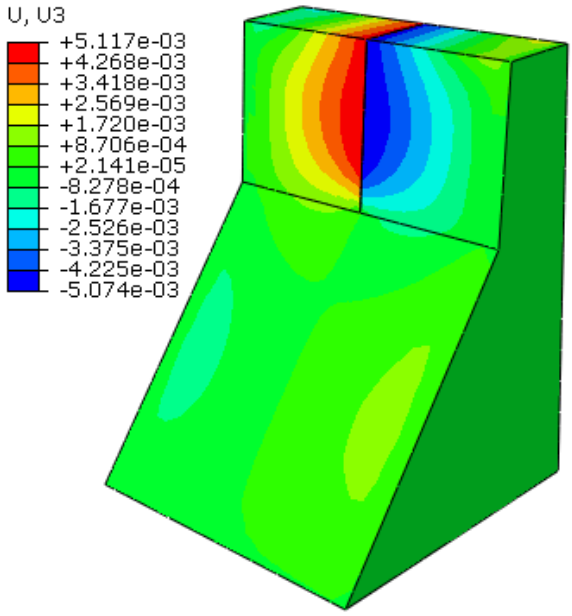


**Figure 8-11.** Contour of transverse displacement (U3) in global Z direction after 20 years.

As mentioned earlier the main goal of this study is to simulate the stress history of the dam which is affected by ASR swelling and resulting material deterioration with and without slot cutting. Figure 8-12 represents the variations of the stress (S33) in global Z direction at Point A of the dam before and after the slot cutting. For the dam without slot cutting stress increases during time until it reaches a maximum compressive stress value of 17 MPa. This value can be roughly obtained using the theoretical maximum value of the stress: $E_c \,.\, \varepsilon_{t=20}^{asr}$. (Note that the Young' modulus ($E_c$=22.1 GPa) is reduced by the ASR damage variable ($d_{asr}$) which is linked to the ASR expansion and $\varepsilon_{t=20}^{asr} = 8.0 \times 10^{-4}$). See Figure 8-9. In Figure 8-12, for the dam with a slot cut made 4.8 years after the start of the simulation, the stress is reduced once the cut is created and gradually increases until it stabilizes again to a compressive stress of 6.5 MPa. This value is in good agreement with the theoretical value of the stress in the transverse direction of the dam which is obtained using equation (8-1):

$$\sigma_{33} = E_c.\varepsilon_{t=20}^{asr} - E_c.\frac{e_{sc}}{L} = 6.63 \text{ MPa} \qquad (8\text{-}1)$$

where in this equation $L$ is the length of the dam equal to 20 m. By comparison of this stress with of the stress results of the dam modelled with the slot cut it can be concluded that the SU-ASR model can effectively model the effects of slot cutting on the assumed dam. This is achieved by analysing and predicting the applicable material parameters and the stress state before and after slot cut.

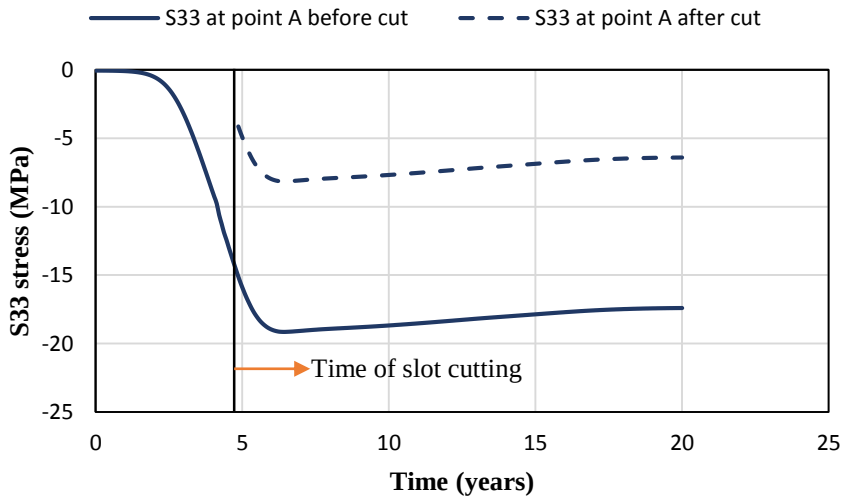


**Figure 8-12**. Stress history of point A in the global Z direction for the reference dam before and after slot cutting.

From this preliminary finite element modelling of a dam with assumed slot cut of 10 mm at the centre of its crest, it can be concluded that the SU-ASR model:

1. could predict the displacement and strain field in the dam affected by ASR,
2. sufficiently predicts the material deterioration due ASR swelling effects,
3. shows the corresponding stresses before and after slot cut in the dam.

Finally, it is worth noting that the actual modelling of slot cut in a dam affected by ASR is a complex process. Hence great care must be exercised in the planning and implementing of any slot cutting programme.

## 8.4 Summary

This chapter was devoted to study the rehabilitation, repair and remedial strategies for dams suffering from ASR. So far there is no way to stop or decrease the ASR in the current concrete structures. Hence, remedial and rehabilitation techniques to relieve the pressure and associated damage in the dam structures are inevitable. Typical extents of manifestation of the ASR impacts on the dam are presented and analytically reviewed. Among the several intervention strategies, slot cutting is one of the main techniques that has been applied successfully to some dams in the real world.

A specialized numerical software tool should be used for analysis and prediction of the impact of slot cutting on deteriorated structures such as dams suffering from ASR. A model which simulates the slot cutting technique is implemented to a synthetic dam structure using SU-ASR code is developed and discussed. Parameters such as temperature, non-uniform time dependent material degradation, confining stresses are considered in analysis. The model could predict the ASR strain and displacements fields, the material deterioration effects and most importantly the stress state before and after slot cut closure. The results were in good agreement with the theoretical solid mechanics based formulation which can be used to calculate the theoretical value of the stress state associated with the slot cutting.

# CHAPTER 9

# Conclusions and recommendations

**Highlights:**

Summary of the research

Main contribution of this thesis

Future research

## 9.1 General

In this research a chemo-thermo-mechanical model is developed to analyse and predict the multi-scale, multi-phase ASR problem in concrete structures such as dams. On the material level, the reduction of ASR expansion under multiaxial confinement, a 3D stress state, is clearly demonstrated. A model was developed to facilitate the prediction of the expansion rate from ASR during the service life of a structure and serves as a tool to investigate structural performance and possible instability due to irreversible displacements and cracks.

## 9.2 Thesis contribution

In this research, the SU-ASR FE-code model is developed and implemented as a user subroutine in Abaqus, a commercial finite element code. In this model, the heat-diffusion analysis is decoupled from the mechanical analysis, and the output from preliminary thermal analysis is used as a predefined field for the subsequent analysis including ASR and mechanical damage. The model is validated at the material scale on the basis of selected published papers

in the literature on experimental modelling of ASR considering the axial stress state based on the experimental work done by Multon and Toutlemonde (2006).

On structural level, a finite element model is constructed for gravity dams suffering from ASR. The reaction extent and damage parameters are presented and the results are compared with real dam behaviour. One of the primary features of the model presented is inclusion of the material stiffness degradation with ASR evolving during time. Considering this feature of the model, it may result in better prediction of structural damage, strains and displacements during the service life of the structure.

In the chemo-thermo-mechanical model developed for this research, the nonlinear responses of the three ASR affected concrete gravity dams in the long term operation condition and the subsequent seismic event are presented. ASR kinetics is combined with a damage plasticity model (CDP) using a finite element approach which takes the ASR expansion with the effects of temperature, humidity, gel absorption by micro cracks, confinement from 3D stress state and time dependent material degradation, into account. The model is then applied to the Fontana dam, Kleinplaas dam and Koyna dam to predict the long term behaviour of the dams. The simulated crack pattern and displacements of Fontana dam are in good agreement with the field observations. Following, the Kleinplaas dam which is located in Stellenbosch and has been suffering from ASR for many years is modelled and analysed. The model is calibrated with the measured data and the ASR parameters are identified. The model is then used to simulate the past and current swelling behaviour of the dam and the associated damage. The results could successfully predict the displacements and ASR strain rates plus the formation of irreversible plastic cracks.

The Koyna dam was selected to carry out a seismic analysis considering the state of the structure at the end of ASR analysis as in initial state for the subsequent seismic analysis. Three assumptions are used for modelling the water-dam interaction i.e.: i) empty reservoir, ii) added-mass technique and iii) FFSI using the Helmholtz wave equation. It is shown that the FFSI modelling strategy predicts the damage pattern better than the other approaches by comparing the crack pattern and crest displacement. It can be concluded that there is a difference in displacement response between ASR affected and non-affected concrete dam indicating that the vibration characteristic of the dam is significantly changed due to crack opening and non-uniform material degradation caused by the ASR. The seismic displacement response of the

ASR affected dam is larger than those from the non-affected dam. During the earthquake cracks propagate through the upper face of the dam which may cause collapse of the dam.

Another contribution of this thesis is the modelling of slot cutting technique which is implemented for a synthetic dam structure using the SU-ASR code. Parameters such as temperature, non-uniform time dependent material degradation, 3D confining stresses and the effect of gel absorption by micro cracks on the ASR delay mechanism are fairly considered. The model predicts the displacement and strain field in the dam affected by ASR, sufficiently predicts the material deterioration due ASR swelling effects, and shows the corresponding stresses before and after slot cutting in the dam.

## 9.3 Future research

Currently, it is still difficult to conduct a comprehensive assessment of the actual condition of a dam structure suffering from internal swelling reactions such as ASR. Prediction of the strain rate and displacement in the dam as well as the accurate analysis of the deterioration of the material and mechanical properties are required to estimate the period during which the structure will effectively perform its function.

In this research, long term strains such as creep, relaxation and shrinkage are not considered and future research and modelling should be conducted to include these phenomena. Also, comprehensive FE modelling of a rehabilitated dam to assess the effectiveness of the remedial actions is another topic for future research. Topics which could be considered in future research in this field can include one or more of the following:

1. inclusion of creep, shrinkage and relaxation strains to the model,
2. research on rehabilitation, repair and remedial countermeasures,
3. modelling more complicated hydraulic structures such as arch dams and other
4. structures such as bridges,
5. modelling of slot cutting of an actual dam and predict the future behaviour of the dam.

## 9.4 Final remarks

The impact of fresh water shortages manifests itself in arid regions and at present especially in the Western Cape Province of South Africa. The impact of concrete material degradation and earthquake damage as well as resulting structural failure have highlighted the vulnerability of aged dam systems. The loss of these critical systems can have major socio-economic consequences, losses and other cascading effects on water supply, power generation and irrigation. Hence, considerable efforts have been devoted to evaluating the safety of aged dams and in some cases to pursue suitable remedial action and rehabilitation strategies.

Although extensive research has been done to model ASR and other internal swelling reactions in concrete structures, limited attention has been paid to develop an engineering solution to solve these problems for real life dams exposed to these problems. It is foreseen that this research could stimulate research activity by other researchers and engineers active in this field to further develop and extend the models of the different mechanisms involved in these deleterious phenomena, presented here.

# References

Alaud, S. (2016). *Durability of Concrete under Combined Action: Mechanical Load and Alkali-Silica Reaction*. PhD thesis, Stellenbosch University, Stellenbosch, South Africa.

Alaud, S., & van Zijl, G. P. A. G. (2017). Combined Action of Mechanical Pre-Cracks and ASR Strain in Concrete. *Journal of Advanced Concrete Technology*, *15*(4), 151–164. https://doi.org/10.3151/jact.15.151

ASTM C1260. (2007). *ASTM, Standard Test Method for Potential Alkali Reactivity of Aggregates (Mortar-Bar Method,D)*. American Society for Testing and Materials, United States.

ASTM C1293. (2008). *Determination of length change in concrete due to Alkali-Silica reaction*. American Society for Testing and Materials, United States.

Bazant, Z. P., & Oh, B. H. (1983). Crack band theory of concrete. *Materials and Structures*, *16*, 155–177. https://doi.org/10.1007/BF02486267

Bazant, Z. P., & Steffens, A. (2000). Mathematical model for kinetics of alkali-silica reaction in concrete. *Cement and Concrete Research*, *30*(3), 419–428. https://doi.org/10.1016/S0008-8846(99)00270-7

Ben Haha, M., Gallucci, E., Guidoum, A., & Scrivener, K. L. (2007). Relation of expansion due to alkali silica reaction to the degree of reaction measured by SEM image analysis. *Cement and Concrete Research*, *37*(8), 1206–1214. https://doi.org/10.1016/j.cemconres.2007.04.016

Blight, G. E., & Alexander, M. G. (2011). *Alkali-Aggregate Reaction and Structural Damage to concrete*. UK: CRC Press.

Bournazel, J. P., & Moranville, M. (1997). Durability of concrete: The crossroad between chemistry and mechanics. *Cement and Concrete Research*, *27*(10), 1543–1552. https://doi.org/10.1016/S0008-8846(97)00168-3

Calayir, Y., & Karaton, M. (2005). Seismic fracture analysis of concrete gravity dams including dam-reservoir interaction. *Computers & Structures*, *83*(19–20), 1595–1606. https://doi.org/10.1016/j.compstruc.2005.02.003

Camacho, G. T., & Ortiz, M. (1996). Computational modelling of impact damage in brittle materials. *International Journal of Solids and Structures*. https://doi.org/10.1016/0020-7683(95)00255-3

Capra, B., & Bournazel, J. P. (1998). Modelling of induced mechanical effects of alkali-aggregate reactions. *Cement and Concrete Research*, *28*(2), 251–260. https://doi.org/10.1016/S0008-8846(97)00261-5

Capra, B., & Sellier, A. (2003). Orthotropic modelling of alkali-aggregate reaction in concrete structures: Numerical simulations. *Mechanics of Materials*, *35*(8), 817–830. https://doi.org/10.1016/S0167-6636(02)00209-0

CEB-fib. (2013). *Fib Model Code for Concrete Structures 2010*. *Ernst & Sohn*. Ernst & Sohn.

Charlwood, R. G. (2009). *AAR in Dams and Hydroelectric Plants*. *Short Course on Management of Alkali Aggregate Affected Structures: Analysis, Performance & Prediction*.

Charlwood, R. G. (2009). *Predicting the long term behaviour and service life of concrete dams*. *Conference on Long Term Behaviour of Dams*. LTBD09-Graz.

Charlwood, R. G., Scrivener, K., & Sims, I. (2012). Recent developments in the management of chemical expansion of concrete in dams and hydro projects - Part 1 : Existing structures. In *Hydro 2012* (pp. 1–17). Bilbao, Spain.

Chen, W. F. (2007). *Plasticity in reinforced concrete*. *Computer Methods in Applied Mechanics and Engineering*. USA: J. Ross. https://doi.org/10.1016/0045-7825(82)90016-0

Chen, W. F., & Saleeb, A. F. (1994). *Constitutive Equations for Engineering Materials Volume I: Elasticity and Modelling* (Vol. 1). Elsevier B.V., UK.

Clough, R. W., & Penzien, J. (2003). Dynamics of structures. In *Computers & Structures, Inc.* (Third Edit). https://doi.org/10.1016/0045-7825(92)90174-I

Comby-Peyrot, I., Bernard, F., Bouchard, P. O., Bay, F., & Garcia-Diaz, E. (2009). Development and validation of a 3D computational tool to describe concrete behaviour at mesoscale. Application to the alkali-silica reaction. *Computational Materials Science*, *46*(4), 1163–1177. https://doi.org/10.1016/j.commatsci.2009.06.002

Cornelissen, H. A. W., Hordijk, D. A., & Reinhardt, H. W. (1986). Experimental determination of crack softening characteristics of normal lightweight concrete. *Heron*, *31*(2), 45–56.

Coussy, O. (2004). *Poromechanics*. Jon Wiley and Sons, UK.

Davies, J. (1996). Observation of the Fracture Path Development in Mortar Beam Specimens. *Advanced Cement Based Material*, (3), 31–36.

De Borst, R. (2002). Fracture in quasi-brittle materials : a review of continuum damage-based approaches. *Engineering Fracture Mechanics*, *69*, 95–112.

Dormieux, L., Kondo, D., & Ulm, F.-J. (2006). *Micorporomechanics*. J. Wiley and Sons, UK.

Dunant, C. F., & Scrivener, K. L. (2010). Micro-mechanical modelling of alkali-silica-reaction-induced degradation using the AMIE framework. *Cement and Concrete Research*, *40*(4), 517–525. https://doi.org/10.1016/j.cemconres.2009.07.024

Dyer, T. (2014). *Concrete Durability*. CRC Press, London, UK. https://doi.org/10.1017/CBO9781107415324.004

Esposito, R., & Hendriks, M. A. N. (2016). A multiscale micromechanical approach to model the deteriorating impact of alkali-silica reaction on concrete. *Cement and Concrete Composites*, *70*, 139–152. https://doi.org/10.1016/j.cemconcomp.2016.03.017

Fairbairn, E. M. R., Ribeiro, F. L. B., Lopes, L. E., Toledo-Filho, R. D., & Silvoso, M. M. (2006). Modelling the structural behaviour of a dam affected by alkali-silica reaction. *Communications in Numerical Methods in Engineering*, *22*(1), 1–12. https://doi.org/10.1002/cnm.788

Farage, M. C. R., Alves, J. L. D., & Fairbairn, E. M. R. (2004). Macroscopic model of concrete subjected to alkali-aggregate reaction. *Cement and Concrete Research*, *34*(3), 495–505. https://doi.org/10.1016/j.cemconres.2003.09.001

Garcia-Diaz, E., Riche, J., Bulteel, D., & Vernet, C. (2006). Mechanism of damage for the alkali-silica reaction. *Cement and Concrete Research*, *36*(2), 395–400. https://doi.org/10.1016/j.cemconres.2005.06.003

Giorla, A. B., Scrivener, K. L., & Dunant, C. F. (2015). Influence of visco-elasticity on the stress development induced by alkali-silica reaction. *Cement and Concrete Research*, *70*(September), 1–8. https://doi.org/10.1016/j.cemconres.2014.09.006

Glasser, L. S. D. (1979). Osmotic pressure and the swelling of gels. *Cement and Concrete Research*, *9*(4), 515–517. https://doi.org/10.1016/0008-8846(79)90050-4

Glasser, L. S., & Kataoka, N. (1981). The chemistry of "alkali-aggregate" reaction. *Cement and Concrete Research*, *11*(1), 1–9. https://doi.org/10.1016/0008-8846(81)90003-X

Gocevski, V., & Yildiz, E. (2017). Numerical analysis of AAR affected structures with slot cuts, In A. Sellier, E. Grimal, S. Multon, & E. Bourdarot (Eds.), *Swelling concrete in dams and hydraulic structures* (First edit, pp. 188–202). Wiley.

Herrador, M. F., Martínez-Abella, F., & Del Hoyo Fernández-Gago, R. (2009). Mechanical behaviour model for ASR-affected dam concrete under service load: Formulation and verification. *Materials and Structures*, *42*(2), 201–212. https://doi.org/10.1617/s11527-008-9378-6

Hillerborg, A., Modéer, M., & Petersson, P. E. (1976). Analysis of crack formation and crack growth in concrete by means of fracture mechanics and finite elements. *Cement and Concrete Research*, *6*(6), 773–781. https://doi.org/10.1016/0008-8846(76)90007-7

Hjalmarsson, F., & Pettersson, F. (2017). *Finite Element Analysis of Cracking of Concrete Arch Dams Due To Seasonal Temperature Variation*. Master's dissertation, Lund University, Sweden.

Huang, M., & Pietruszczak, S. (1999). Modelling of Thermomechanical Effects of Alkali-Silica Reaction. *Journal of Engineering Mechanics*, *125*(4), 476–485.

Ichikawa, T., & Miura, M. (2007). Modified model of alkali-silica reaction. *Cement and Concrete Research*, *37*(9), 1291–1297. https://doi.org/10.1016/j.cemconres.2007.06.008

Ingraffea, A. R. (1990). Case studies of simulation of fracture in concrete dams. *Engineering Fracture Mechanics*, *35*(1–3), 553–564. https://doi.org/10.1016/0013-7944(90)90230-E

ISE. (1992). *Structural effects of alkali-silica reaction*. *The Institution of Structural Engineers*. UK, London.

*Kleinplaas dam, Third dam safety inspection report*. (2009). Department of Water and Sanitation, Pretoria, South Africa.

Larive, C. (1998). *Apports Combin'es de l'Experimentation et de la Modélisation à la Comprehension del'Alcali-Réaction et de ses Effets Mécaniques*. PhD thesis, Paris, France.

Lee, J., & Fenves, G. L. (1998). Plastic-Damage Model for Cyclic Loading of Concrete Structures. *Journal of Engineering Mechanics*, *124*(8), 892–900.

Legar, P., Côte, P., & Tinawi, R. (1996). Finite element analysis of concrete swelling due to alkali-aggregate reaction in dams. *Computers & Structures*, *60*(4), 601–611.

Lemarchand, E., Dormieux, L., & Ulm, F.-J. (2002). Elements of micromechanics of ASR-induced swelling in concrete structures. *Concrete Science and Engineering*, *4*(March), 12–22.

Li, K., & Coussy, O. (2004). Numerical assessment and prediction method for the chemico-mechanical deterioration of ASR-affected concrete structures. *Canadian Journal of Civil Engineering*, *31*(3), 432–439. https://doi.org/10.1139/l04-003

Liaudat, J., Carol, I., López, C. M., & Saouma, V. E. (2018). ASR expansions in concrete under triaxial confinement. *Cement and Concrete Composites*, *86*, 160–170. https://doi.org/10.1016/j.cemconcomp.2017.10.010

Lubliner, J., Oliver, J., Oller, S., & Oñate, E. (1989). A plastic-damage model for concrete. *International Journal of Solids and Structures*, *25*(3), 299–326. https://doi.org/10.1016/0020-7683(89)90050-4

Meijers, J. P. (2018). weather.sun.ac.za. Retrieved from www.weather.sun.ac.za

Metalssi, O., Seignol, J., Rigobert, S., & Toutlemonde, F. (2014). Modelling the cracks opening-closing and possible remedial sawing operation of AAR-affected dams. *Engineering Failure Analysis*, *36*, 199–214. https://doi.org/10.1016/j.engfailanal.2013.10.009

Mhalanga, Z. S. (2014). Rehabilitation of the spillway upstream control facility and reshaping of the plunge pool. In *Proceeding of SANCOLD conference,*. Johannesburg, South Africa.

Morenon, P., Multon, S., Sellier, A., Grimal, E., Hamon, F., & Bourdarot, E. (2017). Impact of stresses and restraints on ASR expansion. *Construction and Building Materials*, *140*, 58–74. https://doi.org/10.1016/j.conbuildmat.2017.02.067

Multon, S., Seignol, J. F., & Toutlemonde, F. (2005). Structural behaviour of concrete beams affected by alkali-silica reaction. *ACI Materials Journal*, *102*(2), 67–76.

Multon, S., Sellier, A., & Cyr, M. (2009). Chemo-mechanical modelling for prediction of alkali silica reaction (ASR) expansion. *Cement and Concrete Research*, *39*(6), 490–500. https://doi.org/10.1016/j.cemconres.2009.03.007

Multon, S., & Toutlemonde, F. (2006). Effect of applied stresses on alkali-silica reaction-induced expansions. *Cement and Concrete Research*, *36*(5), 912–920. https://doi.org/10.1016/j.cemconres.2005.11.012

Nayak, P., & Maity, D. (2013). Seismic Damage Analysis of Aged Concrete Gravity Dams. *International Journal for Computational Methods in Engineering Science and Mechanics*, *14*(5), 424–439. https://doi.org/10.1080/15502287.2013.784380

Newman, J., & Choo, B. S. (2003). *Advanced concrete technology-Concrete Properties*. Elsevier B.V., London, UK.

Owens, G. (2009). *Fulton's Concrete Technology* (Ninth Ed.). Cement and Concrete Institute, Midrand, South Africa.

Pan, J., Feng, Y., Wang, J., Sun, Q., Zhang, C., & Owen, D. (2012). Modelling of alkali-silica reaction in concrete : a review. *Front. Struct. Civ. Eng*, *6*(1), 1–18. https://doi.org/10.1007/s11709-012-0141-2

Pan, J., Xu, Y., Jin, F., & Zhang, C. (2014). A unified approach for long term behaviour and seismic response of AAR-affected concrete dams. *Soil Dynamics and Earthquake Engineering*, *63*, 193–202. https://doi.org/10.1016/j.soildyn.2014.03.018

Pietruszczak, S. (1996). on the Mechanical Behaviour of Concrete Subjected To Alkali-Aggregate Reaction. *Computers & Structures*, *58*(6), 1093–1097. https://doi.org/10.1016/0045-7949(95)00228-6

Ponce, J. M., & Batic, O. R. (2006). Different manifestations of the alkali-silica reaction in concrete according to the reaction kinetics of the reactive aggregate. *Cement and Concrete Research*, *36*(6), 1148–1156. https://doi.org/10.1016/j.cemconres.2005.12.022

Pourbehi, M. S., van Zijl, G. P. A. G., & Strasheim, J. A. B. (2018). Modelling of Alkali Silica Reaction in concrete structures for rehabilitation intervention. In H. Beushausen (Ed.), *Proceeding of International Conference on Concrete Repair, Rehabilitation and Retrofitting*. Cape town, South Africa.

Poyet, S., Sellier, A., Capra, B., Thèvenin-Foray, G., Torrenti, J. M., Tournier-Cognon, H., & Bourdarot, E. (2006). Influence of Water on Alkali-Silica Reaction: Experimental Study and Numerical Simulations. *Journal of Materials in Civil Engineering*, *18*(August), 588–596. https://doi.org/10.1061/(ASCE)0899-1561(2006)18:4(588)

Puatatsananon, W., & Saouma, V. (2013). Chemo-Mechanical Micromodel for Alkali-Silica Reaction. *ACI Materials Journal*, *110*(1), 2011–2289. Retrieved from http://civil.colorado.edu/~saouma/AAR/AAR-Chemo-Mechanical.pdf

Rajabipour, F., Giannini, E., Dunant, C., Ideker, J. H., & Thomas, M. D. A. (2015). Alkali-silica reaction: Current understanding of the reaction mechanisms and the knowledge gaps. *Cement and Concrete Research*, *76*, 130–146. https://doi.org/10.1016/j.cemconres.2015.05.024

Saouma, V. (2014). *Numerical Modelling of AAR* (First edition). CRC Press, London, UK. https://doi.org/10.1201/b16353

Saouma, V. E., Martin, R. A., Hariri-Ardebili, M. A., & Katayama, T. (2015). A mathematical model for the kinetics of the alkali-silica chemical reaction. *Cement and Concrete Research*, *68*, 184–195. https://doi.org/10.1016/j.cemconres.2014.10.021

Saouma, V. E., & Perotti, L. (2006). Constitutive Model for Alkali-Aggregate Reactions. *ACI Materials Journal*, *103*(3), 194–202.

Sellier, A., Grimal, E., Multon, S., & Bourdarot, E. (2017). *Swelling Concrete in Dams and Hydraulic Structures: DSC 2017*. ISTE Ltd, UK, London. Retrieved from http://eu.wiley.com/WileyCDA/WileyTitle/productCd-1786302136.html

Sims, I., & Poole, A. (2017). *Alkali-Aggregate Reaction in Concrete: A World Review*. CRC Press, London, UK.

Simulia. (2016). Abaqus 2016 theory guide. Dassault systemes.

Sloan, R. C., & Abraham, T. J. (1978). TVA cuts deep slot in dam ends cracking problems. *Civil Engineering*, *48*.

Stanton, T. E. (1940). Expansion of concrete through reaction between cement and aggregate. *Proceeding of the American Scociety for Civil Engineering*, *66*, 1781–1811.

Steffens, A., Li, K., & Coussy, O. (2003). Aging approach to water effect on alkali–silica reaction degradation of structures. *Journal of Engineering Mechanics*, *129*(1), 50–59. https://doi.org/10.1061/(ASCE)0733-9399(2003)129:1(50)

Suwito, A., Jin, W., Xi, Y., & Meyer, C. (2002). A Mathematical Model for the Pessimum Size Effect of ASR in Concrete. *Concrete Science and Engineering*, *4*(13), 23–34.

Tan, H., & Chopra, A. K. (1995). Earthquake analysis of arch dams including dam-water-foundation rock interaction. *Earthquake Engineering and Structural Dynamics*, *24*(11), 1453–1474. https://doi.org/https://doi.org/10.1002/eqe.4290241104

Thompson, G., Charlwood, R. G., Steele, R., & Curtis, D. D. (1994). Mactaquac Generating Station Intake and Spillway Remedial Measures. In *Eighteenth international congress on large dams* (pp. 347–368). Durban, South Africa.

Ulm, F., Coussy, O., Li, K., & Larive, C. (2000). Thermo-Chemo-Mechanics Of ASR Expansion In Concrete Structures. *Journal of Engineering Mechanics*, *126*(March), 233–242.

Valliappan, S., & Chee, C. (2009). Ageing degradation of concrete dams based on damage mechanics concepts. In Y. Yuan, J.Cui, & H. A. Mang (Eds.), *Computational structural engineering* (pp. 21–35). Springer Netherlands.

van Zijl, G. P. A. G. (1999). *Computational Modelling of Masonry Creep and Shrinkage*. PhD thesis, Delft University of Technology, Delft, The Netherland.

Wang, G., Wang, Y., Lu, W., Zhou, C., Chen, M., & Yan, P. (2015). XFEM based seismic potential failure mode analysis of concrete gravity dam-water-foundation systems through incremental dynamic analysis. *Engineering Structures*, *98*, 81–94. https://doi.org/10.1016/j.engstruct.2015.04.023

Zienkiewicz, O. C. (2006). *The finite element method for solid and structural mechanics* (6th ed.). Elsevier B.V., London, UK.